NTIA-Report-80-42

Comparison of Available Methods for Predicting Medium Frequency Sky-Wave Field Strengths

Margo PoKempner

U.S. DEPARTMENT OF COMMERCE
Philip M. Klutznick, Secretary

Henry Geller, Assistant Secretary
for Communications and Information

June 1980

TABLE OF CONTENTS

LIST OF FIGURES

LIST OF TABLES

COMPARISON OF AVAILABLE METHODS FOR PREDICTING MEDIUM FREQUENCY SKY-WAVE FIELD STRENGTHS

Margo PoKempner*

The chronological development of the available methods for predicting medium frequency sky-wave field strengths is presented with a brief discussion of each method. Measured field strengths for 36 medium frequency sky-wave paths are compared with the predicted field strengths from several different prediction methods. Based on the rms errors between observations and predictions, the 1938 Cairo Curves provide the best estimates of the sky-wave field strengths for very long paths worldwide. A new prediction method developed for use in North and South America only, provides improved estimates of the sky-wave field strengths for paths <3500 km.

Key words: CCIR; Cairo Curves; FCC Curves; medium frequency; radio propagation predictions; skywaves

1. INTRODUCTION

Since the inception in the early 1920's of medium frequency (MF) AM broadcasting, the steadily increasing demand for stations resulted in a congestion of the medium frequency spectrum by the late 1940's. The need for more precise and detailed information concerning sky-wave propagation of MF radio waves has been mentioned in various sources since World War II (Phillips, 1950; JTAC, 1964). Today, because there is still a demand for an increase in the number of broadcast services, various proposals are being explored to improve the efficiency of this portion of the spectrum and provide for an orderly expansion of broadcast services. However, an increase in broadcast services could also result in substantial interference to adjacent and co-channel stations and reduce the service areas of currently operating stations.

In view of these problems, the International Radio Consultative Committee (CCIR) of the International Telecommunication Union (ITU) has scheduled a Regional Administrative MF Broadcasting Conference (Region 2). The first session of the Conference was held in Buenos Aires in March, 1980, to establish a basis for preparing a frequency assignment plan for the MF broadcasting band in Region 2 (North and South America). This first session considered propagation data, modulation standards, channel spacing, protection ratios including noise levels, required field strengths, transmitting antenna characteristics,

The author is with the U.S. Department of Commerce, National Telecommunications and Information Administration, Institute for Telecommunication Sciences, Boulder, Colorado 80303.

transmitter power, and planning. The second session, to be convened in November 1981, will draw up an agreement and an associated frequency plan of assignments in the MF broadcasting band in Region 2.

Accurate and reliable technical criteria are needed to support the activities in the second session of this conference. This report is concerned with only one technical aspect; i.e., the reliability of existing methods for predicting long-distance propagation of MF radio waves at night. Several prediction methods are available for this purpose. A brief review of these methods and a comparison between measured field strengths and predicted field strengths for some of the methods are presented here.

2. CHRONOLOGICAL DEVELOPMENT OF MF FIELD STRENGTH PREDICTION METHODS

This section presents the various MF field strength prediction methods and their revisions in the chronological order of their documentation.

1938. One of the earliest recognized field strength prediction techniques was the so-called "Cairo Curves." Two curves, one for North-South and one for East-West propagation were adopted by the CCIR at the International Radiocommunications Conference, Cairo, 1938. At the CCIR VIIIth Plenary Assembly, Warsaw, 1956, the International Frequency Registration Board (IFRB) requested CCIR to extend the Cairo Curves to include variations with magnetic latitude, season, and solar activity. However, it was not until 1974 that CCIR recommended a more precise, accurate, worldwide method for predicting MF field strengths, presumably as a replacement for the Cairo Curves.

1946. The U.S. Federal Communications Commission (FCC), in connection with their Clear Channel Hearing, Docket #6741, presented a set of composite curves showing propagation losses for nighttime sky-wave field strengths in North America. They were incorporated in the FCC Rules and Regulations, Part 3, Radio Broadcast Services.

1959. Norton (1959) developed an MF sky-wave field strength prediction method based on a physical model which corresponds to a wavehop treatment.

1963. The CCIR Documents of the Xth Plenary Assembly, Geneva, presented an empirical formula and a set of curves developed by the European Broadcasting Union (EBU) for determining the annual median value of the nighttime field strength for MF for the European Broadcasting Area (Ebert, 1962).

1966. Barghausen (1966) modified Norton's semi-empirical formula for estimating polarization and absorption losses.

1966. The CCIR Documents of the XIth Plenary Assembly, Oslo, formally recommended the provisional use of the EBU formula for the European Broadcasting Area and also presented a modification to the EBU formula to provide predictions of short-distance sky-wave field strengths for the African LF/MF Broadcasting Conference, Geneva, 1966.

1970. The CCIR Documents of the XIIth Plenary Assembly, New Delhi, presented a separate formula for estimating the annual median field strengths for distances <300 km.

1971. Olver et al. (1971) developed a prediction method based on a wavehop approach similar to that of Norton (1959) except that a ray trace procedure is used.

1973. Knight (1973) proposed a manual method of approximating the wavehop method of Olver et al. (1971).

1974. The CCIR Documents of the XIIIth Plenary Assembly, Geneva, included an empirical formula developed by the U.S.S.R. for estimating the dependence of field strength on frequency and distance at a geomagnetic (dipole) latitude of 37° for the U.S.S.R., and a worldwide semi-empirical method based on physical principles proposed by the U.K.

The CCIR Interim Working Party (IWP) 6/4 modified the U.S.S.R. method by incorporating certain features of the U.K. method and recommended the provisional use of the modified U.S.S.R. method for predicting MF sky-wave field strengths worldwide.

1975. The Final Acts of the Regional Administrative LF/MF Broadcasting Conference (ITU, 1975) adopted the CCIR, Geneva, 1974, sky-wave field strength prediction method (150 to 1600 kHz) for Region 1, Australia and New Zealand. For the Asian part of Region 3, North of 11°S, the "Cairo" North-South curve with a modification for polarization coupling loss (L_p) was recommended.

1977. Wang (1977) developed a new MF sky-wave field strength prediction method for North America.

1978. The CCIR Documents of the XIVth Plenary Assembly, Kyoto, further modified the CCIR, Geneva, 1974, sky-wave field strength prediction method for MF (150 to 1600 kHz) and recommended its provisional use worldwide (CCIR, 1978). Several sky-wave field strength prediction methods proposed for various parts of the world also were described. They are:

1) Cairo North-South curve adopted for use in Asian part of Region 3 - mathematical approximation presented.

2) EBU method to be used in European Broadcasting Area with separate formula for distances <300 km.

3) U.S.S.R. method - valid between 37° and 60° geomagnetic latitude for distances up to 6000 km and has no frequency dependence.

4) U.K. method - valid for all distances worldwide except for the auroral zones and has no frequency dependence.

5) Wang's 1977 method given as an alternative method for the U.S.

1979. Wang (1979) proposed a modification of the CCIR Kyoto 1978 method to improve accuracy in Region 2.

1979. The Inter-American Conference on Telecommunications extended the FCC median signal level curve to distances beyond 4300 km using the Cairo North-South Curve and recommended its adoption for Region 2.

3. DISCUSSION OF THE METHODS

In this section, a brief description and mathematical formulation, where applicable, is given for the methods which have been used internationally and for some of the methods that appear to be more scientific approaches but have not been widely applied.

3.1 Cairo Curves

The Cairo Curves (Figure 1) were based on three measurement campaigns conducted by the International Broadcasting Union (IBU) in the northern hemisphere winters of 1934/35, 1935/36, and 1936/37. As many countries had taken measurements on paths up to 2000 km and obtained results that were in close agreement with the propagation curves for similar distances drawn by Dr. van der Pol's committee at Madrid, 1932, and adopted by CCIR, Lisbon, 1934, these campaigns involved paths ranging from 5000 to 11900 km and frequencies between 695 and 1185 kHz. Measurements were made on 23 paths between North America and Europe, North America and South America, and South America and Europe; the great circle paths are shown in Figure 2. For the third campaign, the transmitting stations were selected on the basis of the following considerations: 1) transmitter power (50 to 120 kW), 2) half-wavelength antennas, and 3) frequencies relatively close to 1000 kHz (Knight, 1977). In Figure 1, the North-South curve represents transequatorial propagation, and the East-West represents propagation at high latitudes. The original curves were in terms of the quasi-maximum value for 1 kW radiated, versus distance. This was defined at the Madrid conference as the value exceeded not more than 5% of the time

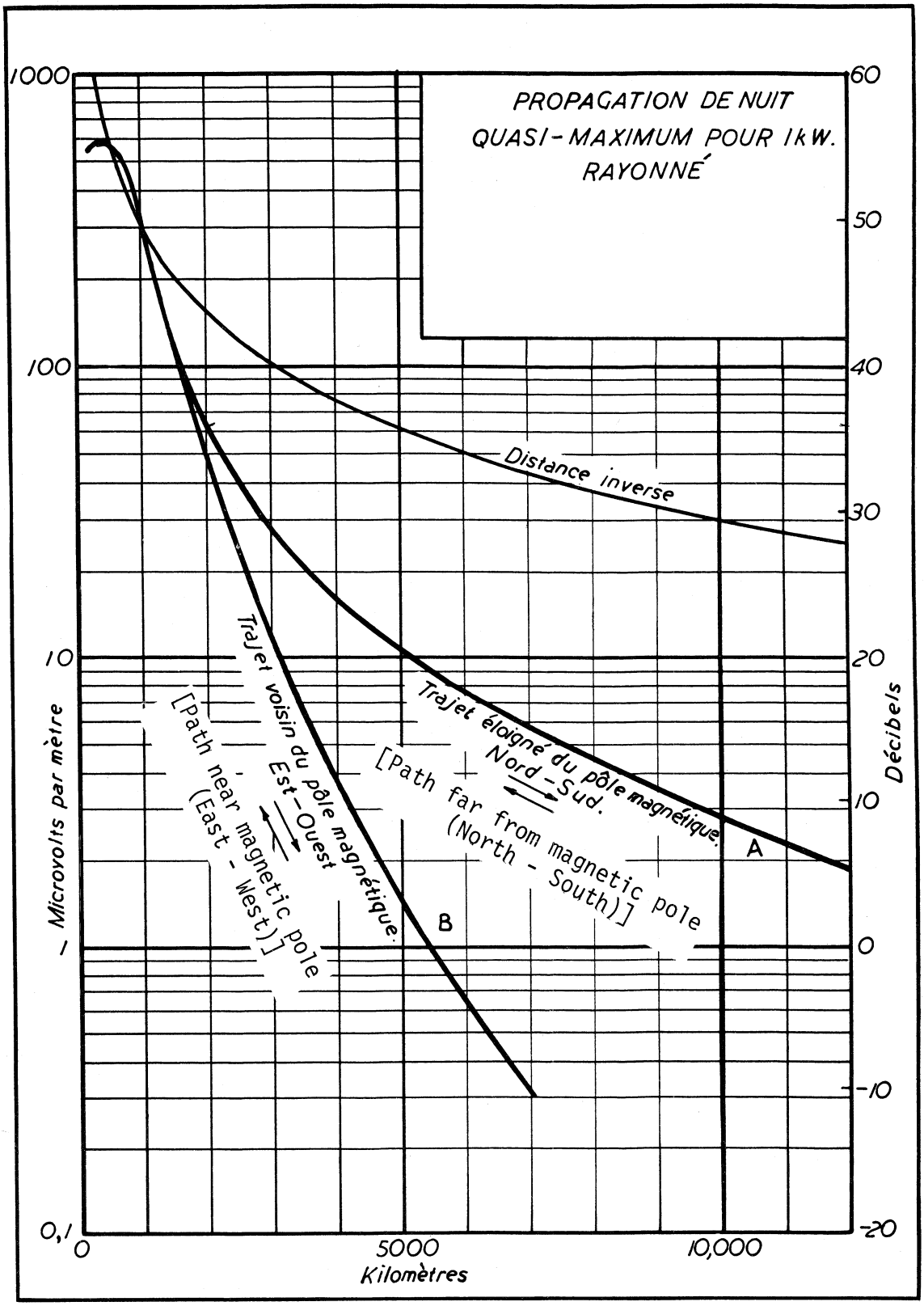

Figure 1. Quasi-maximum field intensity at great distances for propagation at night for a radiated power of 1 kW.

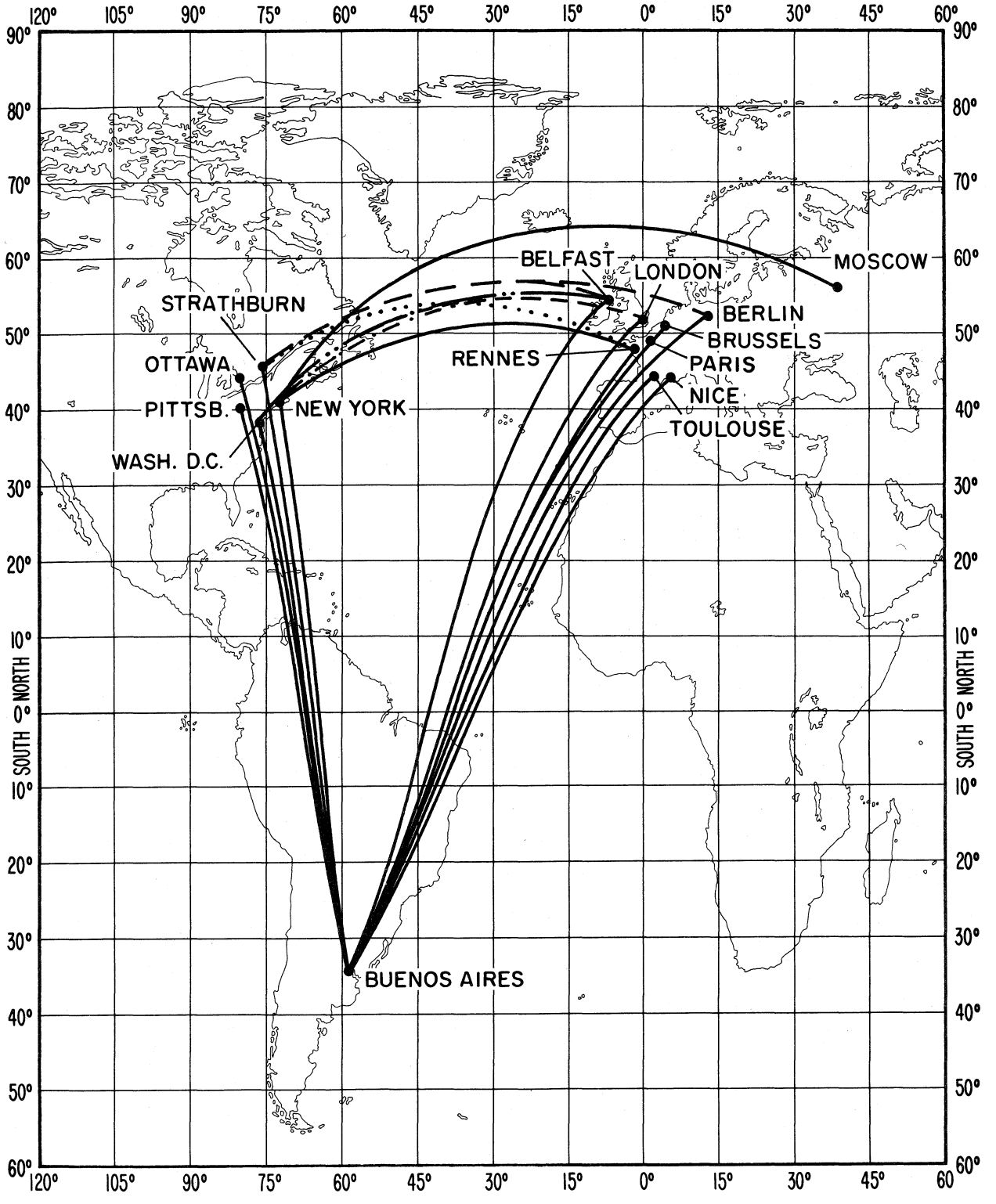

Figure 2. Propagation paths for which MF field strengths were measured during the three campaigns conducted by the International Broadcasting Union, 1934-37.

with the median being about .35 of this quasi-maximum value. Subsequently, CCIR reduced these curves by 9 dB to approximate a median value (CCIR, 1978). These curves were presumably used by the IFRB as a Technical Standard (A6) to determine service areas and interference; by 1956, the IFRB had requested CCIR to revise the Cairo Curves. At this time, new measurements made by the EBU (see Section 3.4 below) showed good agreement with the Cairo Curves out to 2000 km. It was noted that the slope of the Cairo Curves beyond that distance was independent of frequency, geographic location, and solar activity.

3.2 The FCC Curves

There are two sets of FCC curves for sky-wave propagation. The first set, shown in Figure 3, was based on recordings on 500 transmission paths at frequencies ranging from 640 to 1190 kHz and distances of 160 to 4000 km, during February, March, and April 1935, a relatively low solar activity period. The data have been normalized to an equivalent transmitting antenna radiating 160.9 μV/m at 1 km at the vertical angle corresponding to one ionospheric reflection (Barghausen, 1966).

The FCC conducted an extensive measurement campaign in the U.S. and Canada extending from 1939 to 1944. Recordings were made on 23 paths ranging from 400 to 3500 km and transmitting on frequencies ranging from 540 to 1500 kHz. All measurements were made two hours after sunset at the western end of the path. The 1935 measurements were made two hours after the occurrence of darkness on the entire path. As the FCC was primarily interested in engineering standards for frequency assignments, they used only the data for 1944 for the second set of curves (Figure 4). Minimum solar activity occurred in that year and, therefore, presented the highest sky-wave field strengths and represented the worst case for determining service areas and interference. These measurements were made at somewhat higher latitudes than the first set of measurements.

Both sets of curves are contained in the FCC Rules and Regulations (FCC, 1976) and include curves of the field strengths exceeded 10 and 50% of the year or the period of observation, up to distances of 4300 km for the 1935 curves and about 4000 km for the 1944 curves. The 1944 curves are presented as a function of geographic latitude and are used by the FCC for determining frequency assignments for domestic non-clear-channel broadcasting stations. The 1935 curves are used for determining frequency assignments for inter-regional clear-channel broadcasting stations and were adopted by treaty in 1960 by Canada, Cuba, the Dominican Republic, and the Bahama Islands and, at the same time, by Mexico in a separate treaty.

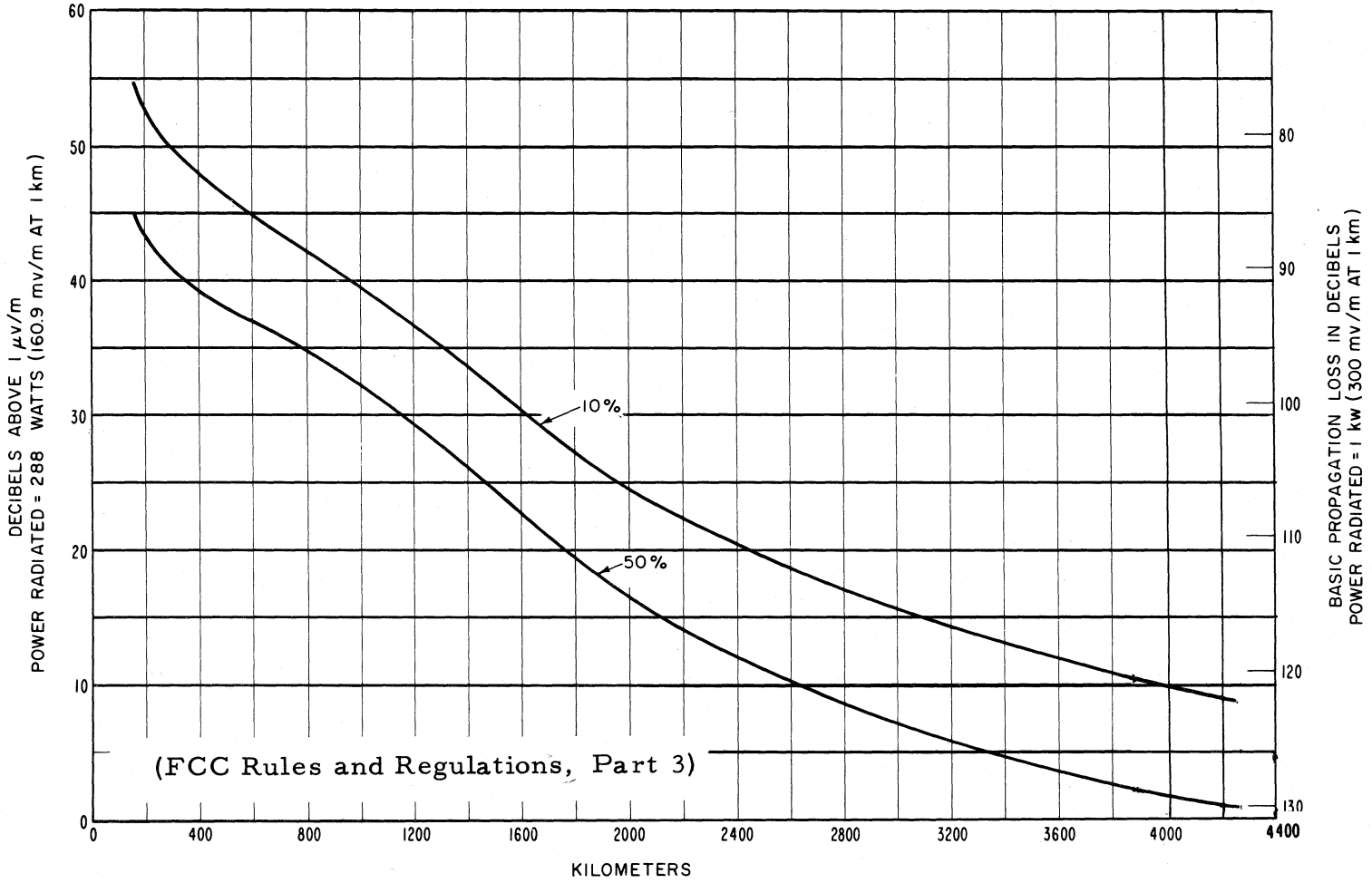

Figure 3. U.S. sky-wave field strength exceeded 10 percent and 50 percent of the time at 1000 kHz. Based on 1935 measurements, vertical polarization, and second hour after sunset at west end of path (Barghausen, 1966).

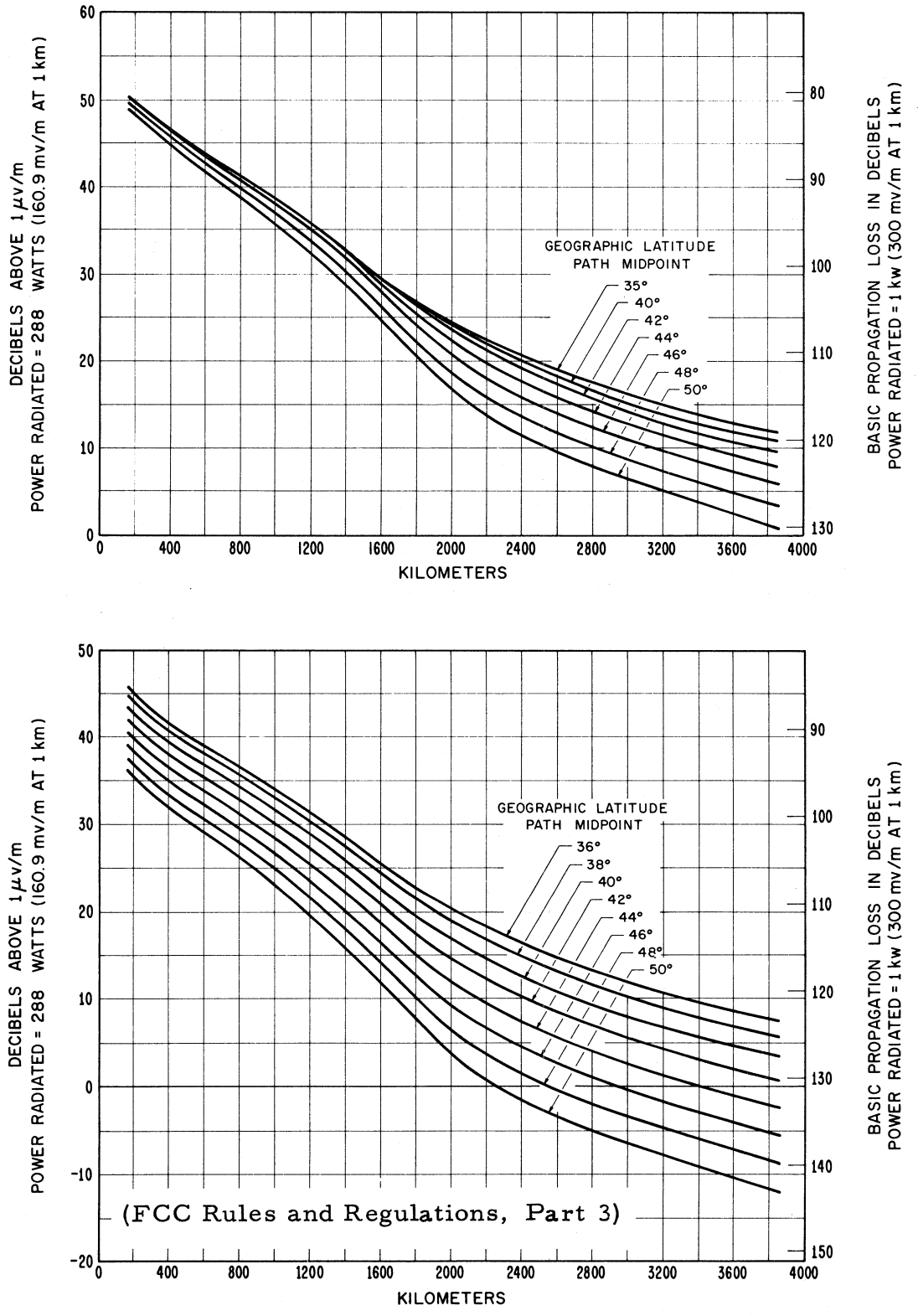

Figure 4. U.S. sky-wave field strength exceeded 10 percent (upper curve) and 50 percent (lower curve) of the time at 1000 kHz. Based on 1944 measurements, vertical polarization, and second hour after sunset at path midpoint (Barghausen, 1966).

3.3 Norton Method

As mentioned before, this is a physical model for MF sky-wave propagation and separates the transmission from transmitter to receiver into parts, analogous to a wavehop treatment. The formula for estimating the basic propagation loss in dB for 1 kW of effective radiated power, assuming a short vertical dipole antenna above a perfectly conducting plane earth and corresponding to a field strength of 300 μV/m at 1 km, is given by Rice et al. (1965) as:

$$L_{pb} = 139.37 - L_{rt} + G_t - G_{pt}(\hat{r}_1) + 20 \log_{10} f_M - E_{1(kW)} \quad dB$$

where

L_{pb} is basic propagation loss, dB,

L_{rt} is the ratio in dB of the transmitting antenna resistance to the radiation resistance of this antenna in free space (3.01 dB),

G_t is the free-space gain of a short vertical dipole transmitting antenna (1.76 dB),

$G_{pt}(\hat{r}_1)$ is the principal polarization directive gain of a short vertical dipole over a half-wave dipole (also 1.76 dB in free space),

r is the resistance of the antenna,

$\hat{r}_1$ is the direction of the most important propagation path from the transmitter to the receiver,

and

f_M is the operating frequency in MHz.

In Norton's method, for hops with one ionospheric reflection,

$$L_{pb} = L_{pbf} + A_t(\psi) + A_r(\psi) + [P + A(\phi,0.5)] - C_1 \quad dB$$

where $A(\psi)$ represents the antenna radiation loss factors for transmitter and receiver for the angle of elevation, ψ (Norton, 1959, Figures 23 and 24), P is the polarization loss, $A(\phi,0.5)$ is the absorption loss exceeded 50% of the time, C_1 is the additional gain due to the focusing of the energy on reflection of the curved surface of the ionosphere for one hop, and

$$L_{pbf} = 32.45 + 20 \log f + 20 \log d \quad dB$$

where

L_{pbf} is the basic free-space transmission loss,

f is in MHz, and d = distance in km.

The expression [P + A(ϕ,0.5)] has been evaluated empirically from measurements at low frequencies between stations in England, Scandinavia, and Germany, and for standard broadcast frequencies in the United States, and results in an increasing sky-wave field strength with increasing frequencies.

The following formula can be used to calculate the basic propagation loss involving more than one ionospheric reflection, m, and a ray path of length, d:

$$L_{pb} = L_{pbf} + A_t(\psi) + A_r(\psi) + (m-1)A_g(\psi) - C_m(d,0.5) + m[P+A(\phi,0.5)] \text{ dB}$$

where the factor $(m-1)A_g(\psi)$ allows for the ground reflection loss.

For a more detailed discussion of this method, refer to Norton (1959), and Barghausen (1966).

3.4 EBU method

The EBU initiated a measurement campaign in 1952 in response to the IFRB's question concerning the adequacy of the Cairo Curves. Recordings were made of MF field strengths from: Allouis, France, (164 kHz); Rome, Italy, (845 kHz); Horby, Sweden, (1178 kHz); and Monte Carlo, Monaco, (1466 kHz) over approximately 50 transmission paths from October 1952 until December 1960 (Ebert, 1962). From measurements made throughout the night, they were able to establish an empirical formula for the diurnal variation of the nighttime sky-wave field strength relative to local midnight at the path midpoint which was set as the reference hour. Empirical relationships also were derived for including the effects of solar activity, the influence of the magnetic field, the antenna gain as a function of the propagation distance, and a frequency dependence. The final form of the EBU method (CCIR, 1978) for determining the annual median field strength, at the reference time, for a small loop receiving antenna is:

$$F = F_0 + P + \Delta_A \quad (\text{dB}\mu\text{V/m})$$

where F_0 is the annual median field strength for the reference hour and a specified ground conductivity, in terms of an effective monopole radiated power (e.m.r.p.) of 1 kW or a cymomotive force (c.m.f.) of 300 V; P is the correction for power actually fed to the antenna; and Δ_A is the correction accounting for the gain of the transmitting antenna in the direction of propagation and covers both the horizontal and vertical radiation pattern.

The value of F_0 is given by:

$$F_0 = 80.2 - 10 \log d - 0.0018f^{0.26}d + \Delta_I - 0.02R \quad \text{dB}(\mu\text{V/m})$$

where

d is the distance measured along the great circle path (km);

f is the frequency (kHz);

Δ_I is the correction to take account of magnetic dip I;

R is the 12-month smoothed Zurich sunspot number.

This method is considered valid under the following conditions:

1) reflection assumed to be from the E region at a virtual height of 100 km above a spherical earth;

2) distances, d, are between 300 and 3500 km.

As mentioned before, the Federal Republic of Germany derived a formula for calculating F_0 for distances under 300 km, and it is included as part of the EBU method. This formula is:

$$F_0 = 60.6 - \left[10 \log \left(1 + 1.0175 \left(\frac{d}{200}\right)^2\right)\right] - 0.54f^{0.26} \quad dB(\mu V/m).$$

Note that both of these empirical formulas indicate decreasing sky-wave field strengths with increasing frequency.

3.5 Barghausen Method

This prediction technique (Barghausen, 1966) is similar to that of Norton (1959) except that in addition to Norton's semi-empirical formula for polarization and absorption losses, Barghausen included the results of measurements of reflection coefficients as a function of frequency for vertical-incidence soundings in South-West Africa (Elling, 1961). These observations showed a greater frequency dependence than those of Norton and also indicated that the sky-wave field strength may increase with frequency. Median sky-wave transmission curves vs. distance were calculated for only one-hop distances and for E-region reflection at 110 km.

3.6 Revision of EBU Method for the African LF/MF Broadcasting Conference

The CCIR IWP 6/4 developed a set of basic curves for determining the annual median field strength, F_0, for this region. These were based on the EBU formula and extrapolated to 6000 km. Further corrections were made to the EBU curves for distances below 750 km. Also, an antenna correction factor for distances up to 300 km was included.

3.7 Olver Method

This method (Olver et al., 1971) uses a wavehop approach and estimates losses due to all the ionospheric and terrestrial factors that affect a radio

wave as it propagates from a transmitter to a receiver. The method requires a model of the electron density profile for a ray trace procedure. As ray tracing is very time consuming and expensive, this method is not considered to be useful for practical applications.

3.8 Knight Method

The Olver et al. method was adopted for manual applications by providing graphs and curves for determining the number of hops, ground loss at transmitter and receiver, polarization coupling loss at transmitter and receiver, ionospheric loss, intermediate reflection loss, and transmitting antenna correction for two or more propagation modes (Knight, 1973). The EBU (CCIR, 1970-1974a, unpublished paper) tested this method for 152 paths. For paths less than 3000 km, 84% of the differences between predicted and measured field strengths are less than 10 dB, and for longer paths, 66% of the differences are in this range. Again, the wavehop method tended to be laborious and time consuming, particularly for long-distance paths. The main source of errors was found to be insufficient knowledge about the variation of ionospheric absorption with latitude and solar activity, and uncertainties about ground conductivity.

3.9 The CCIR Geneva 1974 Methods

3.9.1 U.S.S.R method

Using measured annual median field strengths at local midnight at the path midpoint for 87 paths of different lengths at different latitudes and 14 frequencies between 200 and 1500 kHz, the U.S.S.R. derived an empirical formula which gives the dependence of field strength on distance and frequency as a function of geomagnetic latitude as follows (CCIR, 1970-74b, unpublished paper).

$$F_0 = 105.3 - 20 \log d - .0019\, f^{0.15} d$$
$$- 0.0024\, f^{0.4} d\, (\tan^2 \phi - \tan^2 37^\circ) \quad \text{dB}(\mu\text{V/m})$$

where

F_0 is the annual median of half-hourly median field strengths (dB above 1 μV/m) at the reference time of six hours after ground sunset at the path midpoint or for paths >2000 km, 750 km from the terminal where the sun sets last;

d is ground distance (km);

f is frequency (kHz);

ϕ is geomagnetic (dipole) latitude at path midpoint.

This formula is considered valid for values of ϕ between 37° and 60°; note that it includes two frequency-dependence terms.

3.9.2 U.K. method

The U.K., recognizing that Knight's method was not sufficiently simple, proposed a semiempirical method based on physical principles, but containing coefficients derived from measured field strengths (CCIR, 1970-74c, unpublished paper). The formula is as follows:

$$F_0 = 105 - 20 \log p - 10^{-3} k_R p - L_p \quad dB(\mu V/m)$$

where

F_0 is as defined in Section 3.9.1;

p is slant-propagation distance;

k is a basic loss factor = $3.3[1+2 \sin^4(1.34\phi)]$, where ϕ is the geomagnetic (dipole) latitude at path midpoint(s);

$k_R = k + 10^{-2} bR$, where b = solar activity factor (see Appendix A, Section 2.6) and R is the 12-month smoothed Zurich sunspot number; and

L_p is polarization loss (see Appendix A, Section 2.4).

This method applies to the MF broadcasting bands for paths up to 12000 km worldwide (except auroral zones), but shows no frequency dependence. It includes corrections for terminals located near the sea (sea gain), geomagnetic (dipole) latitude, polarization coupling loss, solar activity, and hourly variation.

3.9.3 Modified U.S.S.R.

The CCIR IWP 6/4, in preparation for the XIIIth Plenary Assembly, Geneva, 1974, considered the above prediction methods and determined that the U.S.S.R. method could be extended to distances less than 300 km and to other regions by making the following modifications:

a. replace ground distance d by slant propagation distance p,

b. add U.K. correction for sea-gain where applicable,

c. apply U.K. correction for polarization-coupling loss in tropical regions,

d. divide paths longer than 3000 km into two equal sections, calculate loss factors separately for each section, and average the two - same as the U.K. method.

This sky-wave field strength prediction method recommended for provisional use by CCIR, Geneva, 1974, but subsequently replaced by CCIR 1978, is presented in Appendix A.

3.10 Wang 1977 Method

This was proposed as an alternative method for the United States of America (Wang, 1977). The basic formula is:

$$F_o = 102.8 - 20 \log p - L_I - L_R \quad dB(\mu V/m)$$

where

F_o is the annual median field strengths (dB above 1 μV/m) for two hours after sunset at path midpoint,

p is slant propagation distance in km,

L_I is ionospheric loss (including other miscellaneous losses),

L_R is ionospheric loss due to solar activity,

and

$$L_R = \left[(\phi_M - 42) - 0.3\left(\frac{f-500}{100}\right)\right] + 10 \log \left(\frac{p}{1000}\right) 0.01R \quad ,$$

$$L_I = bp \times 10^{-3} \quad ; \quad b = (\phi_M - 40) - 0.3\left(\frac{f-500}{100}\right) \quad ,$$

where f is frequency in kHz, R is the 12-month smoothed Zurich sunspot number, b is a solar activity dependence factor, and ϕ_M is the geomagnetic (dipole) latitude at the path midpoint.

Since the North American measurements were made at two hours after sunset, the equivalent formula for F_o for the reference hour of local midnight at the path midpoint is:

$$F = 105.3 - 20 \log - bp \times 10^{-3} - b - 2 + 10 \log \left(\frac{P}{1000}\right) R \quad dB(\mu V/m) \, .$$

The upper limit for b is 12 units, and the lower limit is such that neither L_I nor L_R can be negative.

3.11 The CCIR Kyoto 1978 Method

The current recommended CCIR (Recommendation 435-3) sky-wave field strength prediction method is:

$$F_o = 106.6 - 2 \sin \phi - 20 \log p - 10^{-3} k_R p - L_p + G_s \quad dB(\mu V/m)$$

where

F_o is the annual median field strength (dB above μV/m) at the reference time defined in Appendix B, Section 2.1;

ϕ is a geomagnetic (dipole) latitude parameter;

p is slant propagation distance in km;

k is a basic loss factor;

K_R is a loss factor dependent on R, the 12-month smoothed Zurich sunspot number;

L_p is the excess polarization-coupling loss (dB); and

G_s is the sea gain correction (dB).

The loss factor, $k_R = k + 10^{-2}bR$, where $k = 3.2 + 0.19f^{0.4} \tan^2(\phi + 3)$, f is frequency in kHz, and b, a solar activity dependence factor, is 4 for North American paths, 1 for Europe and Australia, and 0 elsewhere.

The complete prediction method is presented in Appendix B. Section 6, Appendix B contains a caution on the accuracy of the method when applied to the United States of America.

3.12 The Wang 1979 Method

This is a proposed modification of the recommended CCIR 1978 prediction method given in Section 3.11. Wang suggested that the basic loss factor, k, be changed to

$$k = (0.0667\ |\phi| + 0.2) + 3 \tan^2(\phi + 3). \qquad (0 \leq \phi \leq 60°)$$

This improves the accuracy in high- and low-latitude areas without affecting the prediction in average-latitude areas and assumes f = 1000 kHz, i.e., no frequency dependence is needed. The other change relates to the solar activity dependence factor, b. The CCIR recommends setting b = 4 for North America and b = 0 for South America. Wang proposed the following formula:

$$b = 0.4\ |\phi| - 16 \qquad \text{for } |\phi| \geq 45^o$$
$$b = 0.0 \qquad \text{for } |\phi| < 45^o \ .$$

4. COMPARISON OF PREDICTION METHODS

4.1 General Comparison

A study has been conducted of some of the above sky-wave field strength prediction methods to assess the compatibility and/or variability of the different methods. For this comparison, only the very long paths (>4700 km) for which measured field strengths are available were considered. A total of 46 paths met this criteria, and 36 of these paths were selected for this comparison. In selecting the 36 paths, preference was given to those having at least one terminal in either North, Central, or South America. Twenty-two of the paths are in this category, and the remaining 14 paths are representative of regions other than Region 2. Measurements for 18 of these paths were used

to develop the Cairo Curves, and the measurements from most of the 36 paths were probably used to derive the various CCIR methods. The location of the transmitter and receiver, frequency, and great circle distances are given in Table 1.

Only three of the described prediction methods were considered applicable to all of these paths: 1) Cairo Curves, 2) CCIR 1974 method (modified U.S.S.R.), and 3) CCIR 1978. The FCC 1935 Curves are considered valid only within Region 2 and for distances <4300 km; the EBU method is considered valid only for the European Broadcasting Area; Wang's 1979 method is applicable only in Region 2; Barghausen's method was presented only for one-hop reflection; and the Olver et al. and Knight methods were not included because of their complexity and lack of information on certain variables, e.g., electron density profile of the lower ionosphere.

In this analysis, the following conditions were established for both the CCIR methods and for the Wang 1979 method:

F_0 is the annual median of half-hourly median field strengths [dB(μV/m)] for an effective monopole radiated power (e.m.r.p.) of 1 kW, equivalent to a cymomotive force (c.m.f.) of 300 V, relative to local midnight at the path midpoint(s). Average ground conductivity is assumed, typically 3 to 10 mS/m; and the antennas are assumed to be omnidirectional short verticals, therefore, G_V and G_H = 0.

The resulting sky-wave field strength predictions for the three methods for each of the 36 paths are given in Table 2. The Cairo Curve predicted field strengths have been determined using the North-South Curve as well as the East-West Curve, which is applicable only when the propagation path is near the magnetic pole. Both predicted values are shown in Table 2. The predicted field strengths for the Cairo method are shown without and with a correction term for polarization coupling loss (L_p) as suggested by Phillips and Knight (1965) and Barghausen (1966). The inclusion of L_p for MF propagation in the east-west or west-east direction at low latitudes reduces the field strength by about 2 to 6 dB for paths between the Mideast or Asia and Australia (13, 17, 21, and 31). The regional Administrative LF/MF Broadcasting Conference (ITU, 1975) recommended that the Cairo North-South Curve, with a modification for L_p, be used to predict MF field strengths for the Asian part of Region 3, North of 11°S. In this analysis, the modification for L_p has been applied to all the Cairo North-South Curve predicted MF field strengths on the assumption that this correction should be valid everywhere.

Table 1. List of Propagation Paths

PATH NUMBER	TRANSMITTER	RECEIVER	GEOGRAPHIC COORDINATES TRANSMITTER		RECEIVER		FREQUENCY	GREAT CIRCLE DISTANCE (km)
1	Northern Ireland	Ottawa, Canada	5.0°N	7.0°W	45.4°N	75.7°W	977	4797
2	Sackville, Canada	Chatonnaye, France	45.9°N	64.3°W	46.7°N	6.8°E	1070	5272
3	Moncton, Canada	Chatonnaye, France	46.1°N	64.8°W	46.7°N	6.8°E	1070	5298
4	Northern Ireland	Washington, D. C.	55.0°N	7.0°W	39.0°N	77.0°W	977	5346
5	Rennes, France	Ottawa, Canada	48.0°N	1.7°W	45.4°N	75.7°W	1040	5426
6	Rennes, France	New York City, N.Y.	48.0°N	1.7°W	41.0°N	74.0°W	1040	5573
7	Masirah Island, Oman	Leucate, France	20.5°N	58.8°E	42.9°N	3.0°E	1410	5706
8	New York City, N.Y.	Brussels, Belgium	40.9°N	72.7°W	50.8°N	4.4°E	860	5791
9	New York City, N.Y.	Eindhoven, Netherlands	40.9°N	72.7°W	51.4°N	5.5°E	860	5839
10	Masirah Island, Oman	Limours, France	20.5°N	58.8°E	48.7°N	2.1°E	1410	5884
11	Akita, Japan	Darwin, Australia	39.8°N	139.9PE	12.5°S	130.7°E	770	5885
12	Rennes, France	Washington, D. C.	48.0°N	1.7°W	39.0°N	77.0°W	1040	5910
13	Singapore, Malaysia	Brisbane, Australia	1.4°N	103.9°E	27.5°S	152.0°E	790	6055
14	New York City, N.Y.	Berlin, Germany	40.9°N	72.7°W	52.5°W	13.4°E	860	6287
15	Rome, Italy	Tsumeb, S.W. Africa	41.9°N	12.5°E	19.2°S	17.7°E	845	6795
16	Fort-de-France, West Indies	Jurbise, Belgium	14.6°N	61.1°W	50.5°N	3.9°E	1310	7001
17	Ban Phaci, Thailand	Brisbane, Australia	13.7°N	100.5°E	27.5°S	153.0°E	1580	7198
18	M. Ismaning, Germany	Tsumeb, S.W. Africa	48.2°N	11.8°E	19.2°S	17.7°E	1602	7526
19	Akita, Japan	Brisbane, Australia	39.8°N	139.9°E	27.5°S	152.0°E	770	7584
20	Bangkok, Thailand	Helsinki, Finland	13.7°N	100.5°E	60.2°N	25.1°E	1580	7882
21	Cairo, Egypt	Klang, Malaysia	29.9°N	31.7°E	3.1°N	101.4°E	620	7886
22	Rome, Italy	St. Denis, Reunion	41.7°N	12.6°E	20.9°S	55.5°E	845	8240
23	Buenos Aires, Argentina	Washington, D.C.	34.4°S	58.6°W	39.0°N	77.0°W	1070	8383
24	New York City, N.Y.	Buenos Aires, Argentina	40.9°N	72.7°W	34.6°S	58.5°W	860	8518
25	Buenos Aires, Argentina	New York City, N.Y.	34.4°S	58.6°W	41.0°N	74.0°W	1070	8536
26	Pittsburgh, Pennsylvania	Buenos Aires, Argentina	40.4°N	80.0°W	34.6°S	58.5°W	980	8622
27	Akita, Japan	Melbourne, Australia	39.8°N	139.9°E	37.8°S	145.1°E	770	8644
28	Poro, Phillippines	Helsinki, Finland	15.8°N	120.6°E	60.2°N	25.1°E	1140	8791
29	Buenos Aires, Argentina	Ottawa, Canada	34.4°S	58.6°N	45.4°N	75.7°W	1070	9043
30	Swan Island, Caribbean	Helsinki, Finland	17.4°N	83.9°W	60.2°N	25.1°E	1157	9333
31	Kuwait, Kuwait	Darwin, Australia	29.2°N	48.0°E	12.5°S	130.7°E	1345	9986
32	Rennes, France	Buenos Aires, Argentina	48.0°N	1.7°W	34.6°S	58.5°W	1040	10786
33	Buenos Aires, Argentina	London, England	34.4°S	58.6°W	51.5°N	0.2°W	1070	11127
34	Buenos Aires, Argentina	Brussels, Belgium	34.4°S	58.6°W	50.8°N	4.4°E	1070	11298
35	Buenos Aires, Argentina	Eindhoven, Netherlands	34.4°S	58.6°W	51.4°N	5.5°E	1070	11400
36	Buenos Aires, Argentina	Berlin, Germany	34.4°S	58.6°W	52.5°N	13.4°E	1070	11903

Table 2. Comparison of MF Field Strengths (F_o in dB relative to 1 μV/m) Predicted by Different Methods for R=0

Path Number	Frequency kHz	GCD km	Cairo E-W	Cairo N-S	Cairo -Lp	CCIR 1974 Without G_s	CCIR 1974 With G_s	CCIR 1978 Without G_s	CCIR 1978 With G_s
1	977	4797	-3.8	12.3		-29.3		-30.0	
2	1070	5272	-7.6	11.2		-22.2	-18.8	-22.2	-17.8
3	1070	5298	-7.7	11.0		-22.7	-20.6	-22.7	-19.4
4	977	5346	-8.0	10.8		-26.8		-26.9	
5	1040	5426	-9.0	10.6		-26.6		-26.6	
6	1040	5573	-9.8	10.0		-22.2	-20.0	-22.0	-18.5
7	1410	5706		9.6	7.9	1.4	17.8	1.5	16.9
8	860	5791	-11.5	9.4		-23.7	-14.8	-23.5	-14.5
9	860	5839	-11.7	9.3		-24.7	-15.8	-24.5	-15.5
10	1410	5884		9.2	7.9	-2.3	6.6	-2.2	4.9
11	770	5885		9.2	9.3	9.9	17.9	11.2	15.4
12	1040	5910	-12.1	9.1		-23.2		-22.9	
13	790	6055		8.9	6.3	3.5	12.4	7.3	16.4
14	860	6287	-14.4	8.3		-28.8	-19.3	-28.5	-18.9
15	845	6795		7.0		3.7	9.3	4.6	11.0
16	1310	7001		6.6		-15.6	-11.3	-15.3	-9.9
17	1580	7198		6.2	3.8	-1.1	7.5	2.1	11.0
18	1602	7526		5.2		-2.6		-2.2	
19	770	7584		5.0		1.1		3.1	
20	1580	7882		4.6	3.6	-16.3	-7.7	-16.2	-7.3
21	620	7886		4.6	-.9	-4.8	5.0	-4.0	5.8
22	845	8240		3.7		-3.0	6.3	-1.8	7.6
23	1070	8383		3.4	3.2	-6.6		-5.7	
24	860	8518		3.1	3.0	-7.4	0.3	-6.5	1.7
25	1070	8536		2.9	2.8	-8.1	-0.9	-7.2	0.6
26	980	8622		2.7	2.5	-8.1		-7.2	
27	770	8644		2.6		-5.7		-2.7	
28	1140	8791		2.3	1.5	-20.8	-11.8	-20.5	-9.1
29	1070	9043		1.8	1.7	-12.8		-11.9	
30	1157	9333		1.4		-40.6	-31.6	-40.2	-31.1
31	1345	9986		0.4	-3.3	-11.9	5.7	-10.7	7.4
32	1040	10774		-1.3	-2.1	-19.1	-10.9	-18.2	-12.2
33	1070	11127		-1.8	-2.5	-25.0	-15.9	-24.0	-17.7
34	1070	11298		-2.3	-3.1	-22.5	-13.4	-21.6	-15.3
35	1070	11400		-2.5	-3.3	-23.2	-14.1	-22.3	-16.0
36	1070	11903		-3.2	-4.1	-25.4	-16.3	-24.5	-18.2

Both of the CCIR methods include an explicit expression for determining the additional gain (G_s) when one or both of the terminals are located near sea water. The predicted field strengths for these methods are calculated without the sea gain and with the sea gain when applicable. When sea gain is not included, the minimum difference between the three predictions is about 2 dB, the maximum is about 42 dB, and the median difference is 12 dB. When sea gain is included, the minimum difference between predictions is 3 dB, but the maximum difference is 33 dB, and the median difference is about 10 dB. Even though the addition of sea gain reduces the differences in the field strength predictions somewhat, the median difference of 10 dB would still suggest that the Cairo predictions are not compatible with the CCIR predictions.

4.2 Sea Gain Effect

The increase in field strength which occurs when the antenna is radiating over open sea is treated as an additional gain in the various CCIR methods. In the physical models (e.g., Norton's) the ground conductivity determines the ground losses for the antenna gain and, therefore, this so-called sea gain is included implicitly as a reduction in ground loss. The CCIR method for computing sea gain can produce significantly different answers depending on individual interpretation. For example, according to Knight (1977), the estuary of the River Plate, which is about 50 km wide, could have produced a sea gain of 6 dB at 1 MHz for long paths. However, the instructions for sea gain (see Appendix B, Section 2.3) define the distance, d, as the distance of the terminal from the sea measured along the great circle path. Clearly, for paths between Europe and Buenos Aires, the great circle path is over the estuary of the River Plate; but for the paths 23, 25, and 29 between Buenos Aires and North America this is not the case, as the location of the transmitter is northwest of Buenos Aires. Although the receiver for paths 24 and 26 was southeast of Buenos Aires, it is still questionable as to whether the great circle path is over the estuary of the River Plate. The sea gain included in the predicted field strengths for paths 24 and 25 was determined from the proximity of the northern terminals to the Atlantic Ocean.

4.3 Solar Activity Effect

In both CCIR methods, the relationship between sky-wave field strengths and solar activity is different for different geographical areas. The solar activity dependence factor, b, is 1 for Europe, Australia, and New Zealand, and 4 for North America. For the rest of the world, b = 0; e.g., solar activity

has no effect! In Wang's 1979 modification, for the Americas, the effect of solar activity is included only if the midpoint of the path or half-path is $\geq 45°$. Using these restrictions, the predicted field strengths for only 15 of these 36 paths would be affected by a change in solar activity.

The predicted field strengths for these 15 paths for two levels of solar activity, R = 0 and 100, for both CCIR methods and the Wang 1979 method (where applicable) are given in Table 3. For this comparison, the paths have been ordered according to the geomagnetic latitudes at the midpoint of each half-path (see Appendix A, Section 2.6). In Table 3, the second column indicates the value of b used to determine k_R for each half-path, and the next two columns give the geomagnetic latitude of the midpoint of each half-path. For the CCIR methods, the solar activity effect on the predicted field strengths is primarily dependent on path length. For the paths where b is either 1 or 4, the decrease in the predicted field strengths from solar minimum to solar maximum is 12 dB for path 1, 4797 km, and 16 dB for path 14, 6287 km. For the paths where there is a solar activity effect at only the midpoint of the half-path closest to the receiver, the decrease with solar activity is 3 dB for path 13, 6055 km, and 4.4 dB for path 27, 8644 km. However, in the Wang 1979 method, the predicted field strength is more dependent on geomagnetic latitude than path length. Because of this dependence, the predicted field strength decreases about 34 dB for path 1 from solar minimum to solar maximum; and as the geomagnetic latitude decreases, the predicted field strengths decrease with increasing solar activity but at a slower rate. In other methods, the effect of solar activity is implicit in the ionospheric loss models used; in these methods, the ionospheric loss is a function of geomagnetic latitude, path length, and frequency.

4.4 Comparison of Predicted Field Strengths with Measured Field Strengths

A comparison of measured field strengths with predicted field strengths for different levels of solar activity is shown in Table 4. The first column indicates the measured field strengths either provided to or compiled by the CCIR IWP 6/4 for 35 of the 36 paths. The measured field strengths for paths 6, 9, and 14 for R = 20 and for path 9 for R = 100 were extracted from CCIR (1937).

The paths have been grouped according to regions or geographical areas. In the first three groups, at least one of the terminals is located in Region 2. With the exception of paths 2, 3, 16, and 30, the measured field

Table 3. Comparison of Predicted Field Strengths for Different Solar Activity Levels (without sea gain) (F_o in dB relative to 1 μV/m)

Path Number	b T,R	Geom. Lat. Half-Path Midpoints Xmitter	Receiver	Path Length (km)	Frequency (kHz)	CCIR 1974 R=0	R=100	Predicted Decrease	CCIR 1978 R=0	R=100	Predicted Decrease	Wang 1979 R=0	R=100	Predicted Decrease
1	1,4	58.3	57.3	4797	977	-29.3	-41.3	12.0	-30.0	-42.0	12.0	-34.4	-68.5	34.1
4	1,4	56.7	52.5	5346	977	-26.8	-40.2	13.4	-26.9	-40.3	13.4	-30.6	-61.8	31.2
5	1,4	52.6	55.4	5426	1040	-26.6	-40.2	13.6	-26.6	-40.2	13.6	-29.1	-59.5	30.2
3	4,4	55.2	50.5	5298	1070	-22.7	-36.0	13.3	-22.7	-36.0	13.3	-24.4	-51.6	27.2
2	4,1	55.1	50.5	5272	1070	-22.2	-35.4	13.2	-22.1	-35.3	13.2	-23.8	-50.7	26.9
9	4,1	52.5	52.8	5839	860	-24.7	-39.3	14.6	-24.5	-39.1	14.6	-29.6	-59.1	29.5
8	4,1	52.4	52.5	5791	860	-23.7	-38.2	14.5	-23.5	-38.0	14.5	-28.4	-57.4	29.0
14	4,1	52.4	52.4	6287	860	-28.8	-44.5	15.7	-28.5	-44.3	15.8	-33.8	-65.0	31.2
6	1,4	51.5	52.1	5573	1040	-22.2	-36.1	13.9	-22.0	-35.9	13.9	-23.9	-50.2	26.3
12	1,4	51.0	50.6	5910	1040	-23.2	-38.0	14.8	-22.9	-37.7	14.8	-24.6	-50.0	25.4
30	0,1	35.7	50.2	9333	1157	-40.6	-45.2	4.6	-40.2	-44.8	4.6	-36.7	-55.7	19.0
16	0,1	32.6	45.8	7001	1310	-15.6	-19.1	3.5	-15.3	-18.8	3.5	-10.4	-18.5	8.1
17	0,1	-7.2	-26.2	7198	1580	-1.1	-4.7	3.6	2.1	-1.4	3.5	NA	NA	---
27	0,1	10.4	-27.8	8644	770	-5.7	-10.1	4.4	-2.7	-7.0	4.3	NA	NA	---
13	0,1	-16.5	-29.4	6055	790	3.5	0.5	3.0	7.3	4.2	3.1	NA	NA	---

Table 4. Comparison of Measured Field Strengths with Predicted Field Strengths (F_o in dB relative to 1 μV/m)

Path Number	Observation	R	Cairo Curves	Cairo Curves $-L_p$	CCIR 1974	CCIR 1978	WANG 1979
1. North America to Europe							
1	-14.1	100	-3.8		-41.3	-42.0	-68.5
2	2.6	0	-7.6		-18.8*	-17.8*	-20.4*
3	0.0	0	-7.7		-20.6*	-19.4*	-22.3*
4	-18.2	100	-8.0		-40.2	-40.3	-61.8
5	-13.5	100	-9.0		-40.2	-40.2	-59.5
6	-9.0	20	-9.8		-22.8*	-21.3*	-23.9*
6	-21.0	100	-9.8		-33.7*	-32.4*	-48.0*
8	-17.0	100	-11.5		-29.3*	-29.0*	-48.5*
9	-13.6	20	-11.7		-18.7*	-18.4*	-26.6*
9	-15.1	100	-11.7		-30.4*	-30.1*	-50.2*
12	-18.5	100	-12.1		-38.0	-37.7	-50.0
14	-19.5	20	-14.4		-22.4*	-22.1*	-30.6*
14	-31.0	100	-14.4		-35.0*	-34.7*	-55.5*
RMS Error			8.4		17.5	17.2	31.7
2. North America to S. America							
23	2.0	0	3.4	3.2	-6.6	-5.7	9.3
24	2.0	0	3.1	3.0	0.3*	1.7*	15.6*
25	-2.0	0	2.9	2.8	-0.9*	0.6*	15.0*
26	2.0	0	2.7	2.5	-8.1	-7.2	7.9
29	2.0	0	1.8	1.7	-12.8	-11.9	3.5
RMS Error			2.4	2.3	8.9	8.3	10.6
3. South and Central America to Europe							
16	0.0	0	6.6		-11.3*	-9.9*	-6.1*
30	-22.0	0	1.4		-31.6*	-31.1*	-27.7*
32	-9.9	100	-1.3	-2.1	-10.9*	-12.2*	9.1*
33	-11.5	100	-1.8	-2.5	-15.9*	-17.7*	3.8*
34	-13.5	100	-2.3	-3.1	-13.4*	-15.3*	7.4*
35	-7.5	100	-2.5	-3.3	-14.1*	-16.0*	6.8*
36	-17.0	100	-3.2	-4.1	-16.3*	-18.2*	5.6*
RMS Error			12.5	12.1	6.7	7.1	16.1
4. Europe, Africa, Mideast, & Asia							
7	18.3	0	9.6	7.9	17.8*	16.9*	
10	10.8	0	9.2	7.9	6.6*	4.9*	
15	5.5	0	7.0		9.3*	11.0*	
18	-1.1	0	5.2		-2.6	-2.2	
20	-7.5	0	4.6	3.6	-7.7*	-7.3*	
22	9.8	0	3.7		6.3*	7.6*	
28	-5.2	0	2.3	1.5	-11.8*	-9.1*	
RMS Error			7.2	7.2	3.6	3.6	
5. Mideast, Asia, & Pacific							
11	17.5	0	9.2	9.3	17.9*	15.4*	
13	-1.0	0	8.9	6.3	12.4*	16.4*	
17	3.0	0	6.2	3.8	7.5*	11.0*	
19	8.5	0	5.0		1.1	3.1	
21	0.7	0	4.6	-.9	5.0*	5.8*	
27	5.0	0	2.6		-5.7	-2.7	
31	-7.0	0	0.4	-3.3	5.7*	7.4*	
RMS Error			6.0	4.7	8.9	9.9	
TOTAL RMS Error			8.2	8.0	11.7	11.7	23.4

* Includes sea gain

strengths for these paths were used to derive the Cairo Curves. As would be expected, the Cairo predicted field strength is in closer agreement with the measured field strength for 15 of the 22 observations in these three groups.

As most of the observations for the first group of paths were made during a period of either low or high solar activity, the field strengths predicted by both the CCIR and the Wang 1979 methods include the effect of solar activity. The rms error between the observed and the Cairo predicted field strengths is significantly lower for the paths in group 1 than the rms error for the other three predictions. With the exception of path 14, the Cairo method predictions for the North Atlantic paths, group 1, consistently agree better with the observations than the predictions from the other methods. For the three paths, 6, 9, and 14, for which there are observations for low and high solar activity, there appears to be a solar cycle variation in the observations for only two of the paths, 6 and 14. For path 14, either of the CCIR field strength predictions for R = 20 and 100, are in closer agreement with the observations than either the Cairo or Wang 1979 predictions. But the Cairo predictions, which do not include any solar activity effect, are closer to both observations for path 6 than the other three predictions. The only conclusion that can be made from a sample of this size is that the solar cycle effect cannot be eliminated completely as a contributing factor.

For the paths in group 2 for both CCIR methods, the solar activity factor b has been set to 0 for both half-path midpoints; and in the Wang 1979 method, the geomagnetic latitudes of the half-path midpoints are between 45°N and 45°S. Therefore, none of these predicted field strengths are affected by solar activity. All of the paths in this group were included in the measurement campaigns conducted by the IBU, and again the rms error for the Cairo predictions is significantly lower than the rms error for the other predictions. However, for the two paths that include G_S, the CCIR predictions are somewhat closer to the observations than the Cairo predictions.

The same solar activity restrictions for the paths in group 2 also apply to the paths in group 3; i.e., there is no variation with solar activity. For paths between Central-South America and Europe, the addition of sea gain in the CCIR predictions brings them into closer agreement with the observations than the Cairo predictions, with the exception of path 35. Note that the receiver for path 35 is Eindhoven, the same as for path 9, and the observations for path 9 were also inconsistent with other observations in group 1.

For the fourth group of paths from Europe to Africa, the Mideast, and Asia, the CCIR predictions, in general, are in better agreement with the observations than the Cairo predictions. Again, this is primarily due to the addition of sea gain.

The rms error for the Cairo predictions for the paths in group 5 tend to corroborate the recommendation of the 1975 Regional Administrative LF/MF Broadcasting Conference. In this limited sample, the Cairo field strength predictions with a correction for L_p for paths propagating in the west-east direction (13, 17, 21, and 31) are more compatible with the observations than the CCIR predictions. Although the addition of sea gain is applied to five of these seven paths in the CCIR methods, the CCIR field strength predictions are significantly better than the Cairo method predictions for only one of these paths (11).

When all groups are combined, the rms errors between observations and predictions given in Table 4 indicate that for this limited data sample the field strength predictions based on the Cairo Curves are in closer agreement with the observations than the other methods. However, the differences in the total rms errors are probably not statistically significant. In this analysis, the Cairo East-West Curve was used to predict MF field strengths for the North Atlantic paths in group 1. If the North-South Cairo Curve had been used to predict the field strength for the paths in this group, the corresponding rms error would have been about 26 dB. Similarly, if the variation with solar activity is eliminated in the CCIR 1974 and 1978 and the Wang 1979 predictions, the corresponding rms errors are 11.3, 10.9, and 13.0 dB, respectively. The rms error for the Cairo East-West Curve predictions is still the lowest, but the differences between the rms errors are probably not statistically significant.

There are 15 paths for which the CCIR predictions are better than the Cairo predictions, and sea gain was included in the predictions for all these paths with the exception of path 18. There is essentially no difference between the two CCIR prediction methods (see Table 3) except in the method for determining sea gain. The CCIR 1974 method for computing G_s is much simpler than the CCIR 1978 method, and based on this analysis, predicts the MF field strengths equally as well as the CCIR 1978 method.

The following three sections discuss several factors which, if explicitly taken into account in the prediction methods, might reduce some of the discrepancies between the observations and predictions.

4.4.1 Diurnal effects

The CCIR methods assume that the maximum sky-wave field strength occurs about six hours after sunset, or approximately local midnight at the midpoint(s) of the path. However, many of the measurements were not made at local midnight at the midpoint of the path, and in this case, the data were adjusted to local midnight using the hourly correction factor derived from the European measurements. To assume that this correction is valid everywhere in the world, implies that the absorption properties of the D and E regions of the ionosphere are the same everywhere.

4.4.2 Latitudinal effects

When comparing measurements made in the U.S. with those made in Europe at similar geographical latitudes, it appears that the differences in the measured field strengths are related to the earth's magnetic field. The EBU determined that for Europe there was a significant relationship between measured field strengths and magnetic inclination, but these prediction methods use geomagnetic (dipole) latitude in their empirical relationships. As the dipole latitude is an approximation of the magnetic latitude, the use of the true magnetic latitude might reduce some of the discrepancies between observations and predictions.

4.4.3 Direction of propagation and intermediate ground-reflection loss effects

None of the MF field strength prediction methods currently in use internationally take into account the possibility of nonreciprocal propagation or the intermediate ground reflection losses on multi-hop paths. Crombie (1979) has shown that, at high solar activity, the transmission loss for MF sky-wave paths in the U.S. is greater for transmissions in the east-to-west direction than for the west-to-east direction at these latitudes. The difference, which is statistically significant, is about 9 dB for frequencies between 640 and 1530 kHz. In addition to the possibility of nonreciprocal propagation, the effect of intermediate ground-reflection losses on multi-hop paths should be examined.

4.5 Comparison of Available Methods for Predicting MF Field Strengths in Region 2 (North and South America)

The previous comparisons considered primarily MF prediction methods that are considered to be valid worldwide. Because of the requirement for a reliable MF prediction model for the Regional Administrative MF Broadcasting Conference (Region 2), a separate analysis has been made of the available MF

field strength prediction methods applicable to Region 2. These methods include, in addition to the four previously discussed, the Brasilia method recently recommended by the Inter-American Conference on Telecommunications for Region 2 and a separate MF prediction method developed by CCIR IWP 6/4 and issued December 1979. The Brasilia Curve is an extension of the FCC 1935 median (50%) curve, shown in Figure 3, to distances of 13,000 km by drawing a line parallel to the Cairo North-South Curve and joining the FCC Curve at 4300 km. The IWP 6/4 method differs from the CCIR 1978 method in several respects. One of the more significant differences is the elimination of any solar cycle effect. The equation for the basic loss factor, k, in the CCIR 1978 method has been replaced by the one contained in the Wang 1979 method with the added constraint that k should not be less than 3. The use of the Wang 1979 equation for k and the elimination of solar activity greatly simplifies the calculation of the predicted MF field strengths. The final version of the IWP 6/4 method for Region 2 is presented in Appendix C.

For this comparison, the measured field strengths for 23 MF propagation paths in North America and two propagation paths between the United States and Central America were combined with the measurements for the previous paths, 23, 24, 25, 26, and 29, to form a data base for assessing the validity of these six methods for Region 2. The relevant path information for the additional Region 2 paths is given in Table 5. (Most of these measurements were used to develop the FCC 1944 curves shown in Figure 4.) The comparisons between the measured field strengths for these paths and the predicted field strengths from the Cairo, Brasilia, CCIR 1974 and 1978, Wang 1979, and IWP 6/4 methods are given in Table 6. (When either the measurements or predictions are in terms of a reference time of two hours after sunset, 2.5 dB are added to the field strengths to approximate the field strengths at midnight.)

From the rms errors between observations and predictions, the IWP 6/4 method for Region 2 can be considered the best method for predicting MF field strengths, at least for this group of paths. There is very little difference between the two CCIR and the Wang 1979 methods except for paths >2200 km. The Cairo method results are not as good as in the previous comparison except for the very long paths. The rms error for the Brasilia method is 1 dB less than the rms error for the Cairo method, and although the predicted MF field strengths are less than the Cairo Curve predictions for paths >1500 km, they are also somewhat larger than the field strengths predicted from the other methods for the U.S. paths. The rms errors for the CCIR and Wang 1979 methods

Table 5. List of FCC Propagation Paths in North and Central America

Path Number	Transmitter	Receiver	Geographic Coordinates Transmitter		Receiver		Frequency	Great Circle Distance (km)
US 1	New York City, N.Y	Baltimore, Maryland	40.9°N	73.8°W	39.3°N	76.6°W	880	300
US 2	Des Moines, Iowa	Grand Island, Nebraska	41.6°N	93.4°w	40.9°N	98.4°W	1040	425
US 3	Rochester, New York	Baltimore, Maryland	43.1°N	77.7°W	39.3°N	76.6°W	1180	430
US 4	Raleigh, North Carolina	Baltimore, Maryland	35.8°N	78.8°W	39.3°N	76.6°W	680	432
US 5	Denver, Colorado	Grand Island, Nebraska	39.5°N	104.8°W	40.9°N	98.4°W	850	568
US 6	Cincinnati, Ohio	Atlanta, Georgia	39.1°N	84.6°W	33.8°N	84.4°W	1530	592
US 7	Cincinnati, Ohio	Atlanta, Georgia	39.4°N	84.3°W	33.8°N	84.4°W	700	623
US 8	Minneapolis, Minnesota	Grand Island, Nebraska	45.2°N	93.4°W	40.9°N	98.4°W	830	623
US 9	St. Paul, Minnesota	Grand Island, Nebraska	45.0°N	93.1°W	40.9°N	98.4°W	1500	627
US 10	Cincinnati, Ohio	Baltimore, Maryland	39.4°N	84.3°W	39.3°N	76.6°W	700	662
US 11	Cincinnati, Ohio	Baltimore, Maryland	39.1°N	84.6°W	39.3°N	76.6°W	1530	687
US 12	Dallas Texas	Grand Island, Nebraska	32.9°N	97.0°W	40.9°N	98.4°W	820	898
US 13	Salt Lake City, Utah	Grand Island, Nebraska	40.8°N	112.1°W	40.9°N	98.4°W	1160	1155
US 14	Cincinnati, Ohio	Grand Island, Nebraska	39.4°N	84.3°W	40.9°N	98.4°W	700	1203
US 15	San Antonio, Texas	Grand Island, Nebraska	29.6°N	98.3°W	40.9°N	98.4°W	1200	1262
US 16	Watrous, Canada	Portland, Oregon	51.7°N	105.4°W	45.5°N	112.7°W	540	1434
US 17	Guatemala City, Guatemala	Kingsville, Texas	14.5°N	90.5°W	27.5°N	97.9°W	1020	1636
US 18	Belize, Br. Honduras	Powder Springs, Georgia	17.6°N	88.2°W	33.9°N	84.7°W	834	1850
US 19	Los Angeles, California	Grand Island, Nebraska	33.9°N	118.0°W	40.9°N	98.4°W	640	1900
US 20	Dallas, Texas	Baltimore, Maryland	32.9°N	97.0°W	39.3°N	76.6°W	820	1959
US 21	Minneapolis, Minnesota	Portland, Oregon	45.2°N	93.4°W	45.5°N	122.7°W	830	2278
US 22	St. Paul, Minnesota	Portland, Oregon	45.0°N	93.1°W	45.5°N	122.7°W	1500	2305
US 23	Dallas, Texas	Portland, Oregon	32.9°N	97.0°W	45.5°N	122.7°W	820	2598
US 24	Chicago, Illinois	Portland, Oregon	41.6°N	87.8°W	45.5°N	122.7°W	890	2818
US 25	Cincinnati, Ohio	Portland, Oregon	39.4°N	84.3°W	45.5°N	122.7°W	700	3188
US 26	New Orleans, Louisiana	Portland, Oregon	30.0°N	90.2°W	45.5°N	122.7°W	870	3297
US 27	Atlanta, Georgia	Portland, Oregon	33.8°N	84.2°W	45.5°N	122.7°W	750	3494

Table 6. Comparison of Measured Field Strengths with Predicted Field Strengths (F_o in dB relative to 1 μV/m) for Paths in North and South America

Path Number	Measured Field Strength dBμ(1 kw)	Cairo	Brazilia	CCIR '74	CCIR '78	WANG 79	IWP 6/4
US 1	44.8	46.6	46.6	53.1	52.8	52.6	52.9
US 2	44.8	46.8	46.8	48.8	48.6	48.4	48.7
US 3	44.7	46.8	46.8	48.3	48.0	48.0	48.3
US 4	44.7	46.8	46.8	49.3	49.2	48.8	49.0
US 5	46.5	46.7	46.7	45.6	45.4	45.1	45.3
US 6	47.9	46.6	46.6	44.8	44.7	45.1	45.2
US 7	44.2	46.4	46.4	45.0	44.8	44.4	44.5
US 8	38.0	46.4	46.4	43.5	43.3	42.6	42.9
US 9	41.2	46.4	46.4	42.4	42.2	42.6	42.9
US 10	41.5	46.2	46.2	43.5	43.3	42.6	42.9
US 11	44.9	46.2	46.2	41.9	41.7	42.1	42.4
US 12	43.9	43.9	43.9	39.8	39.7	39.3	39.5
US 13	40.3	37.5	37.5	33.9	33.8	33.8	34.0
US 14	30.6	37.2	37.2	34.0	33.8	32.5	32.8
US 15	39.7	36.6	36.6	34.1	34.1	34.4	34.5
US 16	25.6	33.9	33.9	28.3	27.9	24.3	24.7
US 17	37.5	30.6	30.3	32.9	33.2	34.7	34.4
US 18	35.0	29.1	27.8	30.4	30.6	31.4	31.2
US 19	23.6	28.1	27.4	27.2	27.2	25.9	26.0
US 20	24.2	27.7	26.5	25.4	25.4	24.6	24.7
US 21	10.4	25.2	23.0	16.2	16.0	13.7	13.9
US 22	10.9	25.0	22.6	12.0	11.8	13.4	13.6
US 23	13.9	23.3	20.0	18.0	18.1	16.9	17.0
US 24	0.1	21.4	17.4	10.6	10.6	8.5	8.8
US 25	0.1	19.1	14.8	9.0	9.0	5.4	5.6
US 26	13.3	18.3	13.9	11.3	11.5	10.5	10.6
US 27	-1.9	17.2	13.0	8.3	8.4	5.9	6.1
# 23	2.0	3.2	-3.7	-6.6	-5.7	9.3	-1.9
# 24	2.0	3.0	3.9	0.3	1.7	15.6	4.6
# 25	-2.0	2.8	3.3	-0.9	0.6	15.0	4.1
# 26	2.0	2.5	-4.4	-8.1	-7.2	7.9	-3.8
# 29	2.0	1.7	-4.5	-12.8	-11.9	3.5	-9.0
RMS Error		8.2	7.1	5.8	5.7	5.7	4.7

indicate that there are no significant differences between the field strength predictions using these methods except for the longer paths.

From Table 6, it can be observed that for paths <2000 km, the differences between the predicted MF field strengths for the different prediction methods is insignificant; the rms error is approximately 4.0 dB for all methods. However, for the U.S. paths >2000 km (21 through 27), there is more variability in the predicted MF field strengths. Beyond 2200 km, propagation of the radio wave would involve two ionospheric reflections. The rms error for these seven paths is 15.6 dB for Cairo, 12.4 dB for Brasilia, 7.1 dB for CCIR 1974 and 1978, 5.3 dB for Wang 1979, and 5.4 dB for the IWP 6/4 predictions. From these results, it appears that either the Wang 1979 or the IWP 6/4 predictions are more reasonable for MF paths between 2200 and 3500 km in Region 2.

However, for paths >8000 km (23, 24, 25, 26, and 29), there is less variability between the predictions than for the U.S. paths 21 through 27. The rms error for the predictions for these five paths is 2.3 dB for Cairo, 5.4 dB for Brasilia, 8.9 dB for CCIR 1974, 8.3 dB for CCIR 1978, 10.6 dB for Wang, and 6.5 dB for IWP 6/4. (The Wang 1979 method would give approximately the same results as the IWP 6/4 method if the loss factor, k, is limited to 3 in the calculation of the field strengths for these paths.) The Cairo North-South Curve predictions appear to be the preferred method for very long paths in Region 2.

5. RELIABILITY OF MF FIELD STRENGTH MEASUREMENTS

When comparing measurements with predictions, lack of information about the reliability of the data makes it difficult to realistically assess the accuracy and/or suitability of any prediction method. There are a number of uncertainties concerning the controls and conditions under which many of these observations were made. For example, the measurements used for the Cairo Curves were normalized to 1 kW radiated, but the transmitting antennas were one-half wavelength long. Should an additional correction factor be applied to the measurements before comparing them with predictions that have assumed a short vertical antenna? As the CCIR and Wang prediction methods only approximate the correction to account for the transmitting antenna gains, this could also explain some of the discrepancies between the measurements and predictions. Some of the measurement campaigns extended over several years, and in some areas these measurements indicate a seasonal variation. The Cairo measurements were made only in local winter and summer; if there is a seasonal

dependence, the comparison of these measurements with predictions of an annual median field strength may be biased.

Altogether, there are approximately 300 field strength measurements available for comparisons. In most cases, the measurements have been normalized to represent F_0 as defined by CCIR and include corrections for the transmitting antennas and solar activity when appropriate. In many cases, no information was available concerning the antennas and there were insufficient data to determine a solar activity effect. Some of the measurements were made at intermediate solar activity levels; and, in this case, the annual medians are averaged over all of the years. If the measurements were made at high solar activity in a region where a variation with solar activity is assumed, the measurements were adjusted to represent minimum solar activity. As mentioned in Section 4.4.1, if the measurements were not made at a time when the ionosphere would not be affected by solar radiation, corrections were made to adjust the measurements accordingly.

The intent here is not to criticize the methods used to normalize the measurements, but to emphasize the necessity for the process. Considering the possible deficiencies in the measurements used for the comparisons, the question that needs to be answered is not whether one particular prediction method is better than the others, but are the measurements sufficiently accurate and reliable to make this determination?

6. CONCLUSIONS

The apparent need for the use of so many different variables in the MF field strength prediction methods is indicative of the complexity and uncertainty regarding the physical properties that are involved in long-distance MF sky-wave propagation. Among these is a correlation with a geomagnetic coordinate; however, a correlation between the measurements and the solar zenith angle might be as significant and might also explain the seasonal variation. As annual medians of predicted field strengths are desired, it would seem desirable to perform a multiple regression analysis of all available monthly median MF field strength measurements to determine the interrelationships with variables such as the solar zenith angle, geographic and geomagnetic coordinates, frequency, distance, and solar activity. From this analysis, improved estimates of annual median field strengths could be derived and applied in the development of a more accurate and consistent worldwide MF field strength prediction method.

In addition, and particularly significant for inter-regional applications, there is a need for controlled measurement programs that would provide more reliable measurements, especially for very long paths at low latitudes. Controlled experiments to better determine the effects of multi-hop propagation, sea gain, polarization losses, and to verify nonreciprocal propagation would be useful.

When planning a broadcast service, the service area covered would be determined by the annual hourly median field strengths. For determining interference from one or more signals, it is assumed that interference is produced when the field strength is exceeded at least 10% of the time. The CCIR suggests that 8 dB be added to the annual median of the hourly median field strength to obtain the field strength exceeded 10% of the time. As an estimate of the maximum field strengths or the worst case conditions is required, until a more reliable prediction method is available, the preferred method would be the method that predicts the maximum field strengths. For very long paths, the Cairo Curve method, in general, predicts the highest field strengths. For shorter paths, the preferred method would depend on the geographical area of interest.

7. ACKNOWLEDGMENTS

The author wishes to thank Mr. R. C. Kirby, Director, CCIR Secretariat for permission to reproduce the CCIR texts included in Appendixes A, B, and C, and also A. F. Barghausen for his many suggestions and constructive criticism, and J. S. Washburn for his invaluable assistance in providing the computer calculations for the MF prediction methods.

8. REFERENCES

Barghausen, A. F. (1966), Medium-frequency sky wave propagation in middle and low latitudes, IEEE Trans. Broadcasting BC-12, No. 1, 1-14.

CCIR (1937), Documents of the International Radio Consultative Committee, Bucharest, 1, 368-70.

CCIR, Kyoto (1978), Report 575-1, Methods for predicting sky-wave field strengths at frequencies between 150 kHz and 1600 kHz, ITU, Geneva, 6, 187-198.

Crombie, D. D. (1979), Comparison of measured and predicted signal strengths of nighttime medium frequency signals in the U.S.A., IEEE Trans. Broadcasting BC-25, 86-89.

Ebert, W. (1962), Ionospheric propagation on long and medium waves, EBU Rev., Pt. A (Technical) 71-73, EBU Technical Centre, Brussels.

Elling, W. (1961), Pulse measurements of virtual heights and reflection coefficients of the ionosphere over Tsumeb, South-West Africa in the frequency range from 350-5600 kHz (in German), Arch. Elkt. Ubertragung 15, 115-124.

FCC (1976), Rules and Regulations, 3, Part 73 - Radio Broadcast Services, Washington, D.C., U.S. Government Printing Office.

ITU (1975), Final acts of the Regional Administrative LF/MF Broadcasting Conference (Geneva, 1975) for use in Region 1, ITU, Geneva.

JTAC (1964), Radio spectrum utilization, a program for the administration of the radio spectrum, Inst. of Electrical and Electronics Engineers and Electronic Industries Association, New York.

Knight, P. (1973), MF propagation: a wave-hop method for ionospheric field-strength predictions, BBC Engineering 100, 22-34.

Knight, P. (1977), LF and MF sky-wave propagation: the origin of the Cairo Curves, BBC Research Department 1977/42.

Norton, K. A. (1959), Transmission loss in radio propagation: II. NBS Technical Note 12, U.S. Dept. of Commerce, Washington, D.C.

Olver, A. D., A. G. Lyner, and P. Knight (1971), A computer programme for calculating sky-wave field strengths at medium frequencies, EBU Review, Part A - Technical, No. 125, 18-27.

Phillips, M. L. (1950), Study of medium and long wave propagation, Statement of CCIR U.S. Preparatory Committee No. 4.

Phillips, G. J., and P. Knight (1965), Effects of polarization on a medium-frequency sky-wave service, including the case of multihop paths, Proc. Inst. Elec. Engrs. (London) 112, No. 1, 31-39.

Rice, P. L., A. G. Longley, K. A. Norton, and A. P. Barsis (1965), Transmission loss predictions for tropospheric communication circuits, Vol. 1 NBS Technical Note No. 101, (access. no. AD687-820, NTIS, Springfield, VA 22161).

Wang, J. C. H. (1977), Prediction of medium-frequency skywave field strength in North America, IEEE Trans. Broadcasting BC-23, 43-49.

Wang, J. C. H. (1979), Medium-frequency skywave propagation in region 2, IEEE Trans. Broadcasting BC-25, 79-85.

9. BIBLIOGRAPHY

CCIR, Geneva (1963), Report 264, Predictions of ionospheric field-strength or propagation loss for the frequency range between 150 and 1500 kc/s, ITU Geneva, 2, 313-325.

CCIR, Oslo (1966), Report 264-1, Predictions of ionospheric field strength and propagation loss for the frequency range between 150 and 1500 kHz, ITU, Geneva, 2, 297-324.

CCIR, New Delhi (1970), Report 431, Extension of the sky-wave propagation curves for the frequency range 150 kHz to 1600 kHz, ITU, Geneva, 2(2), 164-187.

CCIR, Geneva (1974), Report 575, Methods for predicting sky-wave field strengths at frequencies between 150 kHz and 1600 kHz, ITU, Geneva, 6, 186-205.

The information contained within Appendix A is taken from CCIR Report 575, Sky-wave Field Strength Prediction Method for the Frequency Range 150 to 1600 kHz, published in Volume VI of the Proceedings of the XIIIth Plenary Assembly, Geneva, 1974.

APPENDIX A: CCIR, 1974 MF FIELD-STRENGTH PREDICTION METHOD

ANNEX

SKY-WAVE FIELD STRENGTH PREDICTION METHOD
FOR THE FREQUENCY RANGE 150 TO 1600 kHz

Method proposed by Interim Working Party 6/4
(Modified U.S.S.R. method)

List of symbols

b	Solar-activity factor given in § 2.6.
d	Ground distance between transmitter and receiver (km).
F_0	Annual median field strength at the reference time defined in § 2 (dB (μV/m)).
F_t	Annual median field strength at time t (dB (μV/m)).
f	Frequency (kHz).
f'	A frequency defined in equation (6) (kHz).
G_0	Sea gain for a terminal on the coast (dB).
G_H	Transmitting antenna gain factor due to horizontal directivity (dB).
G_S	Sea gain for a terminal near the sea (dB).
G_V	Transmitting antenna gain factor due to vertical directivity (dB).
h	Transmitting antenna height (Fig. 6).
h_r	Height of reflecting layer (km).
I	Magnetic dip angle (degrees).
k	Basic loss factor.
k_R	Loss factor.
L_P	Excess polarisation coupling loss (dB).
L_t	Diurnal loss factor (dB).
P	Radiated power (dB (1 kW)).
p	Slant propagation distance (km).
Q	A sea-gain parameter given in § 2.3.
R	Twelve-month smoothed Zurich sunspot number.
s	Distance of terminal from sea, measured along great-circle path (km).
t	Time relative to sunset or sunrise (hours).
V	Transmitter cymomotive force (dB (300 V)).
θ	Direction of propagation relative to magnetic East-West (degrees).
λ	Wavelength.
Φ	A geomagnetic latitude parameter.
Φ_T	Geomagnetic latitude of transmitter } (degrees, positive in northern hemisphere, negative
Φ_R	Geomagnetic latitude of receiver } in southern hemisphere).

1. Introduction

This method of prediction gives the night-time sky-wave field strength produced for a given power radiated from one or more vertical antennae, when measured by a loop antenna at ground level aligned in a vertical plane along the great-circle path to the transmitter. It applies for paths of lengths up to 12 000 km. However in band 5 it was only verified for paths of up to 5000 km. The accuracy of prediction varies from region to region and may be improved in certain regions by applying modifications such as those shown in § 5. In any case the method should be used with caution for geomagnetic latitudes greater than 60°.

2. Annual median night-time field strength

The predicted sky-wave field strength is given by:

$$F_0 = V + G_S - L_P + 105{\cdot}3 - 20 \log_{10} p - 10^{-3} k_R p \qquad (1)$$

where F_0 = annual median of half-hourly median field strengths (dB above 1 μV/m) at the reference time defined in § 2.1.

V = transmitter cymomotive force, dB above a reference cymomotive force of 300 V,

G_S = sea-gain correction, dB,

L_P = excess polarization-coupling loss, dB,

p = slant-propagation distance, km,

k_R = loss factor incorporating effects of ionospheric absorption, focusing and terminal losses, and losses between hops on multi-hop paths.

2.1 *Reference time*

The reference time is taken as six hours after the time at which the sun sets at a point S on the surface of the Earth. For paths shorter than 2000 km, S is the mid-point of the path. On longer paths, S is 750 km from the terminal where the sun sets last, measured along the great-circle path.

2.2 *Cymomotive force*

The cymomotive force V is given as:

$$V = P + G_V + G_H \qquad (2)$$

where P = radiated power, dB above 1 kW,

G_V = transmitting antenna gain factor (dB) due to vertical directivity, given in Fig. 6,

G_H = transmitting antenna gain factor (dB) due to horizontal directivity. For directional antennae, G_H is a function of azimuth. For omnidirectional antennae, $G_H = 0$.

2.3 *Sea gain*

G_S is the additional signal gain when one or both terminals is situated near the sea. G_S for a single terminal is given by:

$$G_S = G_0 - 10^{-3}\left(\frac{Q\,s\,f}{G_0}\right) \quad \text{dB} \qquad (3)$$

where G_0 is the gain when the terminal is on the coast, f is the frequency in kHz and s is the distance in km of the terminal from the sea, measured along the great-circle path. $Q = 0{\cdot}44$ in band 5 and $1{\cdot}75$ in band 6. G_0 is given in Fig. 7 as a function of d for bands 5 and 6. In band 6, $G_0 = 10$ dB

when $d > 6500$ km. Equation (3) applies for values of s such that $G_S > 0$. For larger values of s, $G_S = 0$. If both terminals are near the sea, G_S is the sum of the values of G_S for the individual terminals.

2.4 *Polarisation coupling loss*

L_R is the excess polarization coupling loss. In band 5, $L_P = 0$. In band 6 at low latitudes, for $|I| \leqslant 45°$

$$L_P = 180\,(36 + \theta^2 + I^2)^{-1/2} - 2 \quad \text{dB/terminal} \tag{4}$$

where I is the magnetic dip in degrees at the terminal and θ is the path azimuth measured in degrees from the magnetic E-W direction, such that $|\theta| \leqslant 90°$. For $|I| > 45°$, $L_P = 0$. L_P should be evaluated separately for the two terminals, because of the different θ and I that may apply, and the two L_P values added. The most accurate available values of magnetic dip and declination should be used in determining θ and I.

2.5 *Slant propagation distance*

For paths longer than 1000 km, p is approximately equal to the ground distance d (km). For shorter paths

$$p = (d^2 + 4h_r^2)^{1/2} \tag{5}$$

where $h_r = 100$ km if $f \leqslant f'$ and 220 km if $f > f'$, where f' (in kHz) is given by

$$f' = 350 + [(2{\cdot}8d)^3 + 300^3]^{1/3} \tag{6}$$

Equation (5) may be used for paths of any length with negligible error.

2.6 *Loss factor*

The loss factor k_R is given by

$$k_R = k + 10^{-2}\,bR \tag{7}$$

where R = twelve-month smoothed Zurich sunspot number. In band 5, $b = 0$. In band 6, $b = 4$ for North American paths, 1 for Europe and Australia and 0 elsewhere.

$$k = 1{\cdot}9 f^{0{\cdot}15} + 0{\cdot}24 f^{0{\cdot}4}\,(\tan^2\Phi - \tan^2 37°) \tag{8}$$

where f = frequency (kHz).

For paths shorter than 3000 km

$$\Phi = (\Phi_T + \Phi_R)/2 \tag{9}$$

where Φ_T and Φ_R are the geomagnetic latitudes at the transmitter and receiver respectively, determined by assuming an Earth-centred dipole field model with northern pole at 78·5°N, 69°W geographic co-ordinates. Φ_T and Φ_R are taken as positive in the northern hemisphere and negative in the southern hemisphere. Paths longer than 3000 km are divided into two equal sections which are considered separately. The value of Φ for each half-path is derived by taking the average of the geomagnetic latitudes at one terminal and at the mid-point of the whole path, the geomagnetic latitude at the mid-point of the whole path being assumed to be the average of Φ_T and Φ_R. As a consequence:

$$\Phi = (3\Phi_T + \Phi_R)/4 \quad \text{for the first half of the path and} \tag{10}$$

$$\Phi = (\Phi_T + 3\Phi_R)/4 \quad \text{for the second half.} \tag{11}$$

The values of k calculated from equation (8) for the two half-paths are then averaged and used in equation (7).

If $|\Phi| > 60°$, equation (8) is evaluated for $\Phi = 60°$.

3. Nocturnal variation of annual median field strength

$$F_t = F_0 - L_t \quad (12)$$

where F_t = annual median field strength at time t, dB (μV/m)

F_0 = annual median field strength at reference time defined in §2.1, dB (μV/m), given by equation (1)

L_t = diurnal loss factor, dB, given in Fig. 8.

Fig. 8 shows the average of the annual median nocturnal variations for Europe and Australia, derived from Fig. 8 of Report 264-3 and Fig. 5 of Report 431-1 respectively. The time t is the time in hours relative to the sunrise or sunset reference times as appropriate. These are taken at the ground at the mid-path position for $d < 2000$ km and at 750 km from the terminal where the sun sets last or rises first for longer paths.

4. Day-to-day and short-period variations of field strength

The field strength exceeded for 10% of the total time on a series of nights, during short periods centred on a specific time is:

8 dB greater in band 5

10 dB greater in band 6

than the values of F_0 and F_t given above.

5. Accuracy of the method

This method is believed to be reasonably accurate in I.T.U. Regions 1 and 3. Comparison of predicted and measured values shows, however, that its accuracy in certain regions may be further improved by making the following corrections.

5.1 Since field strengths measured in Australia and New Zealand are 4 to 7 dB higher than those predicted by the method, a better prediction formula for this area is

$$F_0 = V + G_s - L_P + 108 - 20 \log_{10} p - 0{\cdot}8 \times 10^{-3} k_R p \quad (13)$$

The field strength exceeded on band 6 for 10% of the total time on a series of nights, during short periods centred on a specific time, is only 7 dB greater than the annual median in this area.

5.2 The accuracy may be improved in North America by subtracting 3 dB from field strengths predicted by the method.

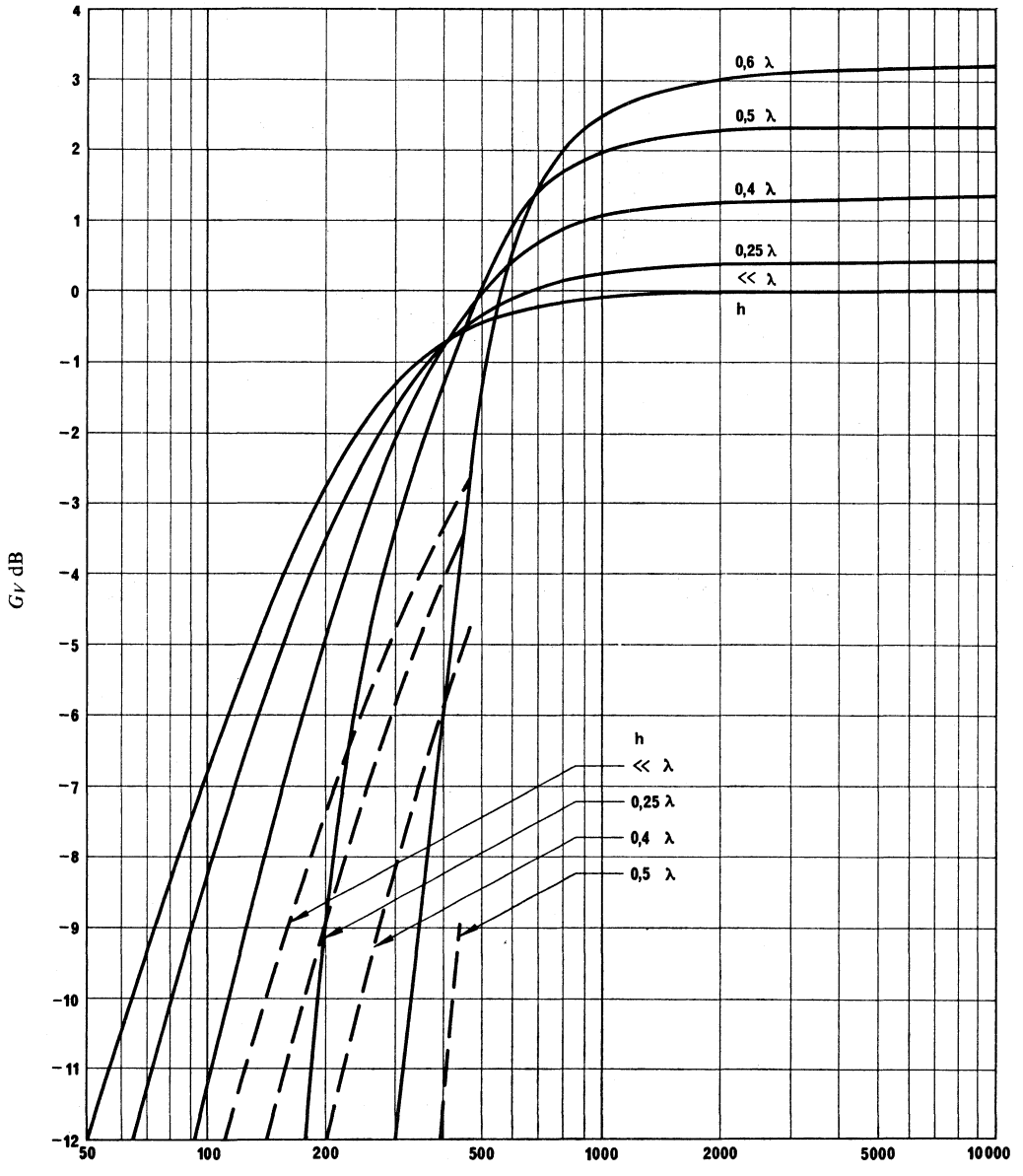

FIGURE 6

Transmitting antenna gain factor (Gv)

h = Antenna height

——— h_r = 100 km (E layer reflection)

– – – – – h_r = 220 km (F layer reflection)

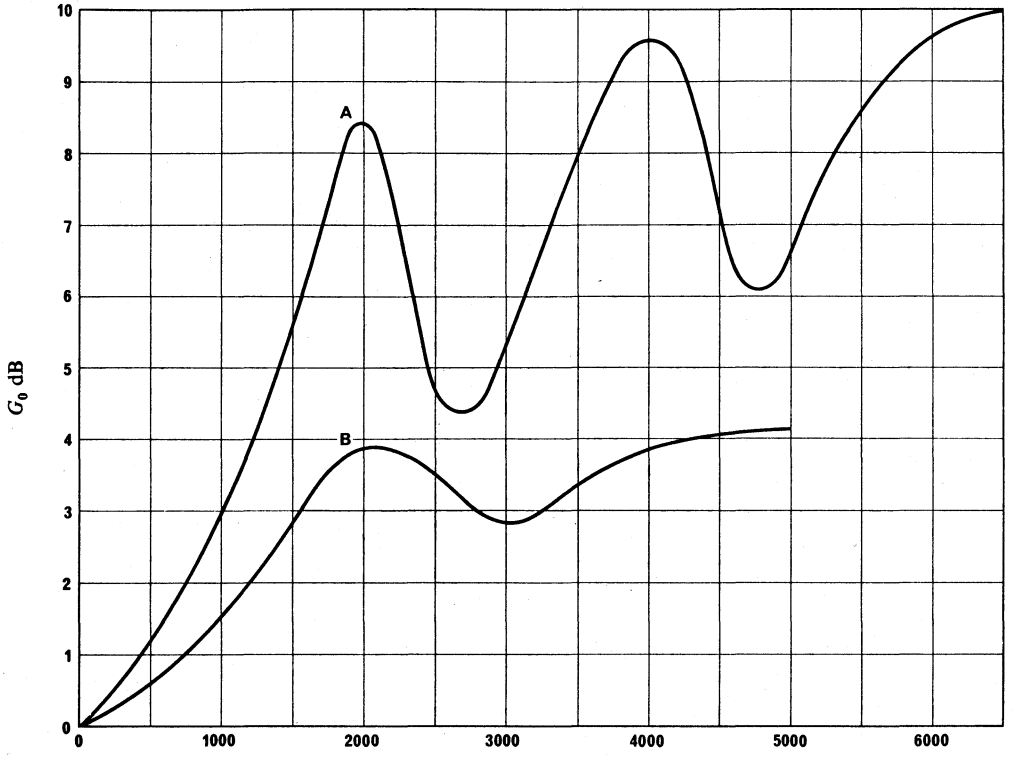

FIGURE 7

Sea gain (G_0) for a single terminal on the coast

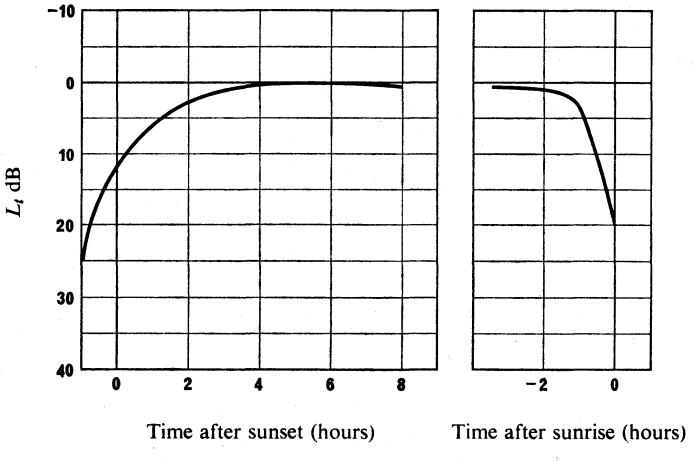

FIGURE 8

Diurnal loss factor (L_t)

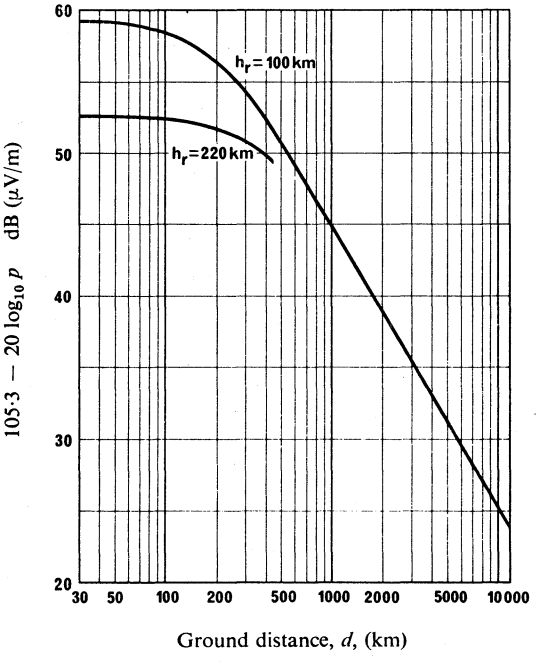

FIGURE 9

Basic field strength

The curves show $105{\cdot}3 - 20 \log_{10} p$

where $p = (d^2 + 4h_r^2)^{1/2}$

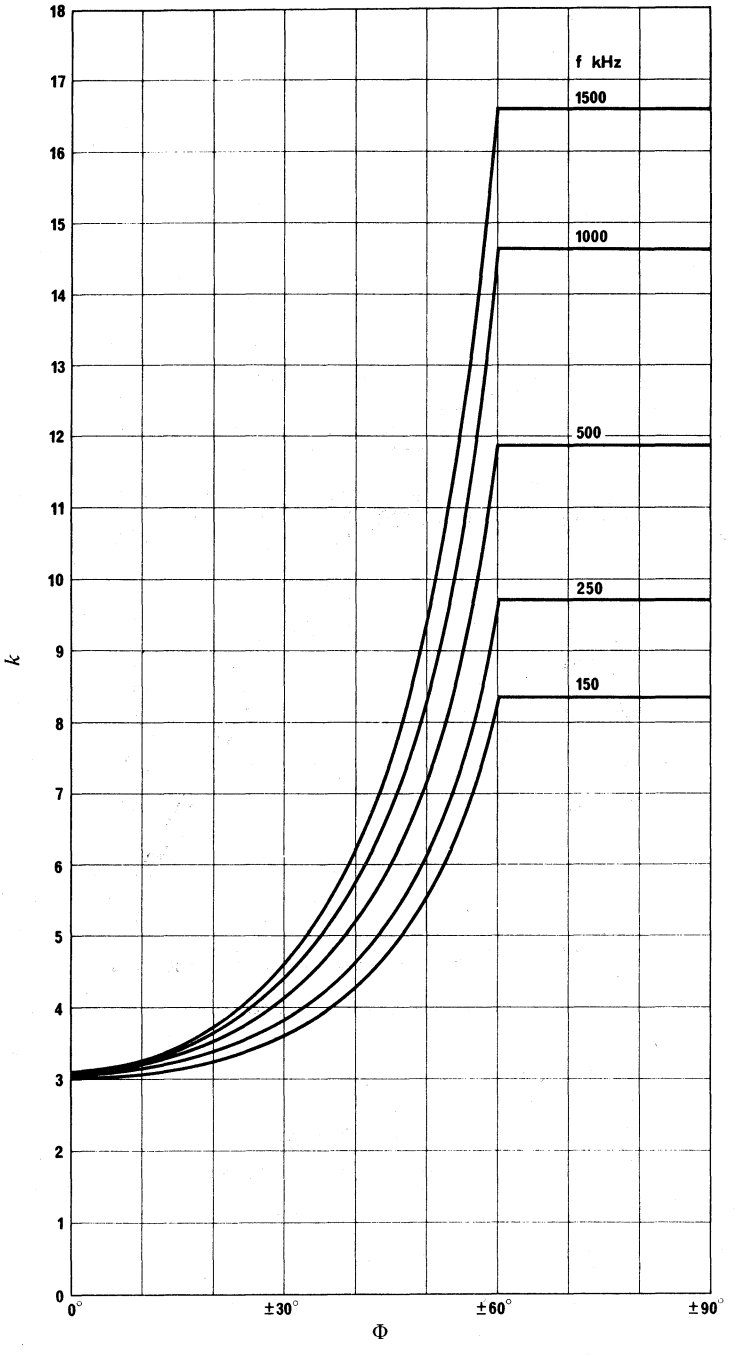

FIGURE 10

Basic loss factor k

$$k = 1{\cdot}9f^{0{\cdot}15} + 0{\cdot}24f^{0{\cdot}4}\,(\tan^2 \Phi - \tan^2 37°)$$

$$(0 \leqslant \Phi \leqslant 60°)$$

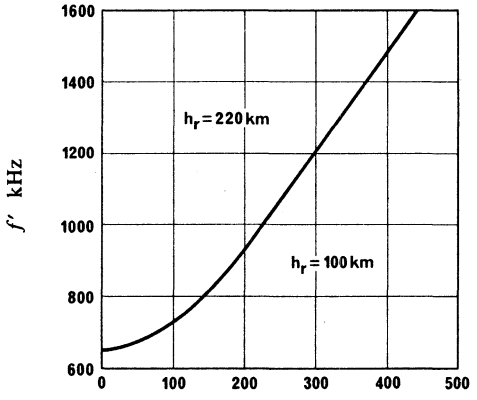

FIGURE 11

Frequency defined in equation (6)

$$f' = 350 + [(2{\cdot}8d)^3 + 300^3]^{1/3}$$

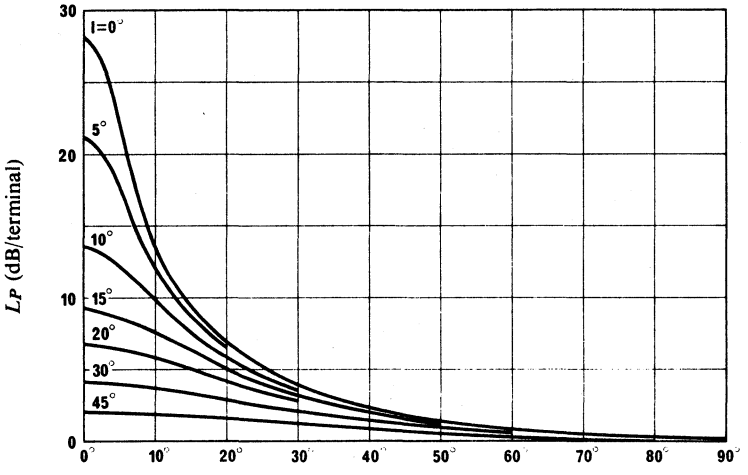

FIGURE 12

Excess polarization coupling loss L_P

$$L_P = 180\,(36 + \theta^2 + I^2)^{-1/3} - 2$$

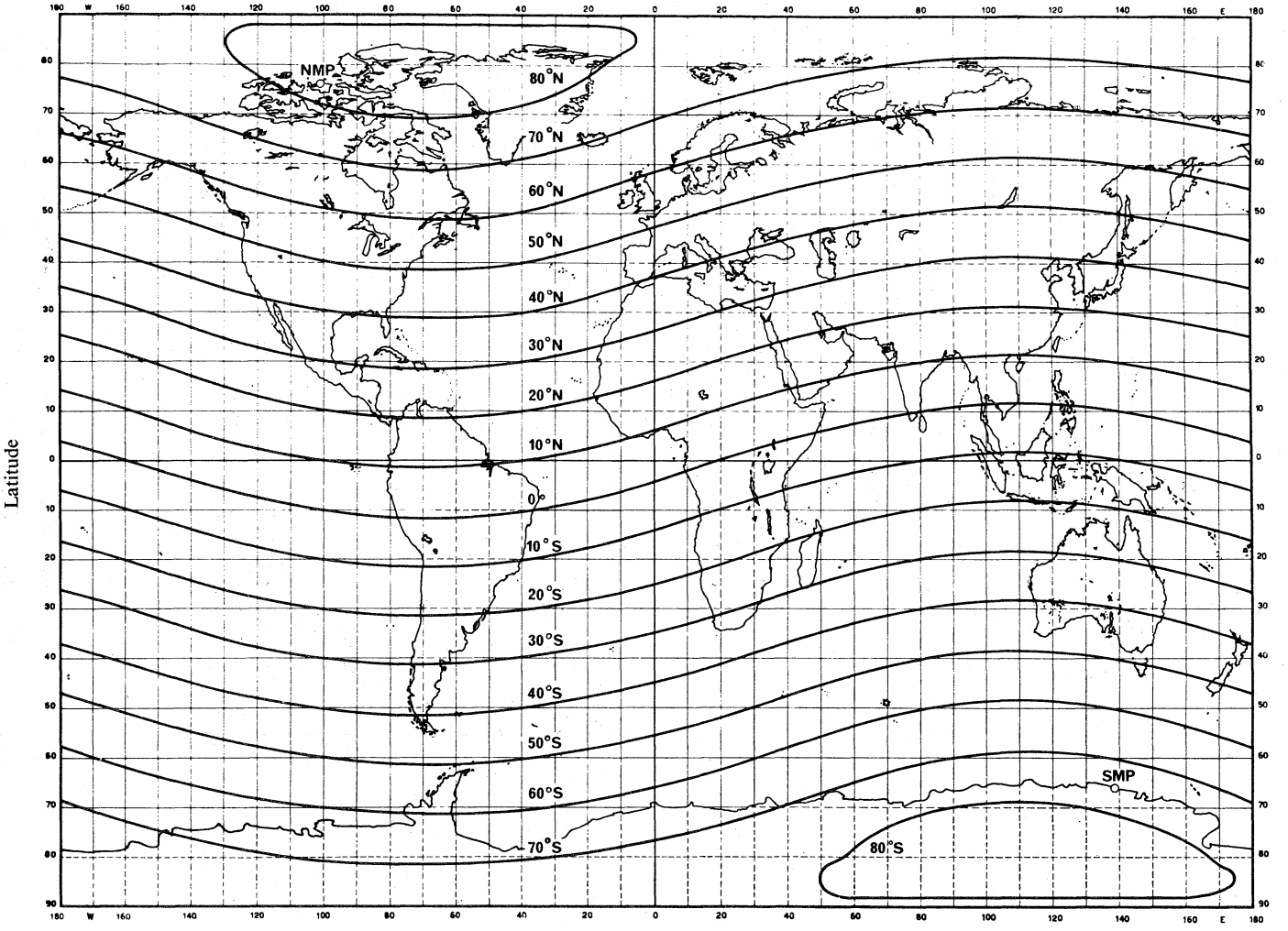

FIGURE 13

Geomagnetic latitudes

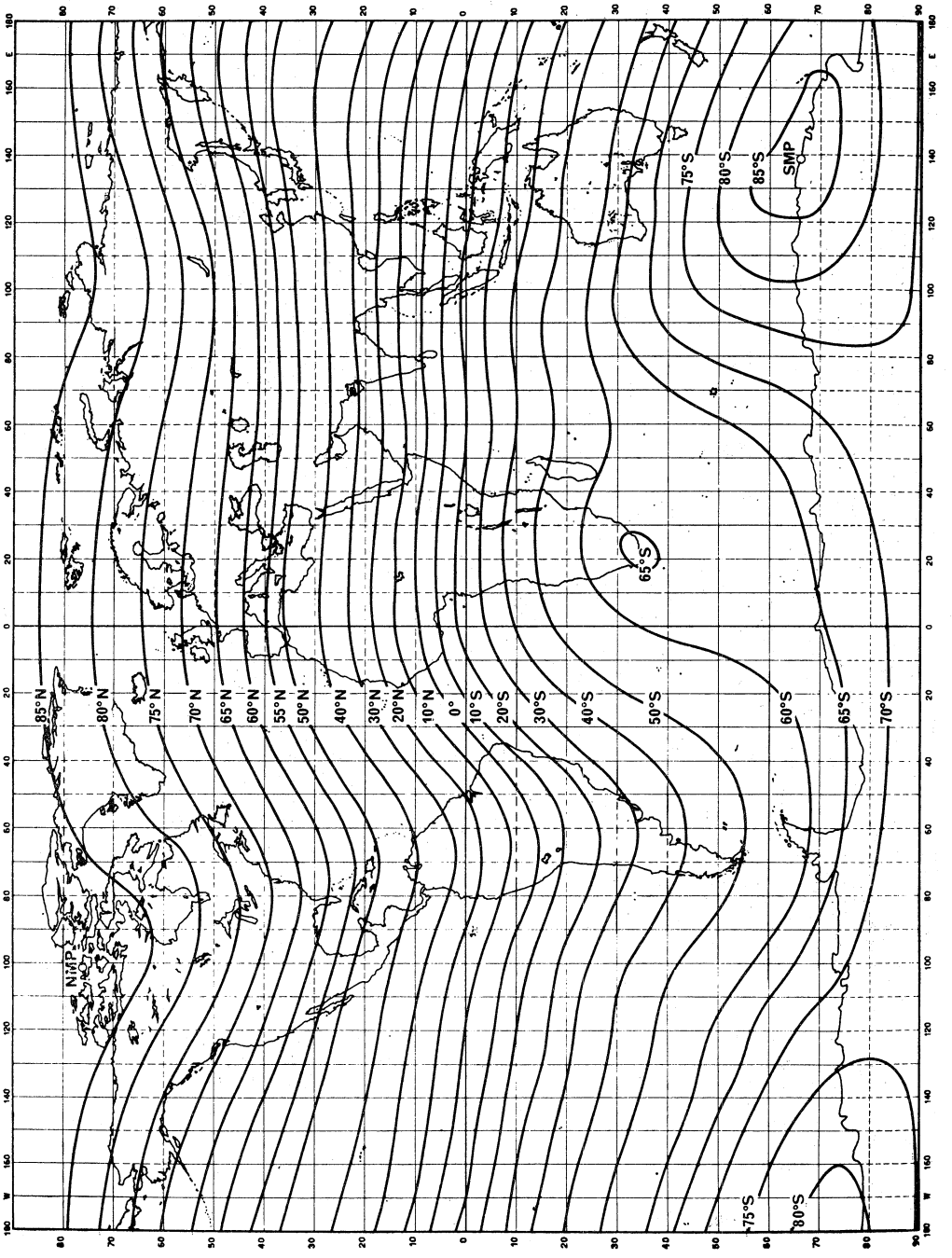

FIGURE 14

Map of magnetic dip

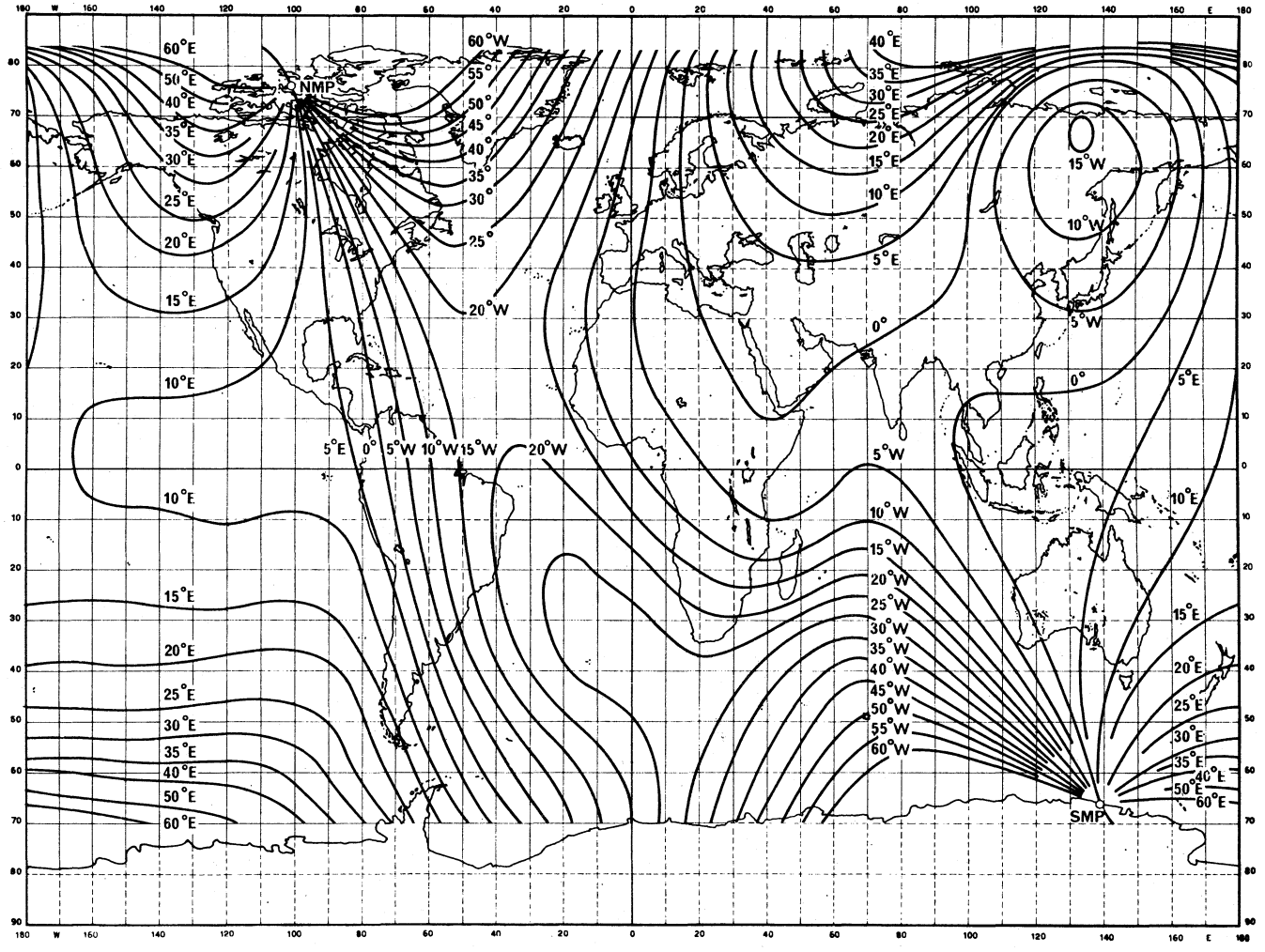

FIGURE 15

Map of magnetic declination (dotted curves east declination, continuous curves west declination)

The information contained within Appendix B is taken from CCIR Recommendation 435-3, Sky-wave Field Strength Prediction Method for the Frequency Range 150 to 1600 kHz, published in Volume VI of the Recommendations and Reports of the CCIR, 1978, as passed at the XIVth Plenary Assembly, Kyoto, Japan.

APPENDIX B: CCIR, 1978 MF FIELD-STRENGTH PREDICTION METHOD

ANNEX I

SKY-WAVE FIELD STRENGTH PREDICTION METHOD FOR THE FREQUENCY RANGE 150 TO 1600 kHz

List of symbols

A: A parameter defined in § 2.

b: Solar-activity factor given in § 2.6.

d: Ground distance between transmitter and receiver (km).

F: Annual median field strength for a given cymomotive force (c.m.f.), V, and at a given time t, relative to sunset or sunrise as appropriate.

F_0: Annual median field strength at the reference time defined in § 2 (dB(μV/m)).

f: Frequency (kHz).

f': A frequency defined in equation (6) (kHz).

G_0: Sea gain for a terminal on the coast (dB).

G_H: Transmitting antenna gain factor due to horizontal directivity (dB).

G_S: Sea gain for a terminal near the sea (dB).

G_V: Transmitting antenna gain factor due to vertical directivity (dB).

h: Transmitting antenna height (Fig. 1).

h_r: Height of reflecting layer (km).

I: Magnetic dip angle, N or S, (degrees).

k: Basic loss factor.

k_R: Loss factor.

L_P: Excess polarisation coupling loss (dB).

L_t: Hourly loss factor (dB).

P: Radiated power (dB(1 kW)).

p: Slant propagation distance (km).

Q_1, Q_2: Sea-gain parameters given in § 2.3.

R: Twelve-month smoothed Zurich sunspot number.

r_1, r_2: Parameters defined in § 2.3.

s_1: Distance of terminal from sea, measured along great-circle path (km).

s_2: Distance of terminal from next section of land, measured along great-circle path (km).

t: Time relative to sunset or sunrise (hours).

V: Transmitter cymomotive force (dB(300 V)).

θ: Direction of propagation relative to magnetic East-West (degrees).

λ: Wavelength.

Φ: A geomagnetic latitude parameter.

Φ_T: Geomagnetic latitude of transmitter
Φ_R: Geomagnetic latitude of receiver
} (degrees, positive in northern hemisphere negative in southern hemishphere).

1. Introduction

This method of prediction gives the night-time sky-wave field strength produced for a given power radiated from one or more vertical antennae, when measured by a loop antenna at ground level aligned in a vertical plane along the great-circle path to the transmitter. It applies for paths of lengths up to 12 000 km in bands 5 (LF) and 6 (MF). * However, in band 5 it was only verified for paths of up to 5000 km. The accuracy of prediction varies from region to region and may be improved in certain regions by applying modifications such as those shown in § 6. In any case the method should be used with caution for geomagnetic latitudes greater than 60°.

* Band 5 covers the frequency range of about 150 to 285 kHz and band 6 covers the range of about 520 to 1600 kHz.

Figs. 1, 2 and 3 are an essential part of the prediction method. Geomagnetic maps are included for convenience in Figs. 11, 12 and 16. The remaining Figs. 4 to 10, 13 to 15 and 17, provide additional information to simplify the use of the method.

2. Annual median night-time field strength

The predicted sky-wave field strength is given by:

$$F = V + F_0 - L_t = V + G_S - L_P + A - 20 \log p - 10^{-3} k_R\, p - L_t \qquad (1)$$

where,

F: annual median of half-hourly median field strengths (dB(μV/m)) for a given transmitter cymomotive force, V, and at a given time, t, relative to sunset or sunrise as appropriate,

F_0: annual median of half-hourly median field strengths (dB(μV/m)) for a transmitter cymomotive force of 300 V at the reference time defined in § 2.1,

V: transmitter cymomotive force, dB above a reference cymomotive force of 300 V, (see § 2.2),

G_S: sea-gain correction, (dB), (see § 2.3),

L_P: excess polarization-coupling loss, (dB), (see § 2.4),

A: 106.6 − 2 sin Φ, where Φ is defined by equation (9),

p: slant-propagation distance, (km), (see § 2.5),

k_R: loss factor incorporating effects of ionospheric absorption, focusing and terminal losses, and losses between hops on multi-hop paths, (see § 2.6),

L_t: hourly loss factor, (dB), (see § 2.7).

To facilitate calculation, Fig. 4 shows the quantity $A - 20 \log p$, for $\Phi = 40°$ as a function of ground distance, d, whereas Figs. 5 to 10 show F_0 as a function of ground distance, d, for various frequencies and for various geomagnetic latitudes when G_S, L_P and R are all zero.

2.1 *Reference time*

The reference time is taken as six hours after the time at which the Sun sets at a point S on the surface of the Earth. For paths shorter than 2000 km, S is the mid-point of the path. On longer paths, S is 750 km from the terminal where the sun sets last, measured along the great-circle path.

2.2 *Cymomotive force*

The cymomotive force V is given as:

$$V = P + G_V + G_H \qquad (2)$$

where,

P: radiated power, dB above 1 kW,

G_v: transmitting antenna gain factor (dB) due to vertical directivity, given in Fig. 1,

G_H: transmitting antenna gain factor (dB) due to horizontal directivity. For directional antennae, G_H is a function of azimuth. For omnidirectional antennae, $G_H = 0$.

2.3 *Sea gain*

G_S is the additional signal gain when one or both terminals are situated near the sea. G_S for a single terminal is given by:

$$G_S = \left(\frac{s_2}{r_2} - \frac{s_1}{r_1}\right) G_0 \qquad \text{(dB)} \qquad (3)$$

where,

G_0: gain when the terminal is on the coast and the sea is unobstructed by further land,

s_1: distance of terminal from sea, measured along great-circle path (km),

s_2: distance of terminal from next section of land, measured along great-circle path (km),

$r_1 = 10^3\, G_0^2/Q_1 f$

$r_2 = 10^3\, G_0^2/Q_2 f$

f: frequency (kHz),

$Q_1 = 0.30$ in band 5 and 1.4 in band 6,

$Q_2 = 0.25$ in band 5 and 1.2 in band 6.

G_0 is given in Fig. 2 as a function of d for bands 5 and 6. In band 6, $G_0 = 10$ dB when $d > 6500$ km. Equation (3) applies for values of s_1 and s_2 such that $G_S > 0$. For larger values of s_1, $G_S = 0$. If $s_2 > r_2$, G_S is calculated with $s_2 = r_2$. If $s_2 < r_2$ and if more than half the distance between s_2 and a great-circle distance equal to r_2 is occupied by land, equation (3) applies, but if less than half the distance between s_2 and r_2 is occupied by land, G_S is calculated with $s_2 = r_2$.

If both terminals are near the sea, G_S is the sum of the values of G_S for the individual terminals.

Equation (3) should not be used for fresh water.

2.4 *Polarization coupling loss*

L_P is the excess polarization coupling loss. In band 5, $L_P = 0$. In band 6, L_P for a single terminal is given by one of the following two formulae:

$$\text{If } I \leqslant 45°: L_P = 180\,(36 + \theta^2 + I^2)^{-1/2} - 2 \quad \text{dB} \tag{4}$$

$$\text{If } I > 45°: L_P = 0$$

where I is the magnetic dip, N or S, in degrees at the terminal and θ is the path azimuth measured in degrees from the magnetic E-W direction, such that $|\theta| \leqslant 90°$. L_P should be evaluated separately for the two terminals, because of the different θ and I that may apply, and the two L_P values added. The most accurate available values of magnetic dip and declination (e.g. see Figs. 11 and 12) should be used in determining θ and I.

Fig. 13 shows values of L_P calculated from equation (4).

2.5 *Slant propagation distance*

For paths longer than 1000 km, p is approximately equal to the ground distance d (km). For shorter paths

$$p = (d^2 + 4h_r^2)^{1/2} \tag{5}$$

where $h_r = 100$ km if $f \leqslant f'$ and 220 km if $f > f'$, as shown in Fig. 14 where f' (in kHz) is given by:

$$f' = 350 + [(2.8d)^3 + 300^3]^{1/3} \tag{6}$$

Equation (5) may be used for paths of any length with negligible error.

2.6 *Loss factor*

The loss factor k_R is given by

$$k_R = k + 10^{-2}\,bR \tag{7}$$

where R = twelve-month smoothed Zurich sunspot number. In band 5, $b = 0$. In band 6, $b = 4$ for North American paths, 1 for Europe and Australia and 0 elsewhere.

The basic loss factor k is given by:

$$k = 3.2 + 0.19\,f^{0.4} \tan^2(\Phi + 3) \tag{8}$$

where f = frequency (kHz). If $\Phi > 60°$, equation (8) is evaluated for $\Phi = 60°$. If $\Phi < -60°$, equation (8) is evaluated for $\Phi = -60°$. Fig. 15 shows values of k calculated from equation (8) according to these rules.

For paths shorter than 3000 km:

$$\Phi = 0.5\,(\Phi_T + \Phi_R) \tag{9}$$

where Φ_T and Φ_R are the geomagnetic latitudes at the transmitter and receiver respectively, determined by assuming an Earth-centred dipole field model with northern pole at 78.5° N, 69° W geographic co-ordinates. Φ_T and Φ_R are taken as positive in the northern hemisphere and negative in the southern hemisphere (see Fig. 16). Paths longer than 3000 km are divided into two equal sections which are considered separately. The value of Φ for each half-path is derived by taking the average of the geomagnetic latitudes at one terminal and at the mid-point of the whole path, the geomagnetic latitude at the mid-point of the whole path being assumed to be the average of Φ_T and Φ_R. As a consequence:

$$\Phi = (3\Phi_T + \Phi_R)/4 \text{ for the first half of the path and} \tag{10}$$

$$\Phi = (\Phi_T + 3\Phi_R)/4 \text{ for the second half.} \tag{11}$$

The values of k calculated from equation (8) for the two half-paths are then averaged and used in equation (7).

2.7 *Hourly loss factor*

The hourly loss factor, L_t, is given in Fig. 3, which shows the average of the annual median hourly variations for Europe and Australia, derived from Figs. 2 and 6 of Report 431-2 respectively. The time t is the time in hours relative to the sunrise or sunset reference times as appropriate. These are taken at the ground at the mid-path position for $d < 2000$ km and at 750 km from the terminal where the Sun sets last or rises first for longer paths.

Fig. 17 shows sunset and sunrise times for a range of geographic latitudes.

3. Day-to-day and short-period variations of night-time field strength

The field-strength exceeded for 10% of the total time on a series of nights at a given season, during short periods centred on a specific time, is

6.5 dB greater in band 5

8 dB greater in band 6

than the value of F_0 given in § 2. Larger values may be observed at the peak of the solar cycle.

4. Seasonal variation of night-time field strength

At night, MF sky-waves propagating in temperate latitudes are strongest in spring and autumn and are weakest in summer and winter, the summer minimum being the more pronounced. The overall variation may be as much as 15 dB at the lowest frequencies in the MF band, decreasing to about 3 dB at the upper end of the band. At LF the seasonal variation at night has the opposite trend, with a pronounced summer maximum. The seasonal variation is much smaller in tropical latitudes.

5. Day-time field strength

In band 5 in Europe the median day-time field strength in winter is 10 dB less than the night-time value of F_0 given in § 2. In summer the daytime field strength is 30 dB less than F_0. The field strength exceeded for 10% of the total time on a series of days in winter, during short periods centred on a specific time, is 5 dB greater than the median day-time value given above.

In band 6 in Europe the median day-time field strength in winter is 25 dB less than the night-time value of F_0 given in § 2. In summer the day-time field strength is about 60 dB less than F_0.

In spring and autumn in Europe, day-time field strengths in bands 5 and 6 have values between the summer and winter values.

6. Accuracy of the method

The accuracy in the United States of America may be improved by using a reference time of two hours after sunset. Field strengths measured in the United States of America tend to be greater at higher frequencies; the frequency variation given by equation (8) is in the opposite sense.

The term in equation (3) which describes how G_S is modified by the distance s_2 to the next section of land is derived from theory and must therefore be regarded as tentative until measurements are available.

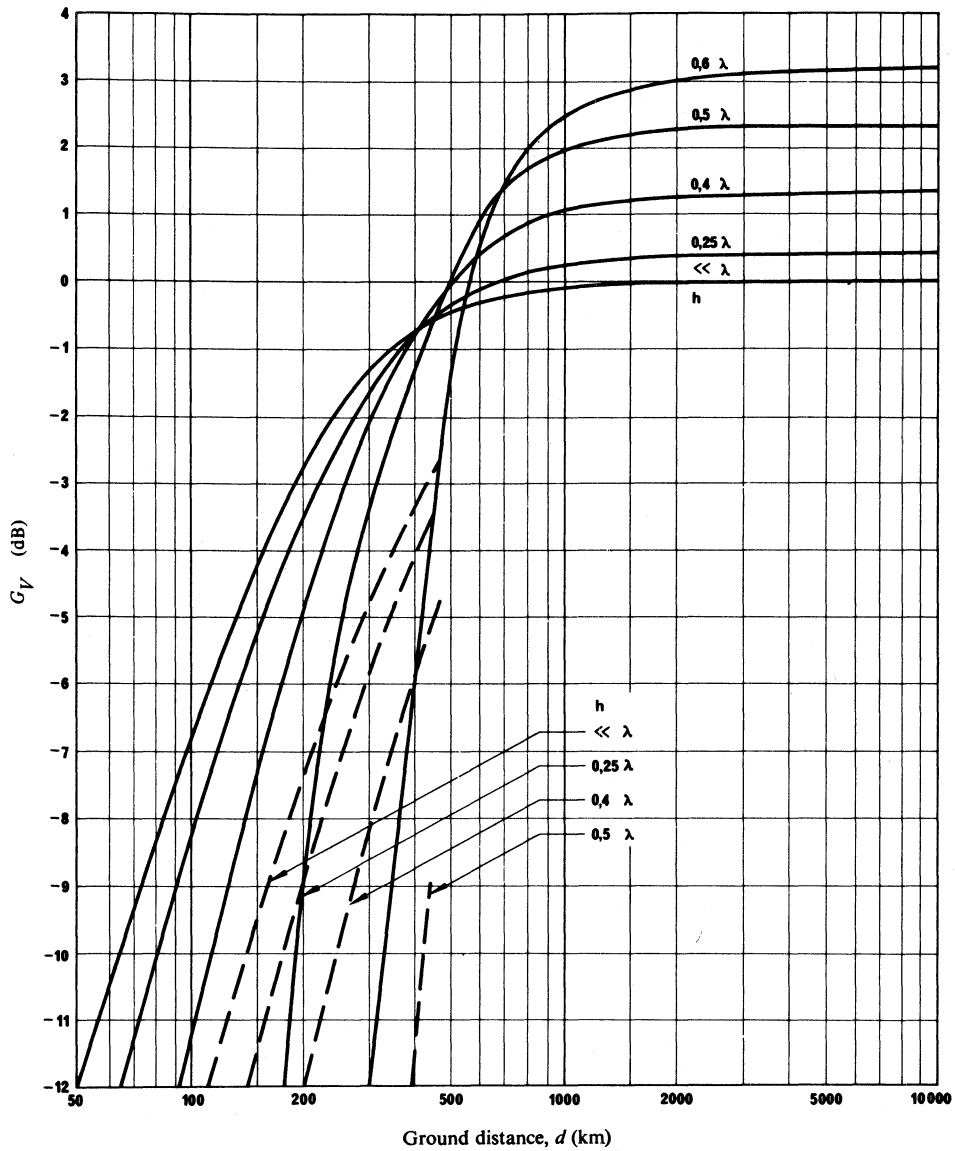

FIGURE 1 – *Transmitting antenna gain factor for monopoles (G_V)*

h = Antenna height

——— h_r = 100 km (E layer reflection)

— — — — h_r = 220 km (F layer reflection)

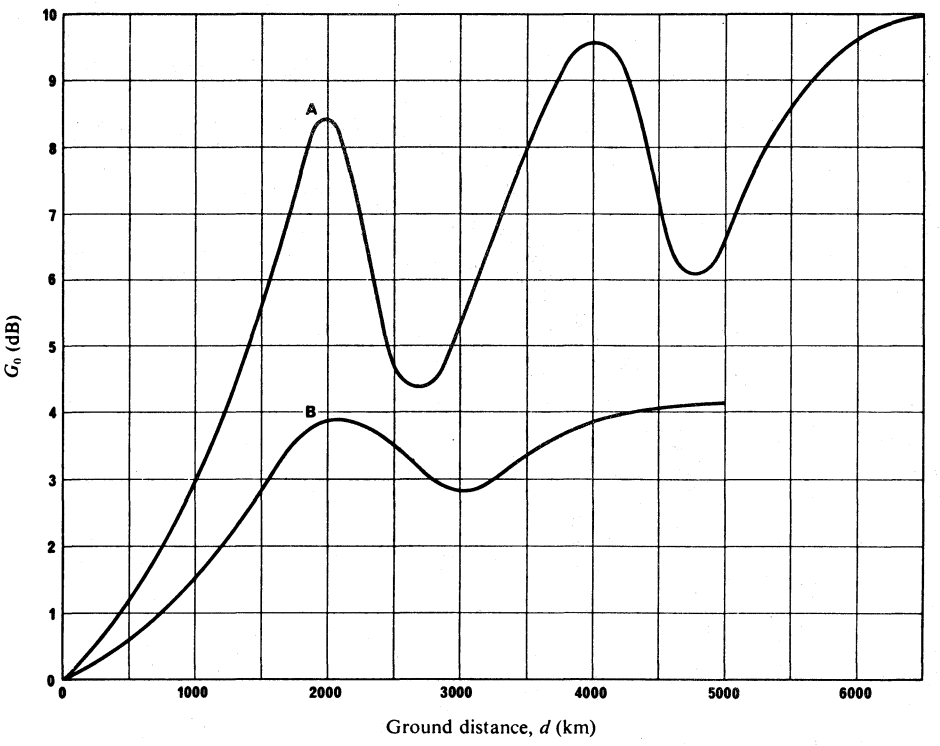

FIGURE 2 – *Sea gain (G_0) for a single terminal on the coast*
A: Band 6 B: Band 5

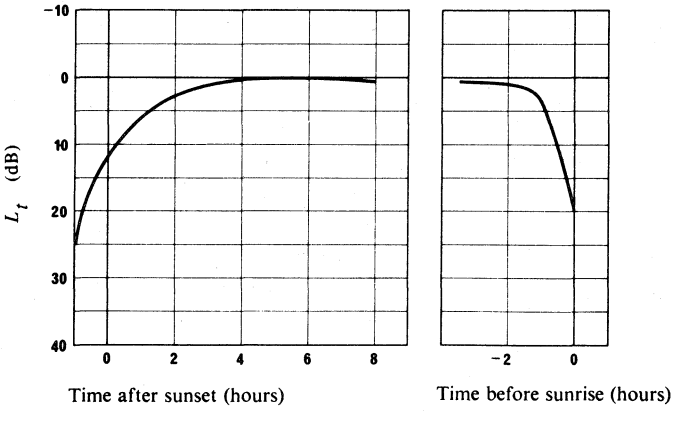

FIGURE 3 – *Hourly loss factor (L_t)*

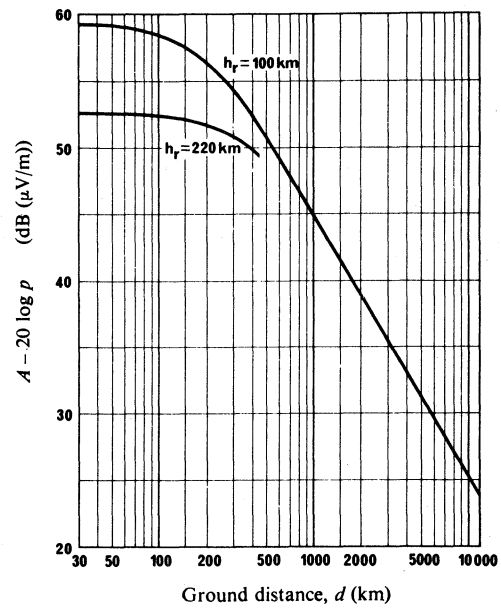

FIGURE 4 - *Basic field strength*

The curves show $= A - 20 \log p$

Where $A = 106.6 - 2 \sin \Phi$
$\Phi = 40°$
$p = (d^2 + 4h_r^2)^{1/2}$

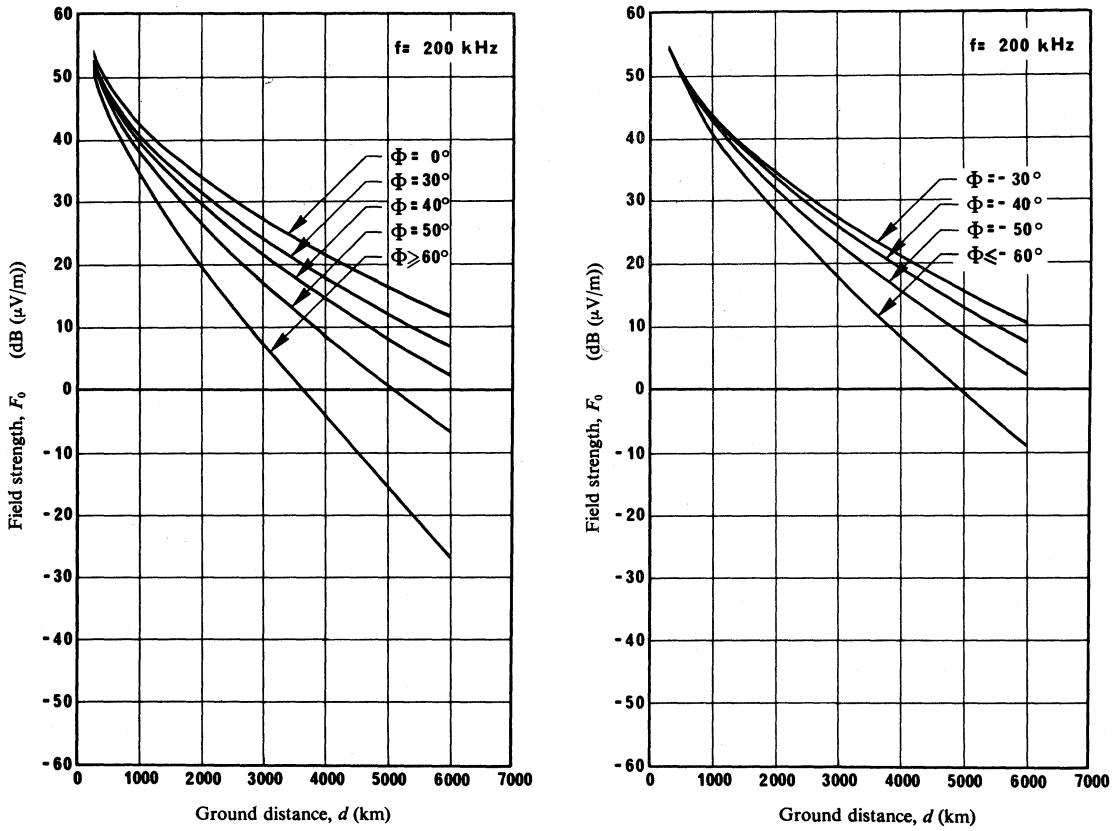

FIGURE 5 – *Curves showing F_0 for 200 kHz when G_S, L_P and R are all zero, for constant geomagnetic latitudes*

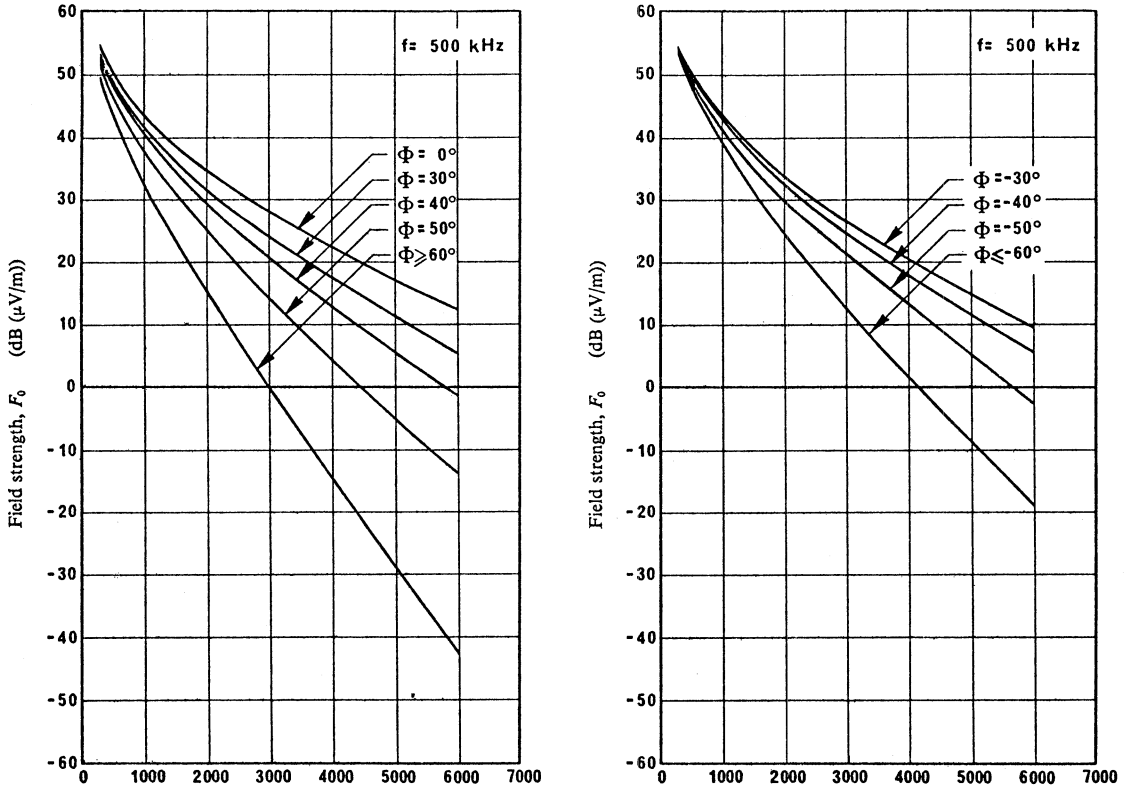

FIGURE 6 – *Curves showing F_0 for 500 kHz when G_S, L_P and R are all zero, for constant geomagnetic latitudes*

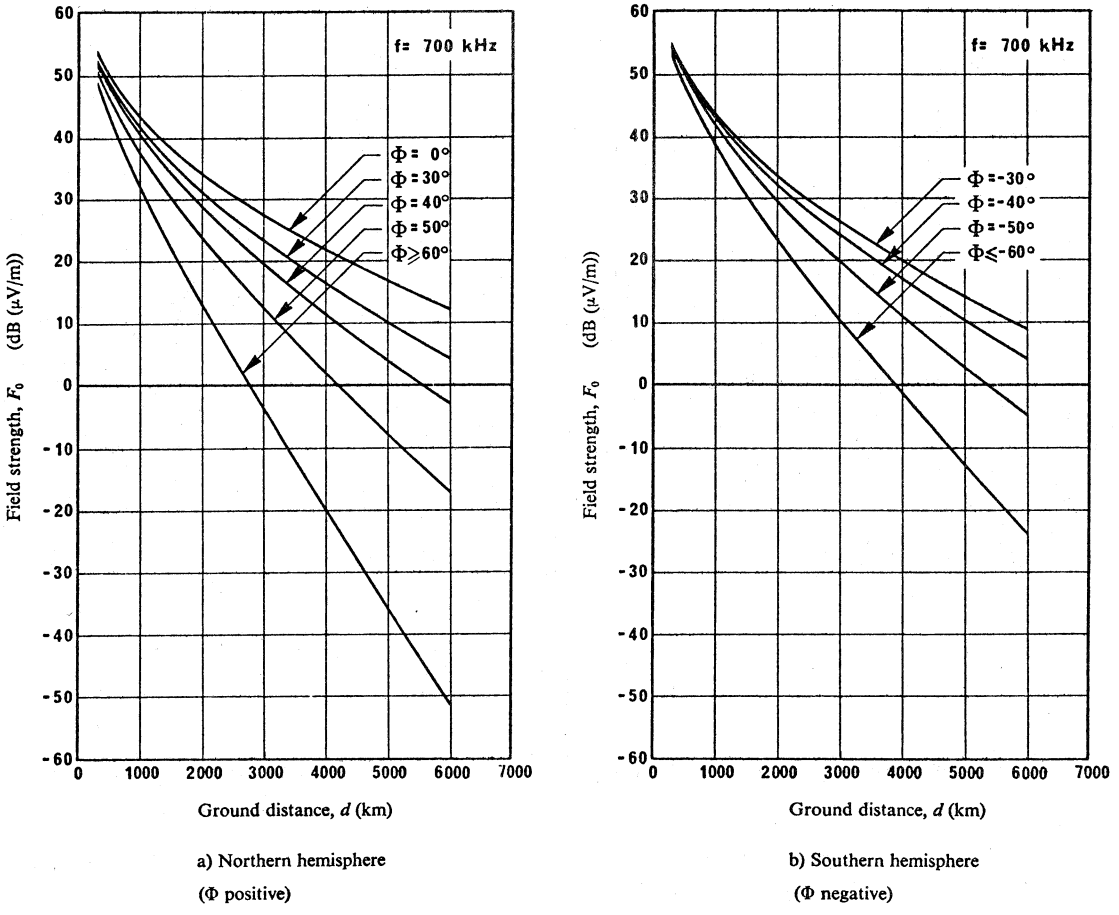

FIGURE 7 – *Curves showing F_0 for 700 kHz when G_S, L_P and R are all zero, for constant geomagnetic latitudes*

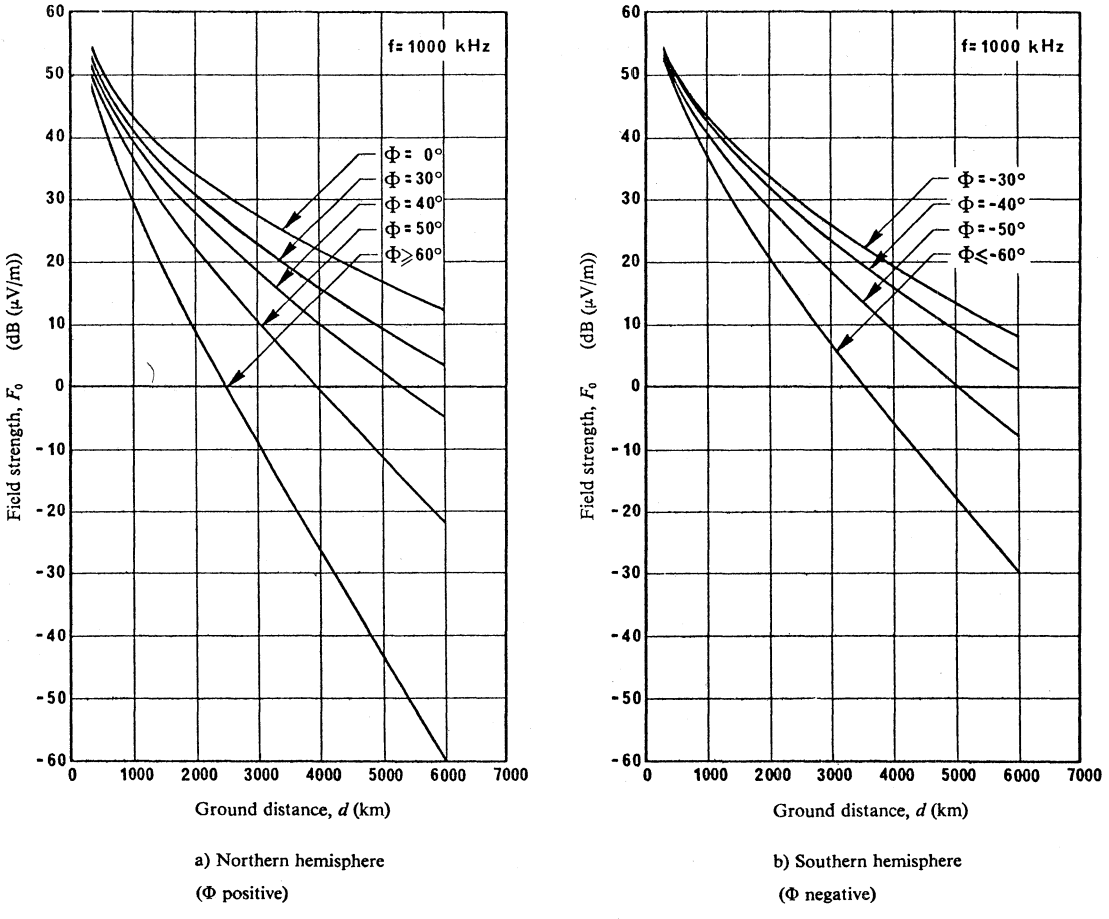

FIGURE 8 – *Curves showing F_0 for 1000 kHz when G_S, L_P and R are all zero, for constant geomagnetic latitudes*

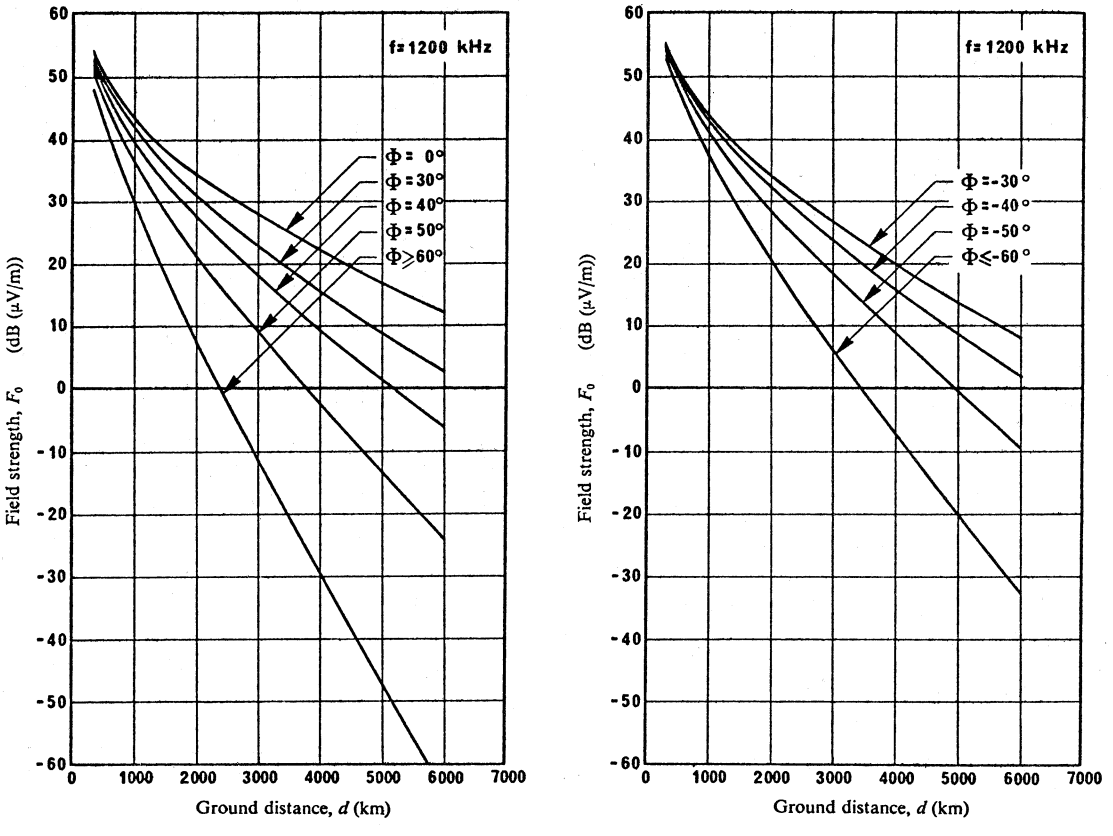

FIGURE 9 – *Curves showing F_0 for 1200 kHz when G_S, L_P and R are all zero, for constant geomagnetic latitudes*

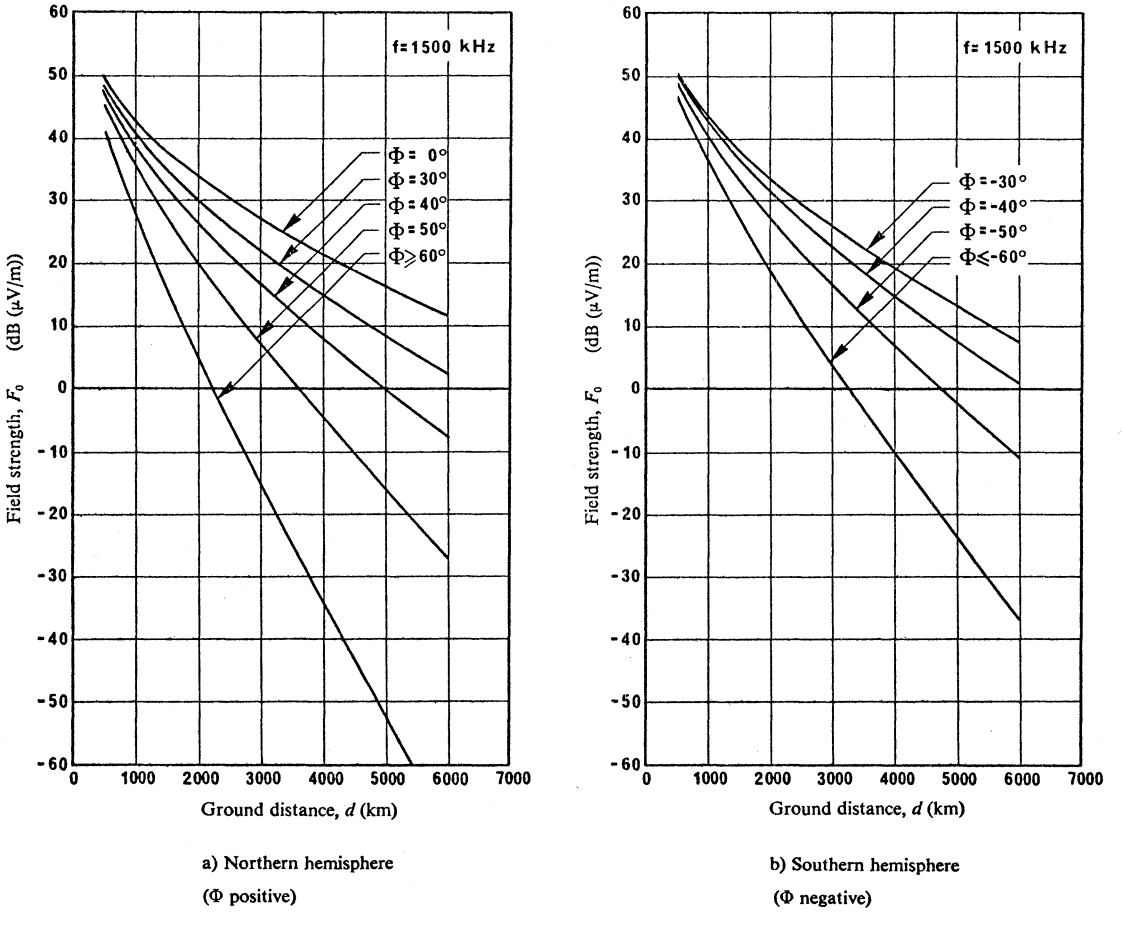

FIGURE 10 – *Curves showing F_0 for 1500 kHz when G_S, L_P and R are all zero, for constant geomagnetic latitudes*

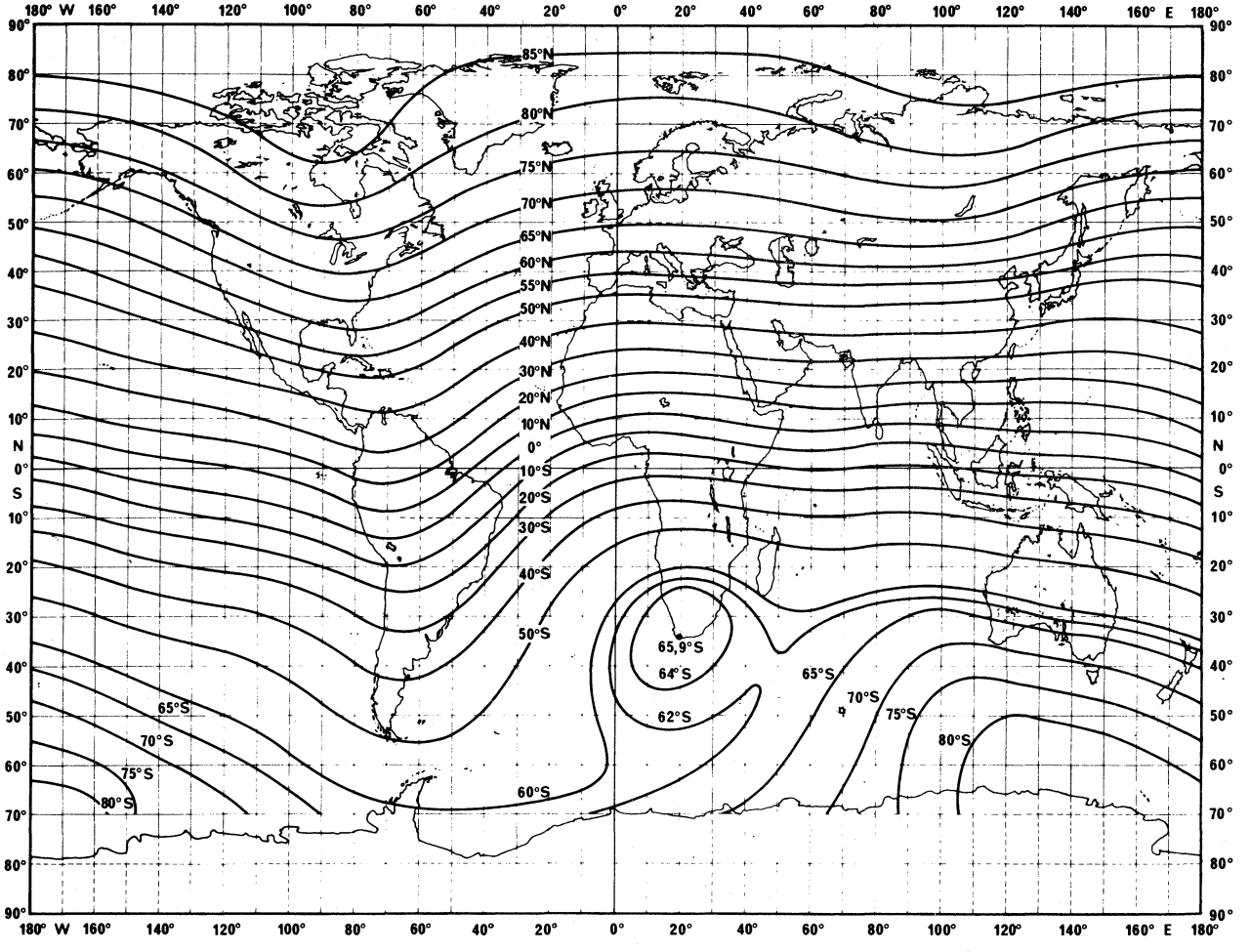

FIGURE 11 – *Map of magnetic dip (epoch 1975.0)*

(Source: Magnetic inclination or dip (epoch 1975.0) Chart No. 30 World U.S. Defense Mapping Agency Hydrographic Center)

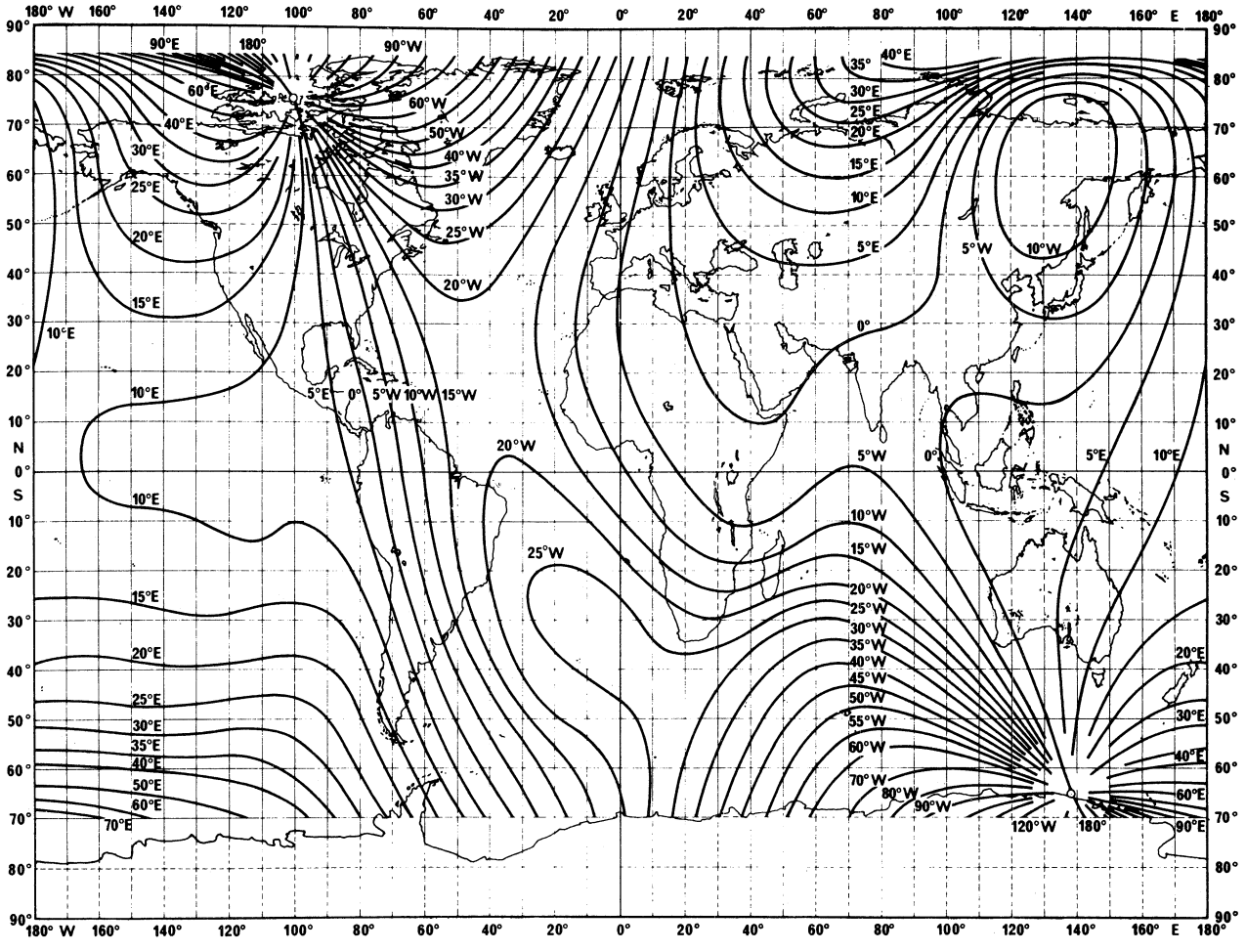

FIGURE 12 – *Map of magnetic declination (epoch 1975.0)*

(Source: Magnetic variation (epoch 1975.0) Chart No. 42, World U.S. Defense Mapping Agency Hydrographic Center)

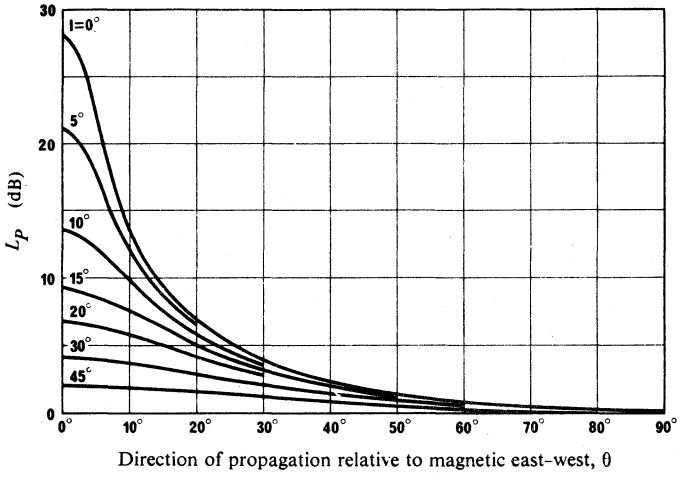

FIGURE 13 – *Excess polarization coupling loss L_P (for a single terminal)*

$$L_P = 180\,(36 + \theta^2 + I^2)^{-1/2} - 2$$

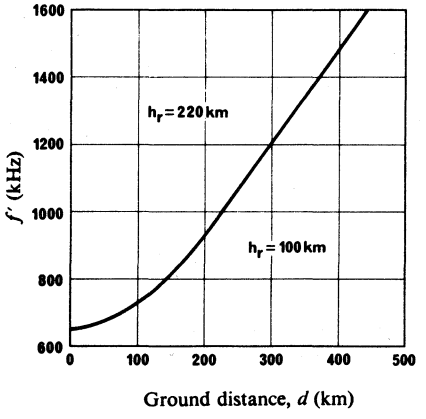

FIGURE 14 – *Frequency f' defined by equation*

$$f' = 350 + [(2.8\,d)^3 + 300^3]^{1/3}$$

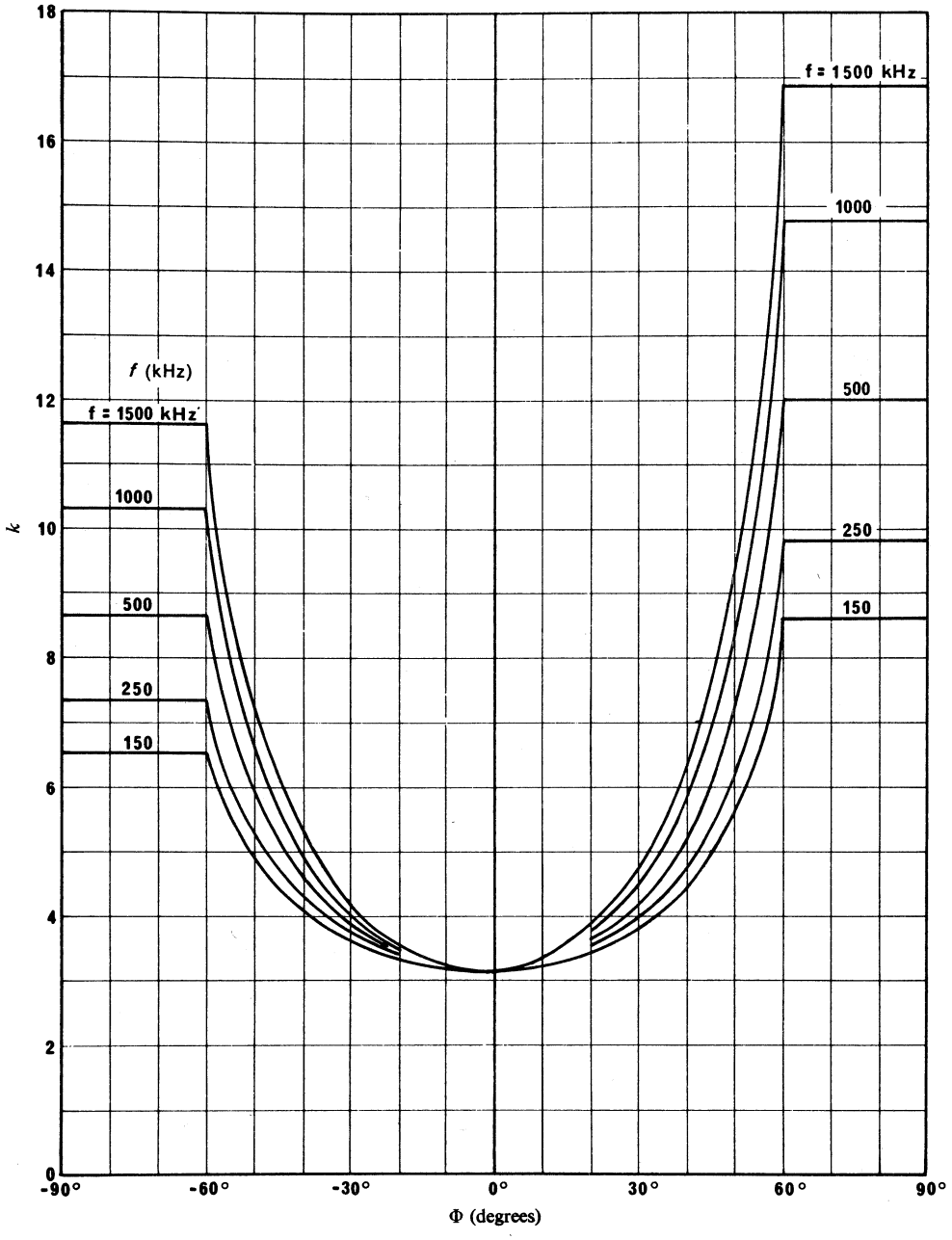

FIGURE 15 – *Basic loss factor*

$k = 3.2 + 0.19 f^{0.4} \tan^2 (\Phi + 3)$

$-60° \leqslant \Phi \leqslant 60°$

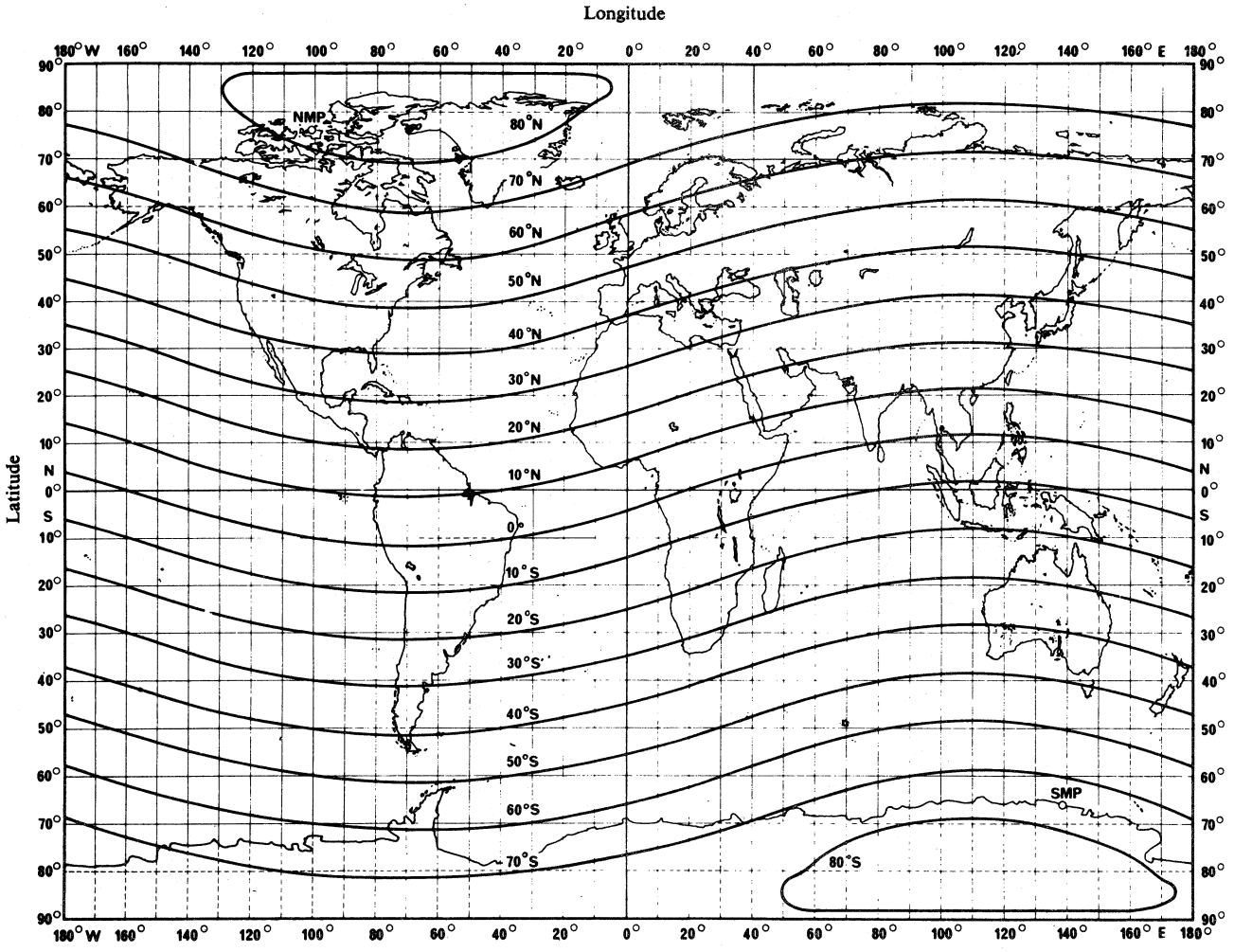

FIGURE 16 – *Geomagnetic latitudes*

The information contained within Appendix C is taken from the CCIR Report to the 1st Session of the Regional Administrative MF Broadcasting Conference, (Region 2), held in Geneva, 1979.

APPENDIX C: CCIR IWP 6/4 MF FIELD-STRENGTH PREDICTION METHOD

CHAPTER 2

SKY-WAVE PROPAGATION

2. Sky-wave field strength prediction method for the frequency range 520 to 1600 kHz in Region 2

2.1 General

This Chapter sets out a method for the prediction of sky-wave field strengths at MF for planning purposes, for the use of the Regional Administrative MF Broadcasting Conference (Region 2). This method is based on the information contained in CCIR Recommendation 435-3, and has been carefully considered in the light of measurements made in Region 2, in particular the information contained in the Final Report of the Fifth Meeting of the Working Group on Radiobroadcasting, Inter-American Telecommunications Conference, Brasilia, 9-13 July 1979. It will be noticed that this present method while being compatible with the basis of the above mentioned Final Report now offers reliable and complete treatment of the entire Region without discontinuities, and contains several important simplifications in the application of the Recommendation 435-3 data considered appropriate for use in the development of a Region 2 plan. These simplifications are based on direct contributions from Region 2 to the meeting of CCIR Interim Working Party 6/4, Geneva, October 2-5, 1979.*

This method of prediction suggested for use in Region 2 for planning purposes is similar to but not identical with that of CCIR Recommendation 435-3. In all cases of inter-Regional interference predictions involving Region 2, the use of the entire method set out in the latest version of Recommendation 435 is considered appropriate.

2.2 List of symbols

c_1, c_2: Sea-gain corrections defined in § 2.4.3.

d: Ground distance between transmitter and receiver (km).

F: Annual median field strength for a given cymomotive force (c.m.f.), M**, at the reference time defined in § 2.4.1.

---

* In order that this CCIR planning data be continually refined, Administrations of Region 2 are specifically requested to contribute additional information on this subject to Study Group 6 of the CCIR.

** A cymomotive force of 300 V is equivalent to a field strength of 300 mV/m at 1 km, which is the field strength due to an ideal short vertical monopole radiating 1 kW (an e.m.r.p. of 1 kW).

F_0: Annual median of half-hourly median field strengths (dB(μV/m)) for a transmitter cymomotive force of 300 V at the reference time defined in § 2.4.1.

f: Frequency (kHz).

G_0: Sea gain for a terminal on the coast (dB), see § 2.4.3.

G_H: Transmitting antenna gain factor due to horizontal directivity (dB), see § 2.4.2.

G_S: Sea gain for a terminal near the sea (dB), see § 2.4.3.

G_V: Transmitting antenna gain factor due to vertical directivity (dB), see § 2.4.2.

h: Transmitting antenna height, see fig. 33.

I: Magnetic dip angle, N or S (degrees), see § 2.4.4.

k: Basic loss factor, see § 2.4.6.

L_P: Excess polarisation coupling loss (dB).

P: Radiated power (dB(1 kW)).

p: Slant propagation distance (km), see § 2.4.5.

r_1, r_2: Parameters defined in § 2.4.3.

s_1: Distance of terminal from sea, measured along great-circle path (km), see § 2.4.3.

s_2: Distance of terminal from next section of land, measured along great-circle path (km), see § 2.4.3.

M: Transmitter cymomotive force (dB(300 V)) , see § 2.4.2.

α: Geographic latitude of terminal, degrees positive in the northern hemisphere, negative in the southern hemisphere, see § 2.4.6.

β: Geographic longitude of terminal, degrees, positive east of Greenwich meridian, see § 2.4.6.

θ: Direction of propagation relative to magnetic East-West (degrees), see § 2.4.4.

λ: Wavelength, see fig. 33.

Φ: A geomagnetic latitude parameter, see § 2.4.6.

Φ_T: Geomagnetic latitude of transmitter

Φ_R: Geomagnetic latitude of receiver

} degrees, positive for northern geomagnetic latitudes, negative for southern geomagnetic latitudes, see § 2.4.6.

2.3 Introduction

This method of prediction gives the night-time sky-wave field strength produced for a given power radiated from one or more vertical antennae, when measured by a loop antenna at ground level aligned in a vertical plane along the great-circle path to the transmitter. It applies for paths of lengths up to 12 000 km but should be used with caution for geomagnetic latitudes greater than 60°. It applies to the period when solar activity is least and field strengths are greatest and is suitable for planning purposes at all periods of solar activity. It gives the median field strength two hours after sunset (see § 2.4.1). The field strength exceeded for 10% of the time at this hour is 8 dB greater (see § 2.5).

Figs. 33 and 34 are an essential part of the prediction method. Geomagnetic maps are included for convenience in figs. 40, 41 and 43. The remaining figs. 35, 36, 37, 38, 39, 42, 44 and 45 provide additional information to simplify the use of the method when using manual calculations.

2.4 Annual median night-time field strength

The predicted sky-wave field strength is given by:

$$F = M + F_0 = M + G_S - L_P + 103 - 20 \log p - 10^{-3} kp \qquad (1)$$

where,

F: annual median of half-hourly median field strengths (dB(μV/m)) for a given transmitter cymomotive force, M*, at the reference time defined in § 2.4.1,

F_0: annual median of half-hourly median field strengths (dB(μV/m)) for a transmitter cymomotive force of 300 V* at the reference time defined in § 2.4.1,

M: transmitter cymomotive force, dB above a reference cymomotive force of 300 V*, see § 2.4.2,

G_S: sea-gain correction, (dB), see § 2.4.3,

---

* A cymomotive force of 300 V is equivalent to a field strength of 300 mV/m at 1 km, which is the field strength due to an ideal short vertical monopole radiating 1 kW (an e.m.r.p. of 1 kW).

L_P: excess polarization-coupling loss, (dB), see § 2.4.4,

p: slant-propagation distance, (km), see § 2.4.5,

k: basic loss factor incorporating effects of ionospheric absorption, focusing and terminal losses, and losses between hops on multi-hop paths, see § 2.4.6.

To facilitate calculation, figs. 35 and 36 show F_0 as a function of ground distance, d, for various geomagnetic latitudes when G_S and L_P are zero. Curves for 1 kW radiated from a short vertical monopole would be identical at distances greater than 1000 km.

2.4.1 Reference time

The reference time is taken as two hours after the time at which the Sun sets at a point S on the surface of the Earth. For paths shorter than 2000 km, S is the mid-point of the path. On longer paths, S is 750 km from the terminal where the Sun sets last, measured along the great-circle path. Fig. 45 facilitates the determination of sunset time.

2.4.2 Cymomotive force

The cymomotive force (c.m.f.) is expressed in volts; it corresponds numerically to the field-strength in mV/m at a distance of 1 km* (see CCIR Recommendation 561).

The cymomotive force M (in dB with respect to 300 V) is given as:

$$M = P + G_V + G_H \qquad (2)$$

where,

P: radiated power, dB above 1 kW,

G_V: transmitting antenna gain factor, dB, due to vertical directivity, given in fig. 33 for omnidirectional antennae,

G_H: transmitting antenna gain factor, dB, due to horizontal directivity.

For omnidirectional antennae, $G_H = 0$. For directional antennae G_H and G_V vary with azimuth and ground distance and may be determined collectively from the antenna radiation patterns.

For ground distances greater than 2000 km, $G_V + G_H$ is approximately equal to the antenna gain in the horizontal plane.

2.4.3 Sea gain

G_S is the additional signal gain when one or both terminals are situated near the sea, but it does not apply to propagation over fresh water. G_S for a single terminal is given by:

---

* A cymomotive force of 300 V, which is the reference level used in this Section corresponds to an effective monopole radiated power (e.m.r.p.) of 1 kW.

$$G_S = G_0 - c_1 - c_2 \quad \text{for} \quad (c_1 + c_2) < G_0 \tag{3}$$

$$G_S = 0 \quad \text{for} \quad (c_1 + c_2) > G_0 \tag{4}$$

where,

G_0: gain when the terminal is on the coast and the sea is unobstructed by further land;

c_1: correction to take account of the distance between the terminal and the sea,

c_2: correction to take account of the width of one or more sea channels, or the presence of islands.

If both terminals are near the sea, G_S is the sum of the values for the individual terminals.

G_0 is given in fig. 34 as a function of d.

G_0 = 10 dB when d > 6500 km.

The correction c_1 is given by

$$c_1 = \frac{s_1}{r_1} G_0 \tag{5}$$

where,

s_1: distance of terminal from sea, measured along great-circle path (km),

r_1: $10^3 G_0^2 \;/\; 1.4\, f$ (km),

f: frequency in kHz.

The correction c_2 is given by

$$c_2 = G_0 \left(1 - \frac{s_2}{r_2}\right) \quad \text{for} \quad s_2 < r_2 \tag{6}$$

$$c_2 = 0 \quad \text{for} \quad s_2 > r_2 \tag{7}$$

where,

s_2: distance of terminal from next section of land, measured along great-circle path,

r_2: $10^3 G_0^2 \;/\; 1.2\, f$ (km).

Equation (6) applies if there is only one sea channel, or if more than half the distance between s_2 and a great-circle distance equal to r_2 is occupied by land. If less than half the distance between s_2 and r_2 is occupied by land, $c_2 = 0$.

To facilitate calculation, fig. 37 shows r_1, the greatest distance from the sea for which sea gain has to be calculated, and fig. 38 shows r_2, the greatest distance to the next section of land for which the correction c_2 is required, for various frequencies.

2.4.4 Polarization coupling loss

L_P is the excess polarization coupling loss. L_P for a single terminal is given by one of the following two formulae:

$$\begin{aligned} &\text{If } I \leq 45^\circ : \quad L_P = 180\ (36 + \theta^2 + I^2)^{-\frac{1}{2}} - 2 \qquad \text{(dB)} \\ &\text{If } I > 45^\circ : \quad L_P = 0 \end{aligned} \tag{8}$$

where I is the magnetic dip, N or S, in degrees at the terminal and θ is the path azimuth measured in degrees from the magnetic E-W direction, such that $|\theta| \leq 90^\circ$ as shown in fig. 39. L_P should be evaluated separately for the two terminals, because of the different θ and I that may apply, and the two L_P values added. The most accurate available values of magnetic dip and declination (e.g. see figs. 40 and 41) should be used in determining θ and I.

Fig. 39 shows values of L_P calculated from equation (8).

2.4.5 Slant propagation distance

For paths longer than 1000 km, p is approximately equal to the ground distance d (km). For shorter paths

$$p = (d^2 + 4 \times 10^4)^{\frac{1}{2}} \tag{9}$$

Equation (9) may be used for paths of any length with negligible error.

2.4.6 Loss factor

The basic loss factor k is given by:

$$k = 0.067\ |\Phi| + 0.2 + 3 \tan^2 (\Phi+3) \tag{10}$$

If $\Phi > 59^\circ$, equation (10) is evaluated for $\Phi = 59^\circ$. If $\Phi < -59^\circ$, equation (10) is evaluated for $\Phi = -59^\circ$. If equation (10) gives a value of $k < 3$, then $k = 3$. Fig. 42 shows values of k calculated from equation (10) according to these rules.

For paths shorter than 3000 km:

$$\Phi = 0.5\ (\Phi_T + \Phi_R) \tag{11}$$

where Φ_T and Φ_R are the geomagnetic latitudes at the transmitter and receiver respectively, determined by assuming an Earth-centred dipole field model with northern pole at 78.5° N, 69° W geographic co-ordinates. Φ_T and Φ_R are taken as positive in the northern hemisphere and negative in the southern hemisphere (see fig. 43), and are given by the equation

$$\Phi_T \text{ or } \Phi_R = \arcsin \left[\sin \alpha \sin 78.5^\circ + \cos \alpha \cos 78.5^\circ \cos (69^\circ + \beta) \right] \tag{12}$$

where α and β^* are the latitude and longitude of the terminal respectively. Paths longer than 3000 km are divided into two equal sections which are considered separately. The value of Φ for each half-path is derived by taking the average of the geomagnetic latitudes at one terminal and at the mid-point of the whole path, the geomagnetic latitude at the mid-point of the whole path being assumed to be the average of Φ_T and Φ_R. As a consequence:

$$\Phi = 0.25\ (3\Phi_T + \Phi_R) \text{ for the first half of the path and} \quad (13)$$

$$\Phi = 0.25\ (\Phi_T + 3\Phi_R) \text{ for the second half.} \quad (14)$$

The values of k calculated from equation (10) for the two half-paths are then averaged and used in equation (1).

2.5 The accuracy of the field-strength prediction method for Region 2, proposed in this Chapter

In Section 2.3 above, it is stated that the field strength exceeded for 10% of the time near to two hours after sunset is 8 dB greater than the median field strength. Although this figure is suitable for planning purposes, it should be noted that in regions of high geomagnetic latitude the 10% field strength will tend to be up to 2 dB higher, and at lower geomagnetic latitudes up to 2 dB lower, than this figure.

Field strengths decrease with increasing solar activity, especially at high geomagnetic latitudes.

Field strengths vary during the night and at sunrise and sunset. Fig. 44 shows the average variation which has been observed in Europe and Australia, and it is reasonable to assume that this curve also applies in Region 2. The horizontal scale shows the time in hours relative to the sunrise or sunset reference times as appropriate. These are taken at the ground at the mid-path position for $d < 2000$ km, and at 750 km from the terminal where the Sun sets last or rises first for longer paths. The vertical scale shows the correction which should be applied to the prediction for two hours after sunset.

Fig. 45 shows sunset and sunrise times for a range of geographic latitudes.

The method predicts the field strength which is likely to be observed if the transmitter and receiver are situated on ground of average conductivity, typically 3 to 10 mS/m. If the ground conductivity is an order of magnitude smaller, as it is in some parts of Region 2, then the field strength will be up to 10 decibels smaller; the amount of attenuation is a function of path length and is greatest for waves approaching grazing incidence.

Information on non-reciprocal sky-wave propagation is to be found in the Annex to this Chapter.

---

* See § 2.2 for sign convention.

2.6 Illustration of Chapter 2 method of prediction of sky-wave field strengths

Case 1: Transmitter XEW, Mexico City, Mexico, 19°19' N, 99°07' W, f = 900 kHz, P = 250 kW, Φ_T = 29.1°, and antenna height (assumed) 0.25λ.

Receiving site Kingsville, USA, 27°26' N, 97°53' W, Φ_R = 37.3°, d = 910 km.

Calculation:

Step	Item	Equation or figure used	Contribution to equation (1)
1	G_V = 0.2 dB	Fig. 33	-
2	M	Equation (2)	24.2
3	G_S = 0	(Path is over land)	0
4	L_P = 0	(I> 45°, both terminals)	0
5	103	-	103
6	p = 931.7 km	Equation (9)	-
7	- 20 log p	-	-59.4
8	Φ = 33.2°	Equation (11)	-
9	k = 4.03	Equation (10)	-
10	-10^{-3} kp	-	-3.7
11	F	Equation (1)	63.9 dB(μV/m)

Case 2: Transmitter WLS, Chicago, USA, 41°33' N, 87°51' W, f = 890 kHz, P = 50 kW, Φ_T = 52.3°, and antenna height = 0.53λ (178 m), omni.

Receiving site Portland, USA, 45°32' N, 122°40' W, Φ_R = 51.4°, d = 2821 km.

Calculation:

Step	Item	Equation or figure used	Contribution to equation (1)
1	G_V = 2.6 dB	Fig. 33	-
2	M	Equation (2)	19.6
3	G_S = 0	(Path is over land)	0
4	L_P = 0	(I > 45°, both terminals)	0
5	103	-	103
6	-20 log p	p = d = 2821	-69
7	Φ = 51.9°	Equation (11)	-
8	k = 9.75	Equation (10)	-
9	-10^{-3} kp	-	-27.5
10	F	Equation (1)	26.1 dB(μV/m)

Case 3: Transmitter, Buenos Aires, Argentine, 34°27' S, 58°34' W, f = 1070 kHz, P = 100 kW, Φ_T = -23.1°, antenna height = 0.5λ, omni.

Receiving site, Recife, Brazil, 8°06' S, 34°53' W, Φ_R = 1.5°, d = 3800 km.

Calculation:

Step	Item	Equation or figure used	Contribution to equation (1)
1	G_V = 2.3 dB	Fig. 33	-
2	M	Equation (2)	22.3
3	G_S = 5.4 dB	Equations (3) to (7) and fig. 34	5.4
		G_0 = 9.2 dB	
		At transmitter:	
		s_1 = 4 km, r_1 = 67 km, c_1 = 0.5 dB;	
		s_2 = 50 km, r_2 = 78 km, c_2 = 3.3 dB;	
		G_S = 5.4 dB	
		At receiver: G_S = 0	
4	L_P = 4.5 dB	Equation (8), figs. 40 and 41	-4.5
		At transmitter:	
		I = 33°S, θ = 43°, L_P = 1.3 dB	
		At receiver:	
		I = 12°S, θ = 32°, L_P = 3.2 dB	
5	103	-	103
6	-20 log p	(p = d = 3800 km)	-71.6
7	Φ	Equations (13) and (14)	
		Φ = -17.0° for first half of path;	
		Φ = - 4.7° for second half of path;	
8	k = 3	Equation (10), but k = 3 for both halves of path	
9	-10^{-3} kp	-	-11.4
10	F	Equation (1)	43.2 dB(μV/m)

ANNEX TO CHAPTER 2

NON-RECIPROCAL SKY-WAVE PROPAGATION

1. Introduction

A recent paper* describes an analysis of measurement made in the United States of America which indicates that sky-wave propagation in the MF broadcasting band is non-reciprocal on east-west paths, the transmission loss being greater on paths from east to west. The paper says that these differences should be considered in any frequency assignment process intended to make optimum use of the MF broadcasting band.

2. General

A theoretical paper** has shown that non-reciprocal transmission losses are to be expected on east-west multihop paths due to the change in polarization occurring at the intermediate ground reflection. The paper shows that greater transmission losses are expected on paths from east to west and that the difference between the two directions of propagation is greatest at magnetic-dip latitudes of about 60°, and increases as the frequency increases. The difference between the two directions of propagation is likely to be most pronounced on paths which are just beyond the range of the one-hop mode and where the intermediate reflection point is on land; at this distance (2000 to 2500 km) the two-hop mode is reflected at angles near the Brewster angle. Little difference between the two directions of propagation is to be expected when the intermediate reflection point falls on sea water.

If non-reciprocal propagation is confined to east-west multi-hop paths over land at about 60° dip latitude it will be significant only within a small part of Region 2. The conditions for non-reciprocal propagation can be satisfied in Canada and the United States of America, and here it appears to have been confirmed by measurements. In Central and South America, two-hop paths with intermediate reflection points on land are possible only at dip latitudes less than 30°, where the non-reciprocal effect is unimportant.

3. Conclusion

In common with the field strength prediction method described in Annex I to CCIR Recommendation 435-3, with all of the earlier methods described in CCIR Report 575-1 and with methods based on the FCC curves, the method recommended here for planning purposes in Region 2 does not take account of non-reciprocal propagation. Any method would become very complicated if such a correction were to be properly applied, while in most parts of Region 2 the improvement in accuracy of the predictions would be small.

---

* CROMBIE, D.D. [1979] Comparison of measured and predicted signal strengths of night-time medium frequency signals in the USA. IEEE Trans. on Broadcasting, BC-25, 86-89.

** KNIGHT, P. [1973] MF propagation: non-reciprocal ionospheric propagation on multi-hop paths. British Broadcasting Corporation Research Report 1973/17.

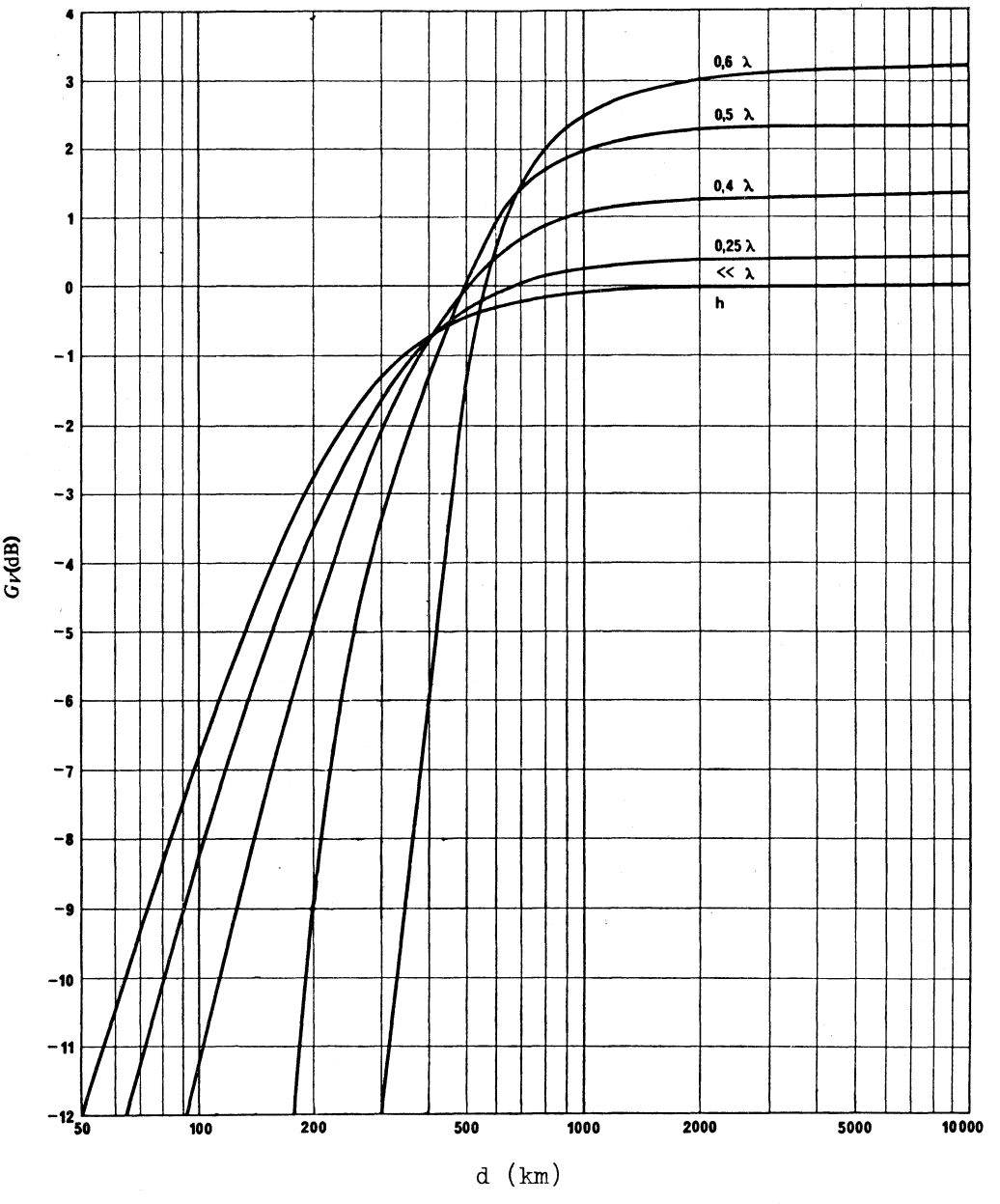

Fig.33 - Transmitting antenna gain factor for single monopoles (G_V)

h= height of antenna

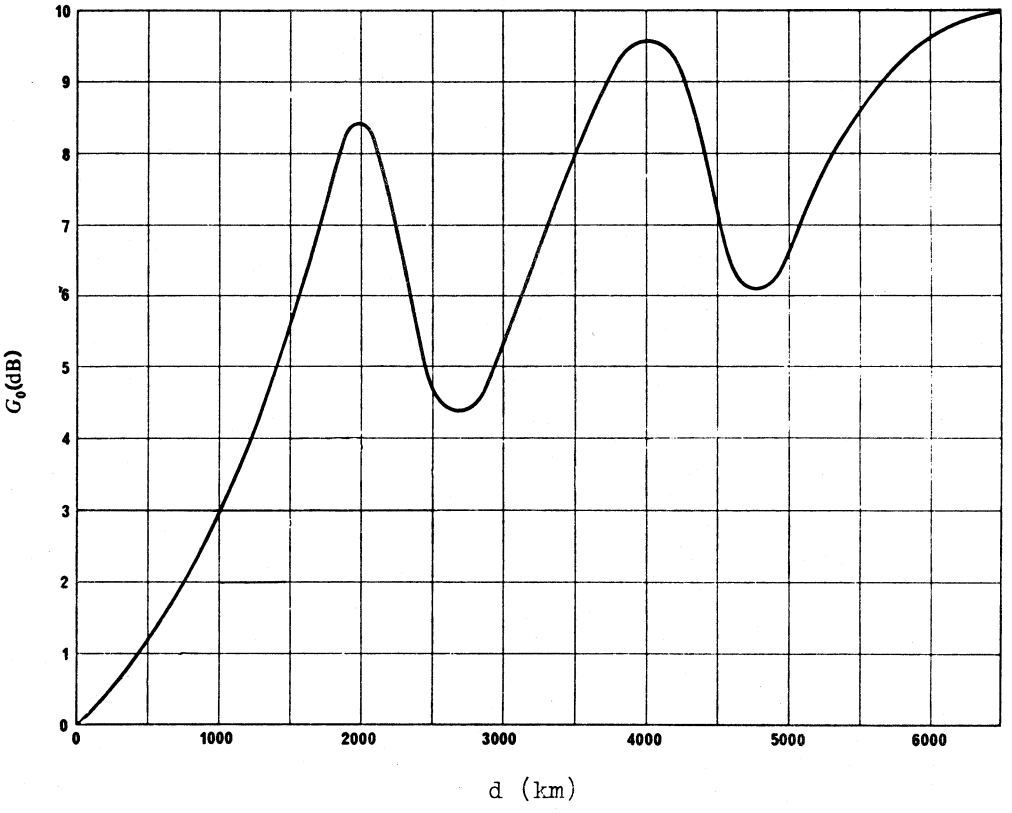

Fig.34 - Sea gain (G_0) for a single terminal on the coast

(G_0 = 10 dB for d>6500km)

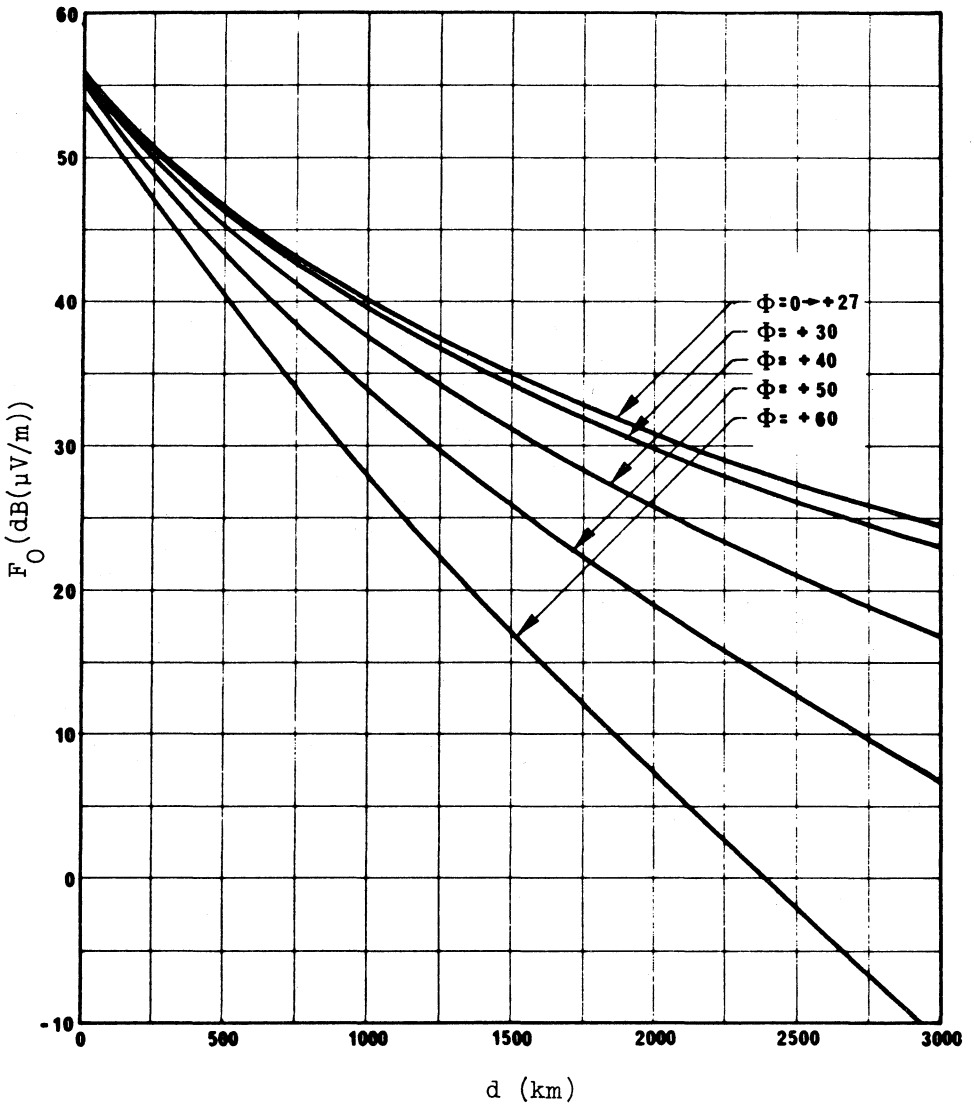

Fig. 35a - F_O for constant Φ, and for G_S and L_P both zero

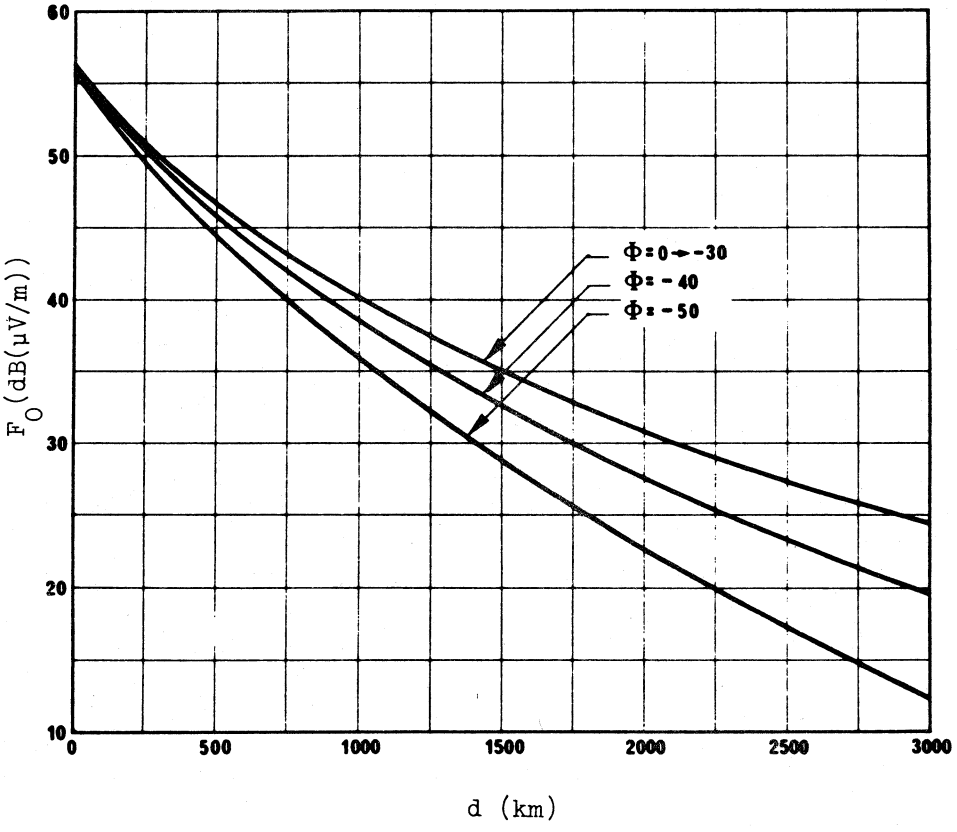

Fig. 35b - F_0 for constant Φ, and for G_S and L_P both zero

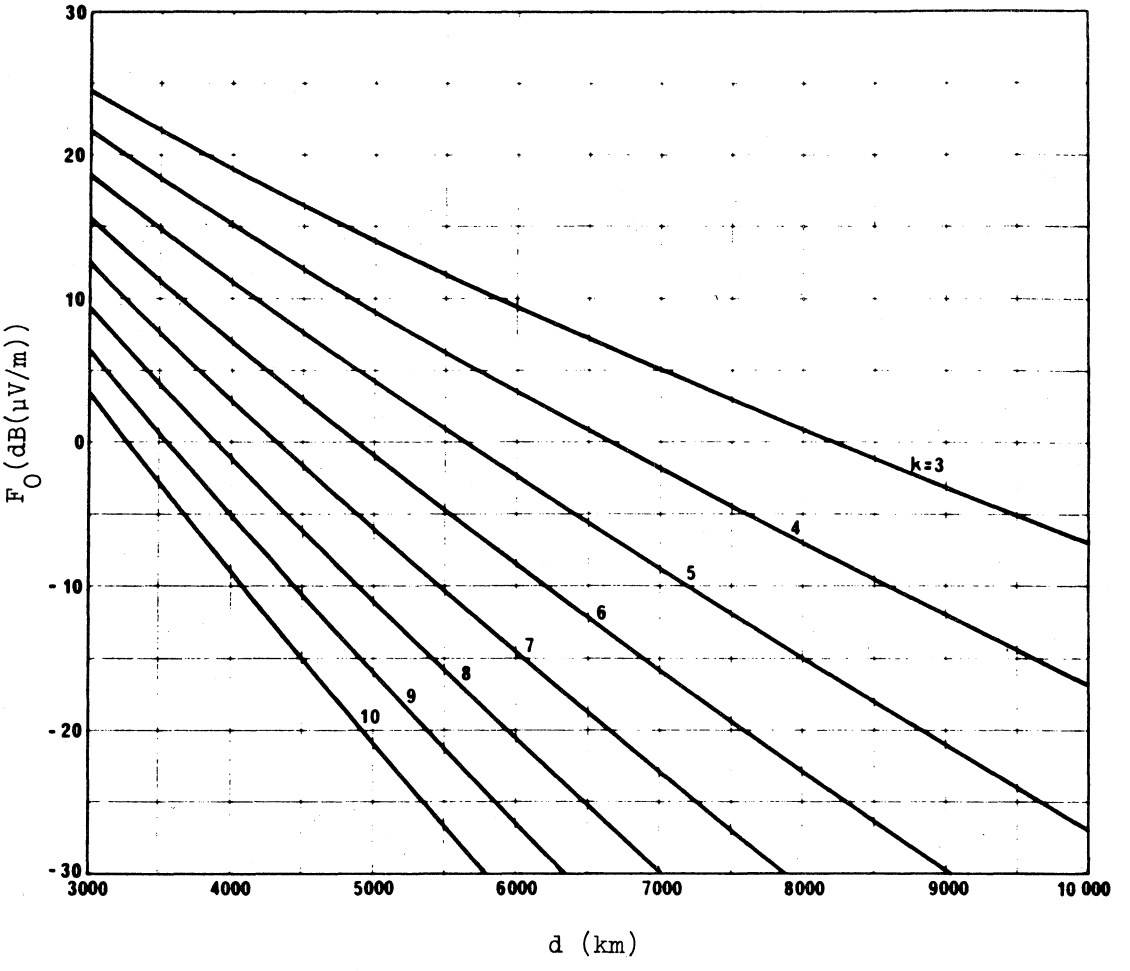

Fig. 36 - F_0 for average values of k, and for G_S and L_P both zero

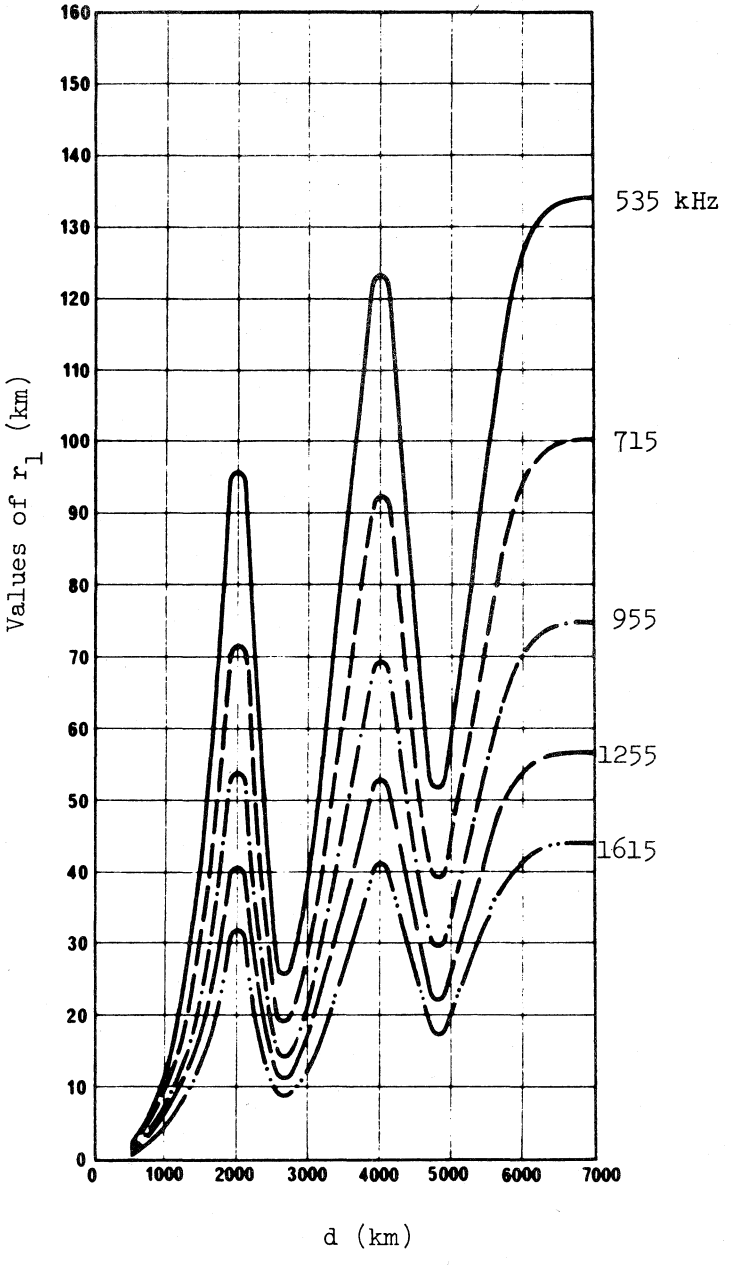

Fig. 37 - Values of r_1 for typical frequencies

——— 535 kHz
— — — — 715
—·—·—·— 955
——— 1255
—··—··— 1615

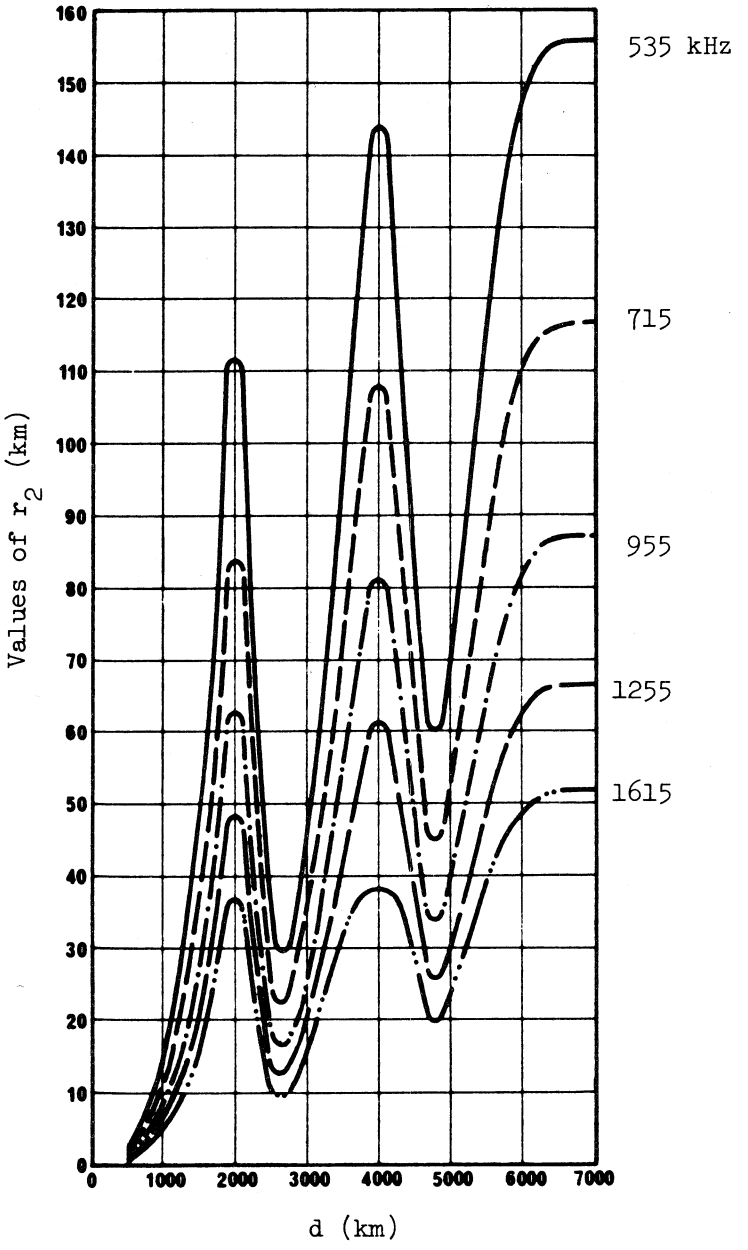

Fig. 38 - Values of r_2 for typical frequencies

——— 535 kHz
– – – – 715
·—·—·—· 955
——— 1255
··—·—·— 1615

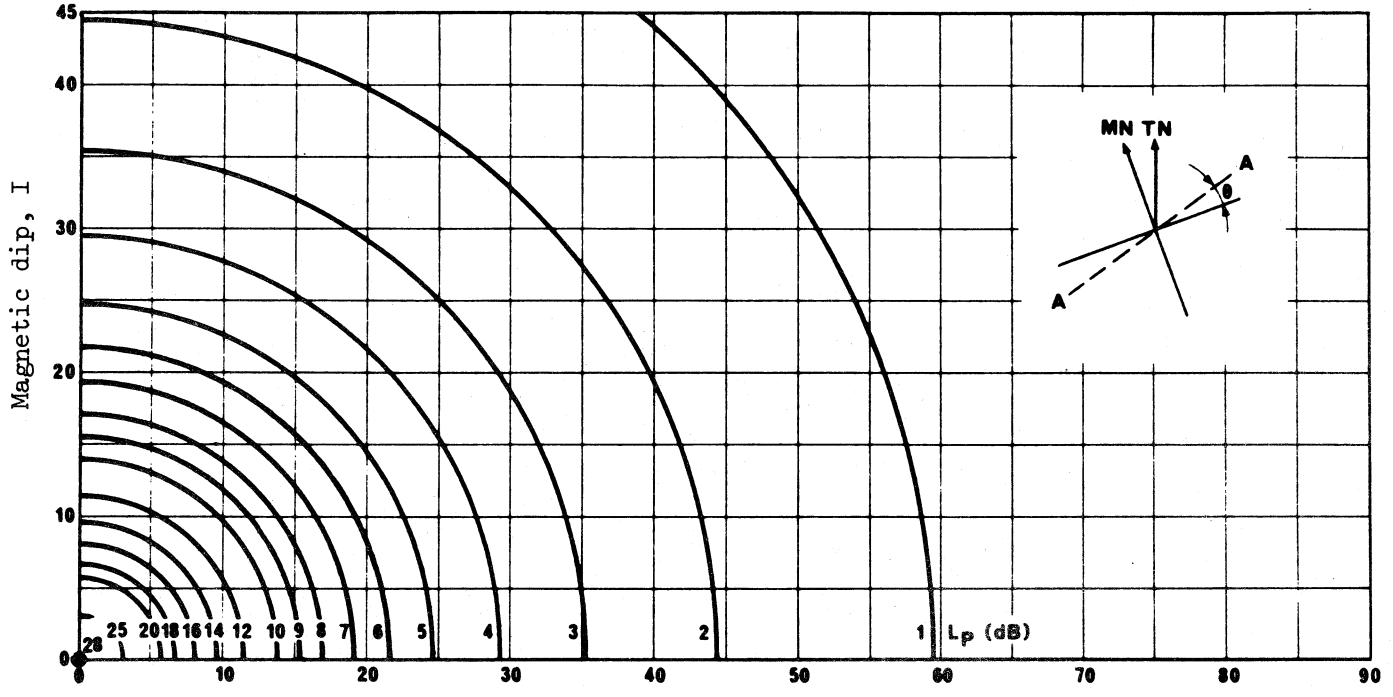

Fig. 39 - Excess polarization coupling loss L_p for a single terminal

$$L_p = 180\ (36 + \theta^2 + I^2)^{-\frac{1}{2}} - 2$$

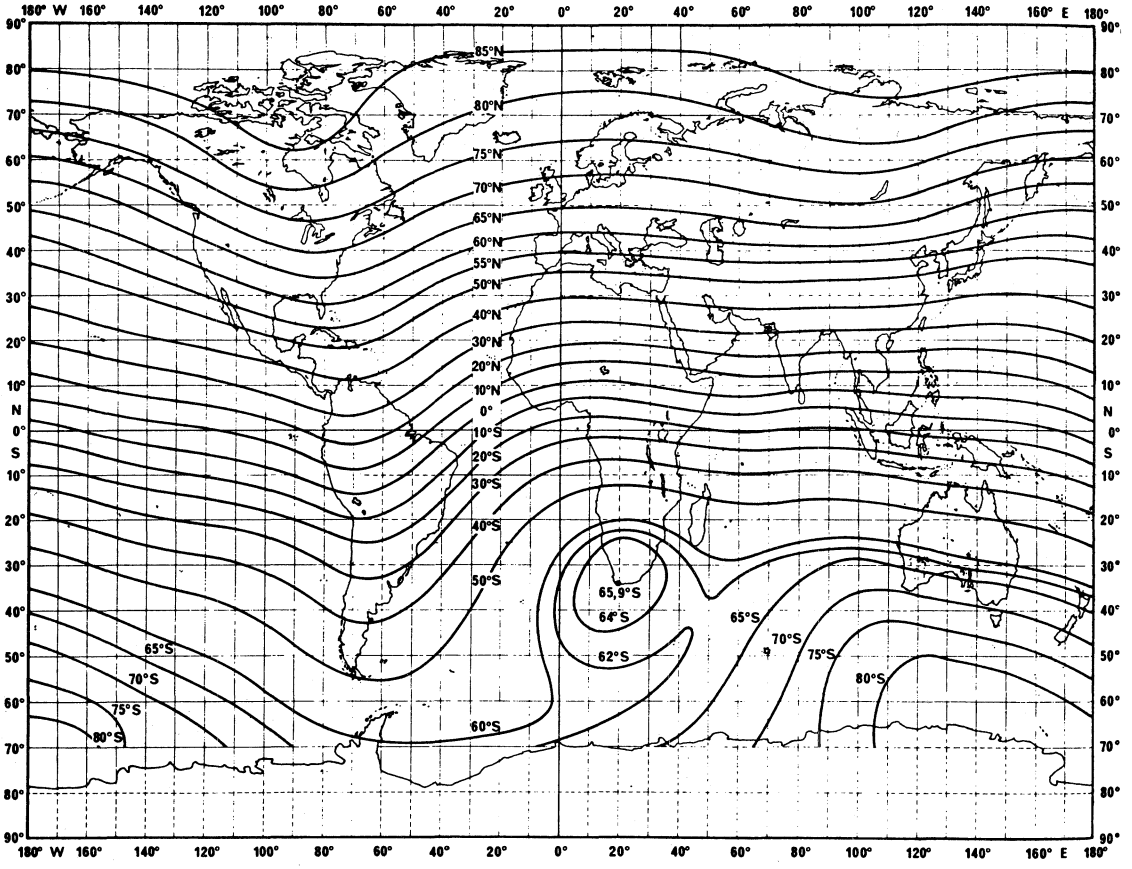

FIGURE 40 – *Map of magnetic dip (epoch 1975.0)*

(Source: Magnetic inclination or dip (epoch 1975.0) Chart No. 30 World U.S. Defense Mapping Agency Hydrographic Center)

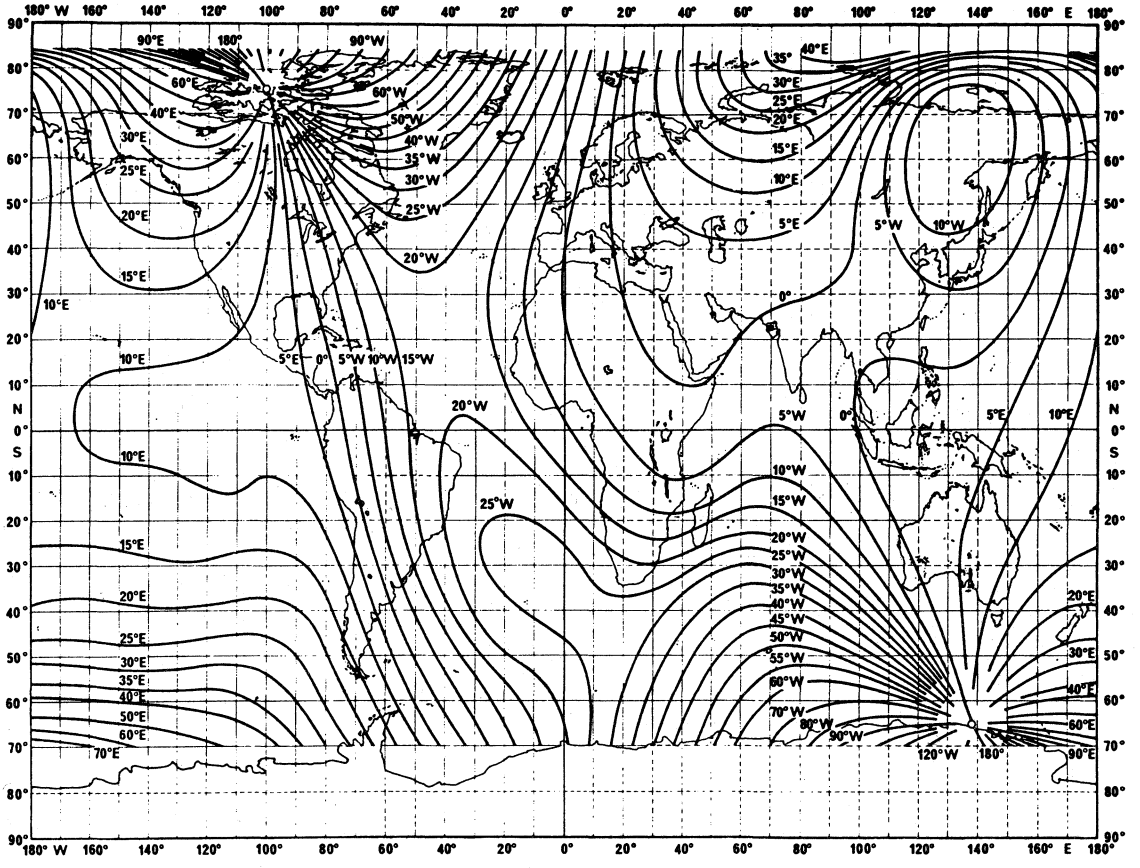

FIGURE **41** – *Map of magnetic declination (epoch 1975.0)*

(Source: Magnetic variation (epoch 1975.0) Chart No. 42, World U.S. Defense Mapping Agency Hydrographic Center)

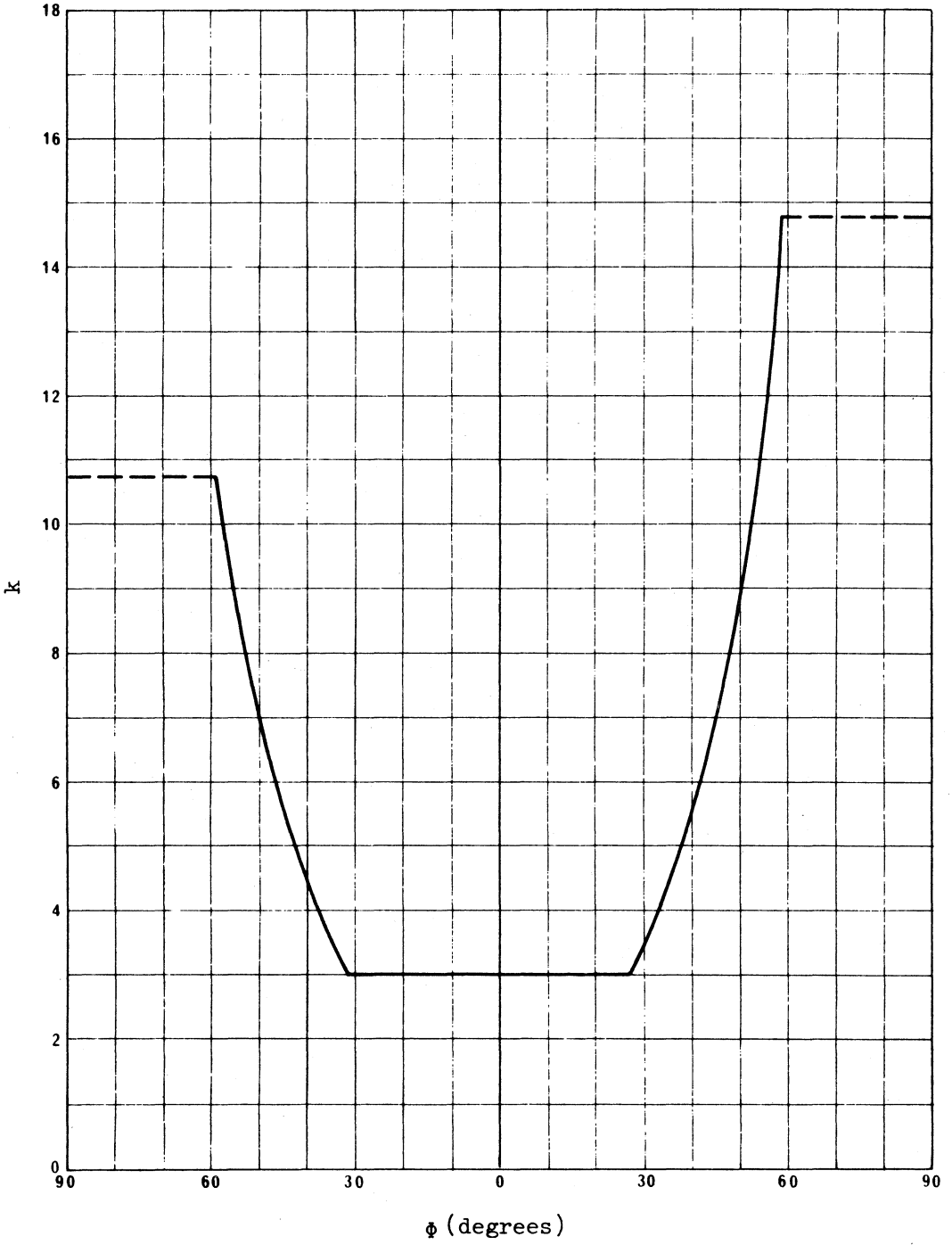

Fig.42 - Basic loss factor k

$-59^{o} \leq \Phi \leq 59^{o}$

$k \geq 3$

$k = 0.67 |\Phi| + 0.2 + 3 \tan^{2}(\Phi + 3^{o})$

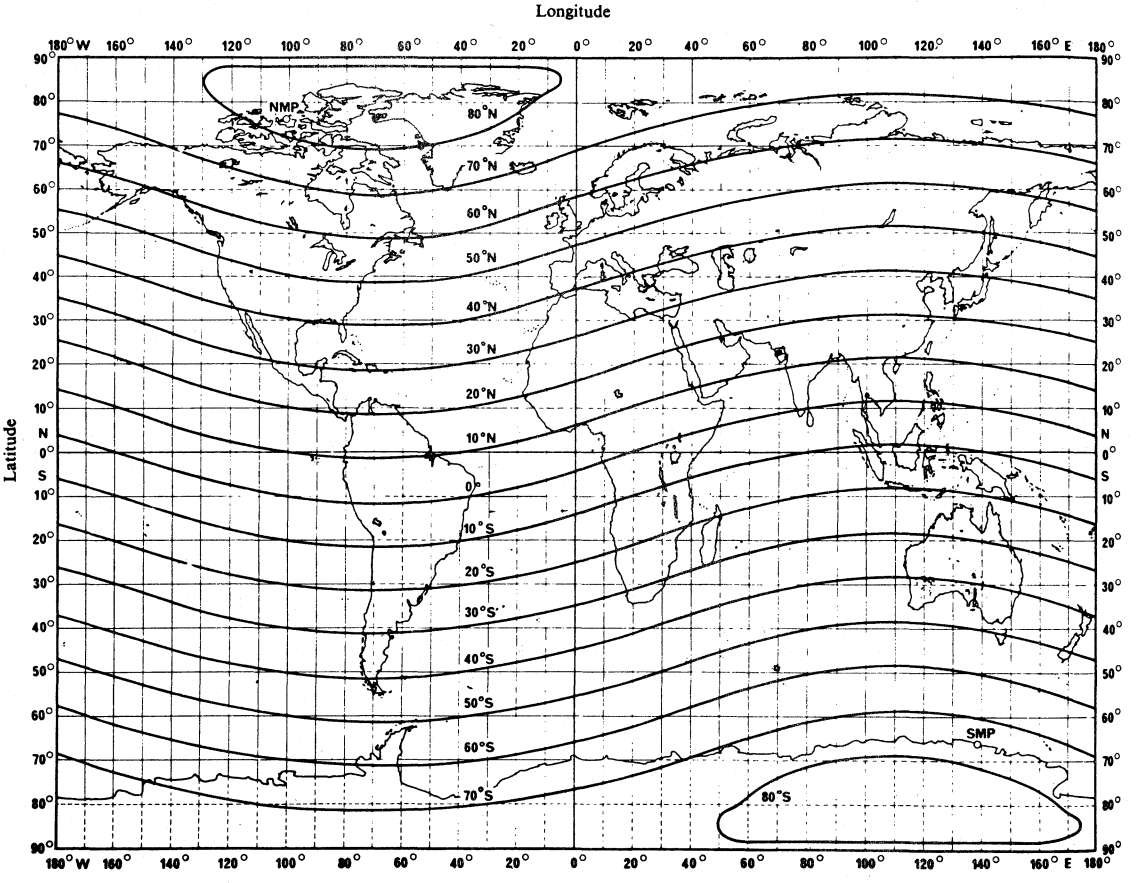

FIGURE 43– *Geomagnetic latitudes*

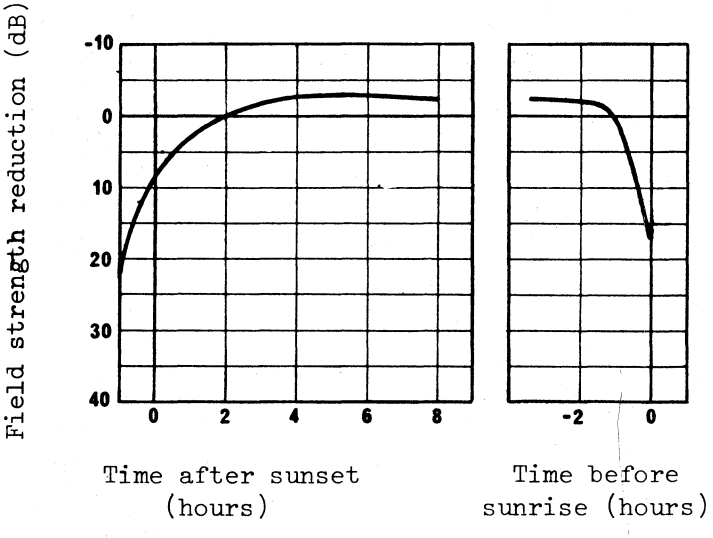

Fig.44 - Field strength variation during the night

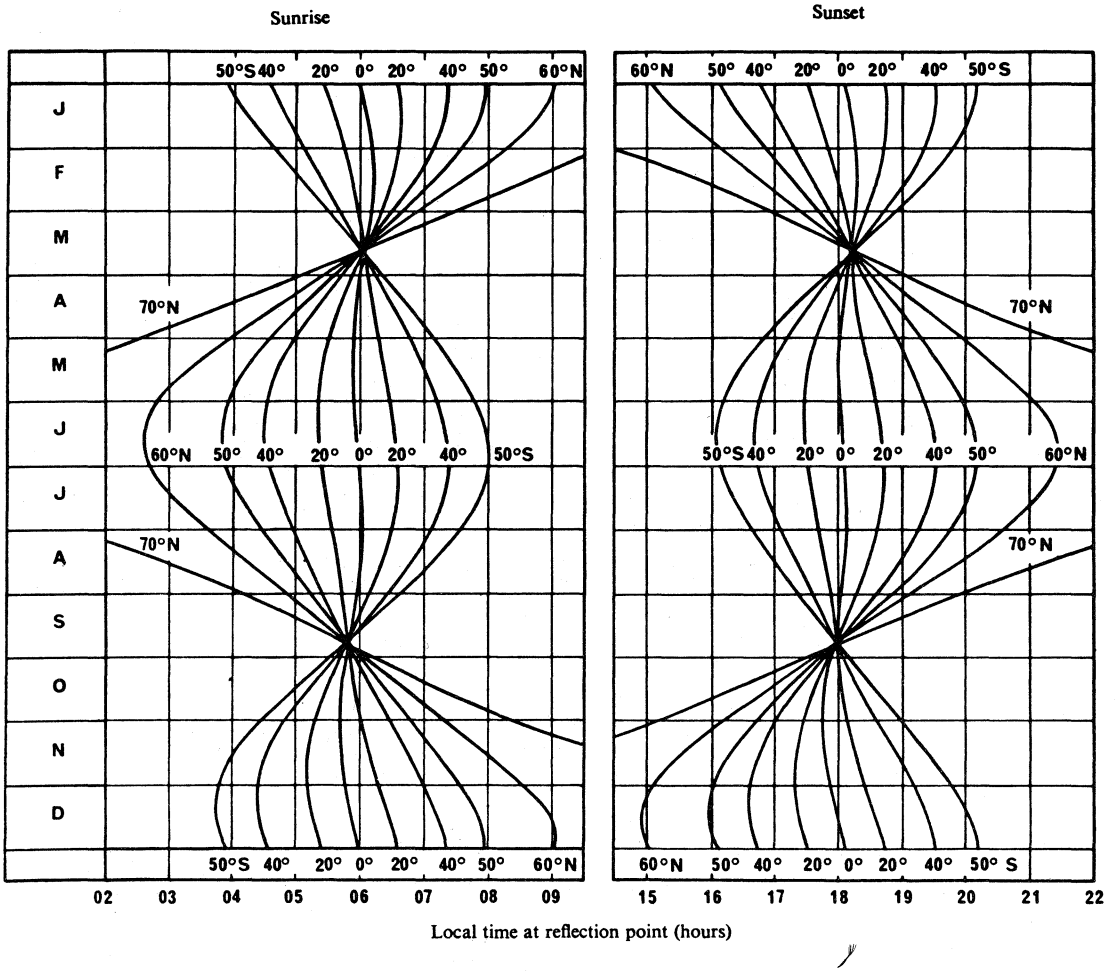

FIGURE **45** – *Times of sunrise and sunset for various months and geographical latitudes*